Journal of Cleaner Production 290 (2021) 125841

Contents lists available at ScienceDirect

Journal of Cleaner Production

journal homepage: www.elsevier.com/locate/jclepro

Review

# Recent development of electrochemical advanced oxidation of herbicides. A review on its application to wastewater treatment and soil remediation

Enric Brillas

*Laboratori d'Electroquímica dels Materials i del Medi Ambient, Departament de Química Física, Facultat de Química, Universitat de Barcelona, Martí i Franquès 1-11, 08028, Barcelona, Spain*

A R T I C L E I N F O

*Article history:*
Received 30 September 2020
Received in revised form
1 January 2021
Accepted 2 January 2021
Available online 5 January 2021

Handling editor: Prof. Jiri Jaromir Klemeš

*Keywords:*
Anodic oxidation
Electro-Fenton
Herbicides
Photoelectrocatalysis
Photoelectro-Fenton
Solar photoelectro-Fenton

A B S T R A C T

Herbicides have been largely utilized during the last decades to maintain the quality and quantity of agricultural crop, ensuring the need of an increasing world food production. However, these synthetic organics are highly biorecalcitrant and stable at mild conditions and cannot be effectively destroyed in conventional wastewater treatment facilities. Among the advanced oxidation processes used to remove herbicides, electrochemical technologies have been recently developed at bench scale as potential powerful treatments. This review presents a critical, exhaustive and detailed analysis on the application of single and combined electrochemical advanced oxidation processes to remediate wastewaters and soils contaminated with common herbicides, covering the period 2010–2019. Nine kinds of treatments, including single methods like anodic oxidation, anodic oxidation with electrogenerated $H_2O_2$, homogeneous and heterogeneous electro-Fenton, photoelectro-Fenton, solar photoelectro-Fenton and photoelectrocatalysis, as well as combined ones involving hybrid and sequential processes, have been examined. The fundamentals of each technology are briefly described, and the main results obtained for the removal of the most used herbicide families from synthetic solutions and soil-washing effluents are carefully exposed and discussed. The role of generated oxidizing agents and/or photolytic reactions in photo-assisted processes is explained to justify the mechanisms proposed for herbicide mineralization. The comparative oxidation ability of the different methods is discussed. Finally, future challenges remarking the need of treating real agricultural wastewaters and contaminated soils, the construction of electrochemical systems with stable electrodes at industrial scale and the realization of techno-economic studies are envisaged.



**Contents**



*E-mail address:* brillas@ub.edu.

https://doi.org/10.1016/j.jclepro.2021.125841

## 1. Introduction

Pesticides or agrochemicals are synthetic substances that are produced for destroying, preventing or controlling unwanted fungal or animal pests. Based on the target organism, they have been classified into herbicides, insecticides, fungicides, rodenticides, and so on. From their chemical structure, herbicides have been categorized into triazine, chlorophenoxy acid, organochlorine, organophosphate and urea families, among others. Herbicides used to crop can act as plant growth regulators, defoliants, desiccants or agents for thinning fruit or preventing the premature fall of fruit (Vagi and Petsas, 2019). The increasing use of herbicides in intensive agriculture during the last decades has maintained the quality and quantity of agricultural crop with the consequent rise in world food production. However, these compounds can enter into aquatic ecosystems via surface run-off, leaching, spray-drift, soil erosion and deposition (Vagi and Petsas, 2019). The occurrence of herbicide residues and their metabolites in aquatic bodies (rivers, lakes, sea) has been well documented, being detected usually at trace contents from ng $L^{-1}$ to μg $L^{-1}$. Despite their low content, they are considered as priority persistent organic pollutants (POPs) due to their potential acute and chronic toxicity that can affect the ecosystems and human health (Mahour et al., 2014).

The majority of herbicides are chemically and photochemically stable at mild conditions. For this reason, they are hardly degraded in wastewater treatment facilities from conventional physicochemical and biological (abiotic and/or biotic) processes. The treatment of soils requires the previous extraction of the herbicides with surfactants to obtain a flushing effluent for remediation (Rodrigo et al., 2014). Among the different techniques developed to remove herbicides from wastewaters and soils, the advanced oxidation processes (AOPs) have been described as the most efficient treatments. AOPs are characterized by the in situ production of hydroxyl radical ($^{\bullet}OH$), which is the second stronger oxidant known with a standard reduction potential ($E^{\circ}$) of 2.72 V/SCE. $^{\bullet}OH$ can non-selective react with most organics up to their mineralization via hydroxylation and dehydrogenation reactions, among others (Oturan and Aaron, 2014). Other weaker oxidants (e.g., $O_2^{\bullet-}$, $O_3$, active chlorine) can be produced depending on the method, operation conditions and matrix tested. Several AOP treatments of herbicide wastewaters have been reported using UV/$H_2O_2$ photolysis and photocatalysis (with $TiO_2$/UV or ZnO/UV) (Ribeiro et al., 2015), as well as pulse electric discharge plasma, gamma irradiation, sulfate radical-based catalysts, sonolysis and $O_3$-based AOPs (Malakootian et al., 2020). More effective processes have been described with electrochemical AOPs (EAOPs) like anodic oxidation (Martínez-Huitle and Panizza, 2018) and electro-Fenton (Nidheesh et al., 2019). The good performance of EAOPs to destroy other kinds of POPs such as pharmaceuticals and personal care compounds (Moreira et al., 2017) and a high number of dyes (Brillas and Martínez-Huitle, 2015). EAOPs are considered as environmental-friendly methods because the injected electrons caused the destruction of organic pollutants. They present several advantages over other AOPs including the absence or addition of low content of non-toxic catalysts, relatively low cost, safety because of their use at mild conditions under ambient conditions and simple equipment with amenability to be easily scaled-up at industrial scale and automatized.

This paper presents an exhaustive critical review over the development of emerging EAOPs that have been applied to herbicide remediation in wastewaters and soils during the last decade. The oxidation power of single and combined (hybrid and sequential) processes including anodic oxidation (AO), Fenton-based treatments like electro-Fenton (EF) and photoelectro-Fenton (PEF), and photoelectrocatalysis (PEC) has been examined as function of their operation parameters for the pre-eminently used herbicide families. The electrochemical systems utilized in these techniques are described. The action of generated oxidizing agents are detailed to explain the degradation and mineralization routes of the herbicides tested.

## 2. Methods

This section analyzes all the literature related to the remediation of herbicide wastewaters by EAOPs identified during the period 2010–2019.

### 2.1. Data sources and search strategy

To select the scientific and review articles dealing with the EAOPs applied to the treatment of herbicides in wastewaters and soils, an exhaustive search of the peer-reviewed literature was made in the Scopus database. Since a low number of papers was found with the keywords electrochemical advanced oxidation processes AND herbicides, the search was extended directly to each technology and the generic name of pesticides, because many articles used the latter general term instead of the particular name of herbicides. Four literature searches were then performed with the following keywords: anodic oxidation AND pesticides, electro-Fenton AND pesticides, photoelectro-Fenton AND pesticides, and photoelectrocatalysis AND pesticides. The literature was limited to publications (scientific articles and reviews) written in English from 2010 to April 2020, covering the period of the last ten years. The name of authors, title, publication data and abstract of each retrieved paper were listed to be further revised individually. In this way, all the publications including herbicides were selected. Presentations, letters to the editors, books and papers related to the electrochemical detection of herbicides were excluded. The full text of all the selected publications was then obtained and was analyzed to decide its inclusion in the present review with the following criteria:

(i) a correct application of single or coupled EAOPs,
(ii) the remediation of single and/or mixtures of herbicides from wastewaters and soils,
(iii) an appropriated information over the experimental methods, including the electrochemical cell and electrodes employed, experimental conditions, equipment for analysis, and degradation and mineralization calculations, and
(iv) a detailed description with adequate discussion of the results obtained, regarding the decay of the herbicide, its removal kinetics, the efficiency of the abatement of total organic carbon (TOC) and/or chemical oxygen demand (COD), the effect of operation variables, comparison between different EAOPs, the energy consumption and if possible, the detection and identification of primary and final by-products, allowing in many cases, the proposal of a degradation or mineralization mechanism. These parameters are remarked for each treatment in the figures and tables presented in this review.

From the aforementioned analysis, the development of 9 kinds of methods involving EAOPs was identified: AO, AO with electrogenerated $H_2O_2$ (AO-$H_2O_2$), homogeneous EF (homo-EF), heterogeneous EF (hetero-EF), PEF, solar PEF (SPEF), PEC and combined (hybrid and sequential) processes. The degraded herbicides were finally ascribed to each of such treatments, regardless of the matrix utilized. Fig. 1 shows the 8 main herbicide families studied by EAOPs, alongside the name and chemical formula of some notable compounds.

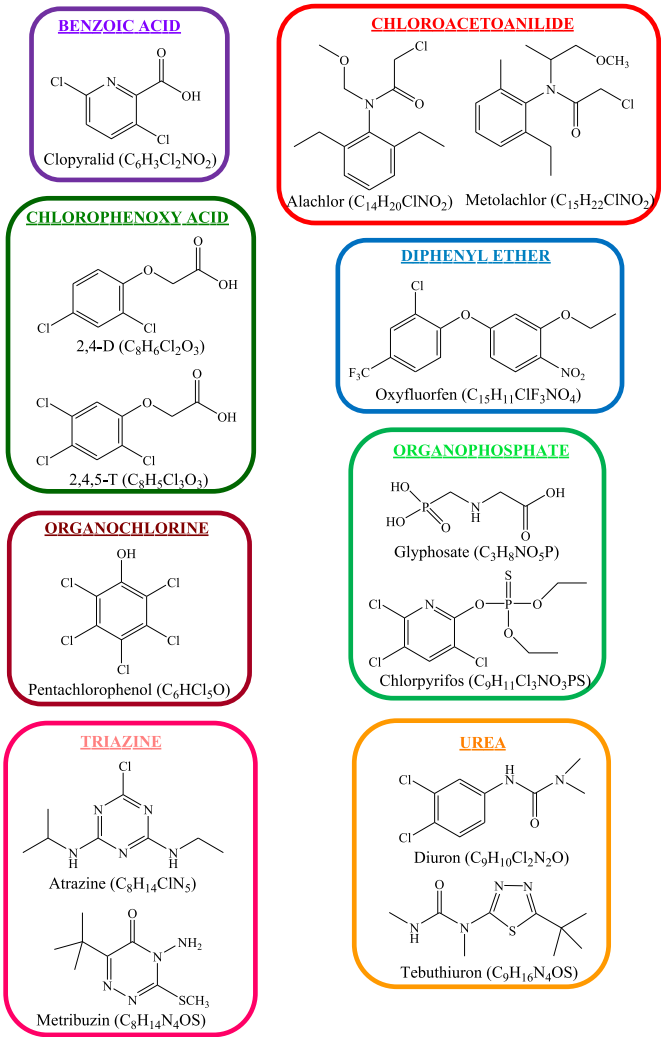


**Fig. 1.** Herbicide families with chemical structure of some compounds treated by electrochemical advanced oxidation processes (EAOPs).

The present review aims to describe the fundamentals and characteristics of each one of the above 9 treatments, followed by a critical analysis of its application to the removal of herbicides. For each process, special emphasis is made over the cell employed, the oxidation ability of the method as function of the operation parameters and the by-products originated.

### 2.2. Bibliometric analysis

Following the above criteria, 6 key review articles were selected. They are focused on a general electrochemical treatment of herbicides up to 2013 (Rodrigo et al., 2014), a general use of AOPs to remove pesticides (Ribeiro et al., 2015) and herbicides (Vagi and Petsas, 2019), and recently, the specific application of boron-doped diamond (BDD) electrodes to the remediation of pesticides in waters (McBeath et al., 2019), wastewaters (Nidheesh et al., 2019) and soils (Trellu et al., 2019). The analysis was completed by selecting 149 scientific articles related to herbicide remediation over the last decade. Fig. 2a shows the annual distribution of the 155 publications (scientific articles and reviews) identified. As can be seen, a growing number of papers has been published since 2015, especially with a higher increase in the last year. This discloses the great interest of the EAOPs to be applied to remediate wastewaters and soils contaminated with herbicides.

A total of 218 different treatments were distinguished within the 149 scientific articles. Fig. 2b makes in evidence that the most utilized EAOP was AO (38.1%), the simplest technique, being applied in many cases as blank assay of other technologies, for example, in PEC. Among the electrochemical Fenton-based processes, the homo-EF (17.9%) was the more largely developed, which comparatively tested AO-$H_2O_2$ (6.9%) as blank treatments. Hetero-EF (2.7%) and photo-assisted methods like PEF (7.3%), SPEF (2.3%) and PEC (6.4%) were explored to smaller extent. It is also noticeable the large study of combined processes, hybrid (11.9%) and sequential (6.4%), mainly developed since 2017.

Regarding the herbicides studied, a total of 165 were considered in the 149 scientific articles selected, corresponding an 84.8% to the 8 families shown in Fig. 1. Fig. 2c highlights that the triazine (23.0%), chlorophenoyacetic acid (20.0%) and urea (17.6%) families were the most largely investigated. In them, atrazine (17.0%), 2,4-D (13.9%) and diuron (7.9%) were the preferential herbicides tested.

It is also noticeable that only 15 scientific articles of the 149 identified reported the remediation of soil-washing effluents, being the rest related to wastewater treatments. That means that greater research efforts have to be made for clarifying the treatment of herbicide in soils since they only represent a 10.1% of the papers published during the period 2010–2019. The EAOP processes could then serve to give an industrial solution to the remediation of these effluents, which has also been poorly studied by different unsatisfactory separation techniques like adsorption, precipitation and membrane technology, as well as by less potent chemical AOPs such as $H_2O_2$/UV and $O_3$ (Gusiatin et al., 2020).

Finally, note that real agricultural wastewaters have not been treated by EAOPs yet. This is an important challenge for future research that is needed to be investigated in order to show the ability of using such treatments at industrial level. Most research in the 149 scientific articles selected was carried out by dissolving the herbicides in synthetic waters (89.3%) and to much less extent, by spiking them into soils (6.7%) or urban or industrial wastewaters (4.0%).

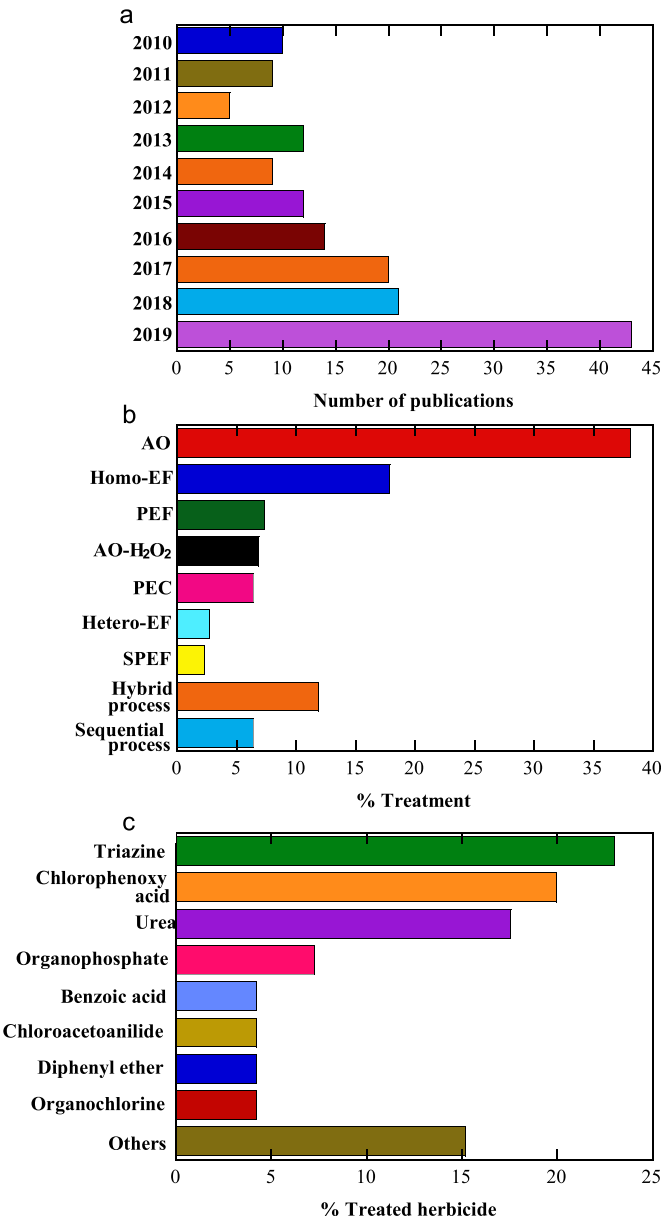


**Fig. 2.** Bibliometric analysis of the literature. (a) Number of publications by year. (b) Percentage of single or combined treatments. (c) Percentage of treated herbicide families.

## 3. Electrochemical systems

The oxidation ability of the EAOPs is determined by the electrochemical system used, including the cell, electrodes and equipment. The treatments identified in this review were performed with small bench-scaled laboratory systems, then being required a next great research effort for scaling up them at industrial scale in order to solve full-scale problems such as cost evaluation and optimization of operation parameters. An interesting advantage of the electrochemical technology is the versatility of a given system to be employed in different EAOPs with little modifications, for example, by changing the nature of electrodes or by exciting the system with ultrasounds (US) or light irradiation.

Figs. 3–5 depict the sketch of several electrochemical systems employed for the treatment of herbicides wastewaters by AO, homo-EF, PEF, SPEF and hybrid processes. The majority of such systems are composed of undivided cylindrical tank reactors and flow cells with two- or three-electrodes. Fig. 3c shows an example of a divided three-electrode H-flow cell for AO where the anodic and cathodic compartments with two BDD electrodes are separated with a Nafion 424 membrane (Valenzuela et al., 2017). The anolyte and catholyte continuously recirculated from two reservoirs driven by two pumps. The third electrode was an Ag|AgCl reference electrode, which served to provide a constant anodic potential ($E_{an}$) by operating under potentiostatic mode. Divided cells are scarcely employed in EAOPs, being preferred the undivided ones because they avoid the potential penalty of the membrane or separator with the consequent lowering of the electric cost of the process.

Tank reactors are the more ubiquitous systems used in AOPs for their easy adaptability to the different operation conditions. These small cells are usually cylindrical, operate in batch mode and are magnetically stirred, not only for the homogenization of the treated solution but also for enhancing the mass transport by diffusion-convection of the reagents toward the electrodes and of the by-products from them. In contrast, Fig. 3b shows a curious three-electrode tank reactor for AO with an inner rotary mixer for stirring (Alves et al., 2012), which has not been more used in the literature. Note that in EF, some authors use three-electrode cells to fix the cathodic potential ($E_{cat}$) for $H_2O_2$ generation (Zhao et al., 2018). Several tank reactors are jacketed to keep a constant solution temperature regulated with an external thermostated water circuit. The temperature regulation and pH adjustment are two necessary requirements for a correct kinetic analysis of the abatement of the target herbicide. An example of a jacketed divided two-electrode cell for AO is given in Fig. 3a (Samet et al., 2010b). Fig. 4a depicts an undivided two-electrode tank reactor for homo-EF characterized by a large carbon-felt cathode (Tran et al., 2019). The versatility of the latter kinds of cells can be corroborated from the feasible immersion of an UVC light in solution for photo-electrolysis (PE) with $H_2O_2$ electrogeneration, as shown in Fig. 4b (Frangos et al., 2016), as well as in other hybrid processes, for example, by coupling US in Fig. 5a giving rise to the sonoelectrolysis (SE) one (Bringas et al., 2011), SPEF with solar photocatalysis (SPC) with $TiO_2$ onto glass spheres in Fig. 5b (Garza-Campos et al., 2014), and granular activated carbon (GAC) for adsorption/AO in Fig. 5c (Pedersen al., 2019). The two-electrode cells run when a constant current ($I$) or current density ($j = I$/electrode area) is provided with a power supply, which determines the cell voltage or potential difference between the electrodes ($E_{cell}$) that serves to calculate the electric consumption of the assay.

It is noticeable that the study with small tank reactors should be limited to the knowledge of the effectiveness of the treatment, including its comparative oxidation ability with others, the kinetics of the herbicide abatement, the effect of operation parameters over the degradation and mineralization processes and the detection of by-products. However, many authors determine from these data, the efficiency and energy consumption of the treatments, which are not useful at industrial scale due to the small volume of treated solutions. A better approach to a full-scale application can be envisaged using flow systems, where greater flowing solution volumes can be treated in batch. Figs. 3d, 4c and 5d present examples of flow systems utilized for AO (de Matos et al., 2020), SPEF with a solar compound parabolic component (CPC) photoreactor (Garcia-Segura et al., 2011) and SE with US (dos Santos et al., 2017a,b). These systems contain a reservoir to introduce the wastewater, which is driven to the cell through a pump with a flow rate regulated by a flowmeter. Heat exchangers can be coupled to the circuit to regulate the temperature. Two main flow cells, cylindrical and filter press, with simple hydrodynamics are employed, as schematized in Figs. 3e–4d. The advantage of the flow systems is that can be easily scaled at industrial level and the information

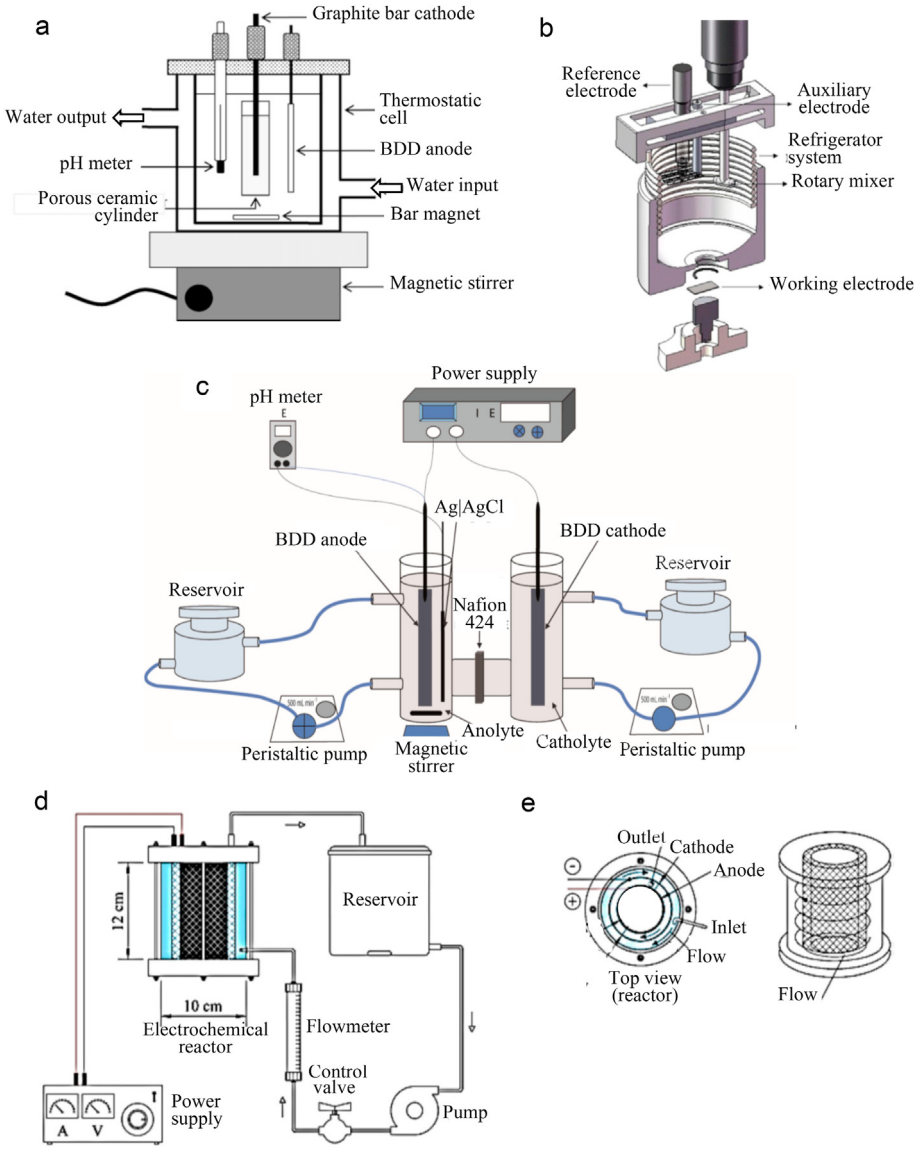


**Fig. 3.** Schemes of experimental setups used for the anodic oxidation (AO) treatments of herbicides in wastewaters operating in batch mode. (a) Stirred two-electrode divided tank reactor with a BDD anode and a graphite bar cathode. Adapted from Samet et al. (2010b). (b) Three-electrode electrochemical cell with rotary mixer. Adapted from Alves et al. (2012). (c) Divided three-electrode H-flow cell equipped with different anolyte and catholyte solutions. Adapted from Valenzuela et al. (2017). (d) Flow plant with (e) a cylindrical two-electrode tank reactor. Adapted from de Matos et al. (2020).

reached at bench scale on the efficiency and energy cost at optimum operation conditions provides a first idea over the possible viability of the process at full-scale.

## 4. Treatment of herbicides from wastewaters and soils by EAOPs

This section is devoted to an exhaustive analysis of each of the 9 identified treatments with EAOPs to remove herbicides from wastewaters and soils, as explained in section 2. First, the fundamentals of each treatment are detailed to understand the origin and oxidation power of the generated oxidizing agents as function of the electrochemical system and the composition of the reaction medium. Second, the application of each EAOP to herbicide remediation is explained, remarking its recent development and main achievements obtained.

### 4.1. Anodic oxidation

The simplest and more popular EAOP for wastewater treatment is AO. The effectiveness of this procedure relies on the nature of the anode material because it determines not only the oxidants electrogenerated, but also their oxidation power. Table 1 summarizes selected results obtained for the AO process of main herbicides belonging to the 8 families specified in Fig. 1. For each assay, the system and best experimental conditions are specified.

#### 4.1.1. Fundamentals

AO is based on the oxidation of organic pollutants in an electrolytic cell by:

(i) Direct electron transfer to the anode, leading to very weak decontamination, and

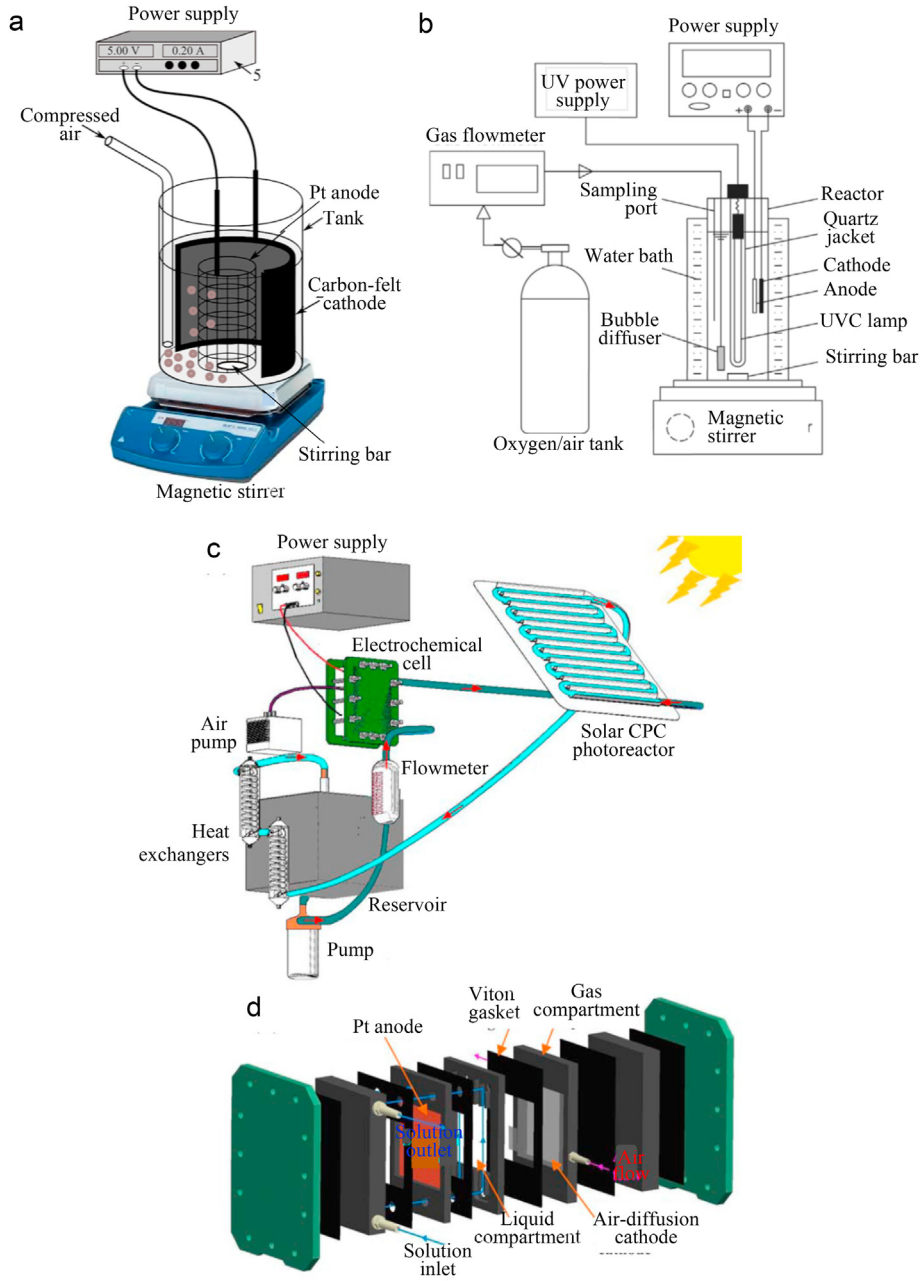


**Fig. 4.** Sketches of experimental setups used for electrochemical Fenton-based/UV treatments of herbicides in wastewaters with a two-electrode cell in batch. (a) Stirred tank reactor with a Pt anode and a carbon-felt cathode for homogeneous electro-Fenton (homo-EF). Adapted from Tran et al. (2019). (b) Stirred tank reactor with an inner UVC lamp for photoelectrolysis (PE) with $H_2O_2$. Adapted from Frangos et al. (2016). (c) Solar pre-pilot flow plant with a CPC photoreactor and (d) a filter-press Pt/air-diffusion electrolytic cell for solar PEF (SPEF). Adapted from Garcia-Segura et al. (2011).

(ii) mediated oxidation with species generated from water discharge or electrolyte oxidation at the anode at high *I*, giving partial or total decontamination.

Comninellis proposed two extreme ideal anodes to explain their oxidation power when only water discharge occurred (Panizza and Cerisola, 2009):

(i) Active anodes, exemplified by Pt and dimensionally stable anodes (DSA) like $RuO_2$ and $IrO_2$, which yield an electrochemical conversion with selective transformation of organics into biodegradable by-products, usually carboxylic acids, and

(ii) non-active anodes, exemplified by metal mixed oxides (MMO) like $SnO_2$ doped with $Sb_2O_5$ and $PbO_2$, along with BDD. These electrodes lead to the electrochemical combustion or incineration of organics with complete mineralization, i.e., oxidation to $CO_2$ and inorganic ions.

For both kinds of anodes (denoted as M), the water discharge to $O_2$ with $E^\circ = 1.23$ V/SHE involves the initial formation of physisorbed $^\bullet$OH (M($^\bullet$OH)) as intermediate as follows:

$$M + H_2O \rightarrow M(^\bullet OH) + H^+ + e^- \quad (1)$$

In the case of active anodes, M($^\bullet$OH) is oxidized to a

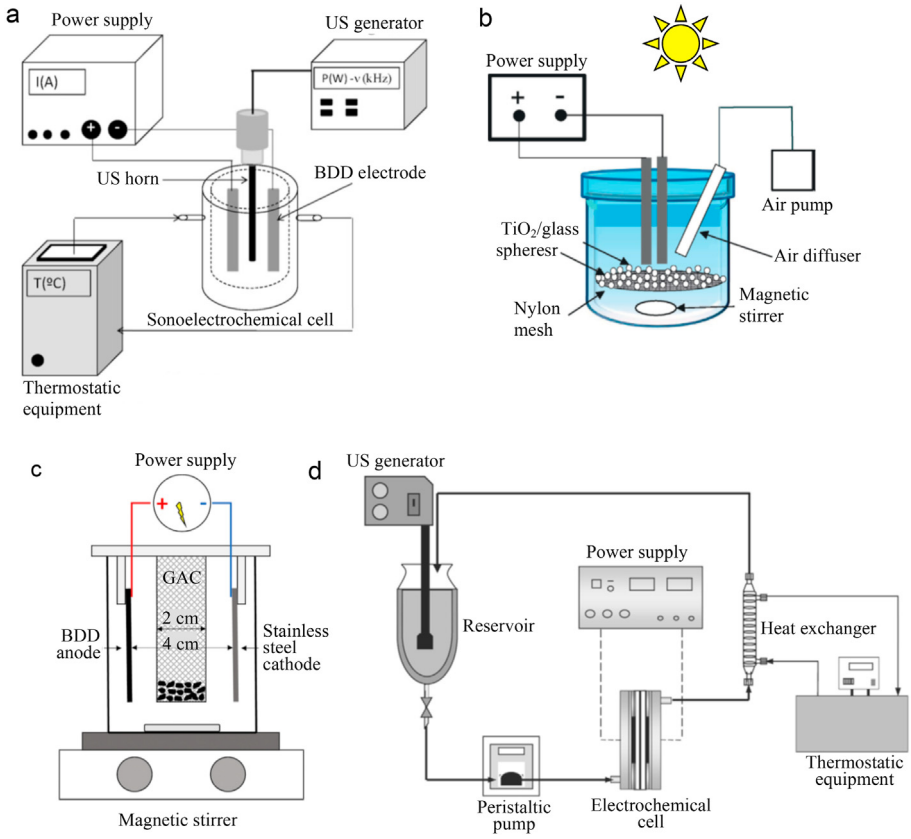


**Fig. 5.** Schemes of experimental setups used for hybrid treatments of herbicides in wastewaters using a two-electrode cell in batch mode. (a) Thermostated sonoelectrochemical cell. Adapted from Bringas et al. (2011). (b) Stirred tank reactor with $TiO_2$/glass spheres for solar photocatalysis (SPC)/SPEF. Adapted from Garza-Campos et al. (2014). (c) Stirred tank reactor with granular activated carbon (GAC) for adsorption. Adapted from Pedersen al. (2019). (d) Flow electrochemical plant with a filter-press reactor and ultrasounds (US) for sonoelectrolysis (SE). Adapted from dos Santos et al. (2017b).

chemisorbed "active oxygen" MO with a higher oxidation state of the metal M, which attacks the organics until carboxylic acids are formed. In contrast, the non-active anodes act as inert electrodes with low M-$^{\bullet}$OH interaction, and M($^{\bullet}$OH) yields full transformation of organics into $CO_2$ as follows:

$$a\ M(^{\bullet}OH) + R \rightarrow M + m\ CO_2 + n\ H_2O + x\ H^+ + y\ e^- \quad (2)$$

where the organic R contains $m$ carbon atoms and its complete mineralization requires $a = (2m + n)$ oxygen atoms. This reaction competes with the parasitic reactions of M($^{\bullet}$OH), like its direct oxidation to $O_2$ by reaction (3), its dimerization to $H_2O_2$ by reaction (4) or its reaction with the latter species to form the weaker oxidant hydroperoxyl radical (M($HO_2^{\bullet}$)) by reaction (5). Another weaker oxidant such as ozone can be produced by reaction (6). Although reactive oxygen species (ROS) like $H_2O_2$, M($HO_2^{\bullet}$) and $O_3$ can be generated from water discharge, the strongest M($^{\bullet}$OH) is the ROS that pre-eminently attacks the organic pollutants (Sirés et al., 2014).

$$M(^{\bullet}OH) \rightarrow M + ½\ O_2 + H^+ + e^- \quad (3)$$

$$2\ M(^{\bullet}OH) \rightarrow 2\ M + H_2O_2 \quad (4)$$

$$M(^{\bullet}OH) + H_2O_2 \rightarrow M(HO_2^{\bullet}) + H_2O \quad (5)$$

$$3\ H_2O \rightarrow O_3 + 6\ H^+ + 6\ e^- \quad (6)$$

High cell voltages are applied to the electrochemical cell in AO to avoid the anode fouling (frequently occurring at low cell voltage values), maintaining the anode activity for the oxidation of water and organic pollutants. It has been found that the change from active to non-active anodes is closely related to the increasing of the $O_2$-evolution overpotential. The BDD anodes are considered as the best electrodes for AO because they possess the highest $O_2$-evolution overpotential as compared to the rest of anodes and then, they produce more quantities of reactive M($^{\bullet}$OH) (Boye et al., 2002). The BDD anodes potentiate the production of other oxidizing agents when sulfate (or hydrogen sulfate), hydrogen carbonate or phosphate are contained in the electrolyte. The anodic oxidation of these anions yields peroxodisulfate, peroxodicarbonate or peroxodiphosphate as follows (Martínez-Huitle et al., 2015):

$$2SO_4^{2-} \rightarrow 2SO_4^{\bullet-} \rightarrow S_2O_8^{2-} + 2e^- \quad (7)$$

$$2HCO_3^- \rightarrow C_2O_6^{2-} + 2H^+ + 2e^- \quad (8)$$

$$2PO_4^{3-} \rightarrow P_2O_8^{4-} + 2e^- \quad (9)$$

The $S_2O_8^{2-}$ ion is a very weak oxidant at mild conditions. It arises from the dimerization of the sulfate radical anion ($SO_4^{\bullet-}$), which is a strong oxidant with a variable $E^{\circ}$ value between +2.5 and + 3.1 V/SHE, that increases with raising pH from pH 0 to pH 12. (Sirés et al., 2014).

The mediated oxidation with ROS, preferentially M($^{\bullet}$OH), becomes less relevant when the AO process is performed in chloride medium because it competes with that of generated active chlorine. The anodic oxidation of $Cl^-$ to $Cl_{2(aq)}$ via reaction (10) is

**Table 1**
Selected results obtained for the anodic oxidation (AO) and AO with $H_2O_2$ generation (AO $H_2O_2$) treatments of several herbicide pollutants in synthetic aqueous matrices using different electrochemical systems.

| Pollutant | System (anode, cathode) | Experimental remarks | Best results | Ref. |
|---|---|---|---|---|
| **Anodic oxidation** | | | | |
| *Chlorophenoxy acid* | | | | |
| 2,4-D | Flow plant with a cell like of Fig. 4d (BDD, BDD) | 2.5 L of 92 mg $L^{-1}$ herbicide ($TOC_0$ = 40 mg $L^{-1}$), 0.050 M $Na_2SO_4$, pH 3.0, Flow rate = 200 L $h^{-1}$, $I$ [a] = 1 A, 300 min | 62% TOC removal, MCE = 10%, $EC_{TOC}$ = 1.13 kWh (g TOC)$^{-1}$. Carboxylic acids detected | García et al. (2014) |
| | Flow plant with a Diacell® 1001 cell, 10 compartments (BDD, SS [b]) | 1.2 L of 100 mg $L^{-1}$ herbicide, 3.0 g $L^{-1}$ NaCl, natural pH, Flow rate = 26.4 L $h^{-1}$, $I$ = 10 A, 250 min | 100% degradation (130 min), $k_1$ = 0.031 $min^{-1}$, 100% TOC removal | Souza et al. (2016a) |
| | Cubic cell (graphite, SS) | 100 mL of 50 mg $L^{-1}$ herbicide, 0.10 M $Na_2SO_4$, pH 7.0, $j$ = 3.0 mA $cm^{-2}$, 50 min | 70% degradation. By-products detected | Samarghandi et al. (2019) |
| | Cubic cell (Ti/$Ru_{0.3}Ti_{0.7}O_2$, Pt) | 100 mL of 100 mg $L^{-1}$ herbicide, 0.050 M $Na_2SO_4$, pH 3.0, $j$ [c] = 50 mA $cm^{-2}$, 120 min | 42% degradation, 21% TOC removal, 19% COD removal, ACE = 20% | Forti et al. (2020) |
| *Diphenyl ether* | | | | |
| Oxyfluorfen | Fig. 3d with a filter-press cell (BDD, SS) | 600 mL of 100 mg $L^{-1}$ herbicide spiked in a soil-washing effluent with SDS [d] surfactant (dosage 5.0 g $kg^{-1}$), Flow rate = 200 L $h^{-1}$, $j$ = 30 mA $cm^{-2}$, Q [e] = 20 Ah $L^{-1}$ | 100% degradation, 98% SDS removal. 650 mg $L^{-1}$ $SO_4^{2-}$ released | dos Santos et al. (2016) |
| *Organochlorine* | | | | |
| Pentachlorophenol | Cylindrical cell (Pt, Pt) | 50 mL of 14 mg $L^{-1}$ herbicide, 0.50 M KCl, pH 3.9–10.0, $E_{an}$ [f] = +1.50 V/Ag\|AgCl, 120 min | 100% degradation at: 20 min (pH 3.9), 60 min (pH 7.8), 120 min (pH 10.0) | Wu (2010) |
| | Cubic cell (Ti/$SnO_2$-Sb, Ti/$SnO_2$-Sb) | 30 mL of 100 mg $L^{-1}$ herbicide, 0.010 M $Na_2SO_4$, pH 6.2, $I$ = 72 mA, 15 min | 99.8% degradation, $k_1$ = 3.94 $min^{-1}$. By-products detected | Niu et al. (2013) |
| *Organophosphate* | | | | |
| Chlorpyrifos | Fig. 3a (BDD or $PbO_2$, graphite) | 150 mL of $COD_0$ = 480 mg $L^{-1}$ of herbicide, 1 M $H_2SO_4$, pH 2, 70 °C, $I$ = 120 mA, 420 min | COD removal: 100% (BDD), 40% ($PbO_2$) | Samet et al. (2010b) |
| Glyphosate | Fig. 3d with a filter-press cell (BDD, SS) | 600 mL of 100 mg $L^{-1}$ herbicide, 3 g $L^{-1}$ $Na_2CO_3$, $Na_2SO_4$ or NaCl, natural pH, $I$ = 7.8 A, 180 min. | TOC reduction: 38% ($Na_2CO_3$), 80% ($Na_2SO_4$), 100% (NaCl). By-products detected | Rubí-Juarez et al. (2016b) |
| | Cylindrical cell (Ti/$Ru_{0.36}Ti_{0.64}O_2$, SS) | 100 mL of 100 mg $L^{-1}$ herbicide, 0.15 M NaCl, pH 3.0, $I$ = 600 mA, 180 min. | 100% TOC removal (pure herbicide), 60% TOC removal (commercial herbicide) | Lima et al. (2019) |
| *Triazine* | | | | |
| Atrazine | Cylindrical cell (BDD, SS) | 100 mL of 30 mg $L^{-1}$ herbicide ($TOC_0$ = 13 mg $L^{-1}$), 0.050 M $Na_2SO_4$, pH 3.0, 35 °C, $I$ = 300 mA, 360 min. | 100% degradation (24 min), $k_1$ = 0.168 $min^{-1}$, 92% TOC removal. By-products detected | Borràs et al. (2010) |
| | Fig. 4a (BDD, carbon felt) | 220 mL of 0.10 mM herbicide, 0.050 M $Na_2SO_4$, pH 6.7, $I$ = 50, 250 and 500 mA, 60 min. | 100% degradation (20 min, 500 mA), $k_1$ = 2.8 × $10^{-3}$ $s^{-1}$ | Oturan et al. (2012) |
| | Cylindrical cell (BDD or DSA [g] anode of Ti/$Ru_{0.3}Ti_{0.4}O_2$, Pt) | 50 mL of 20 mg $L^{-1}$ herbicide, 0.033 M $Na_2SO_4$ or 0.10 M NaCl, natural pH, $I$ = 40 mA, 240 min | TOC removal: 33% (BDD, $Na_2SO_4$), 79% (BDD, NaCl), 13% (DSA, $Na_2SO_4$), 56% (DSA, NaCl) | Malpass et al. (2013) |
| | Cylindrical cell (Pt or graphite, graphite) | 300 mL of 10 mg $L^{-1}$ herbicide, 0.010 M $Na_2SO_4$ or NaCl, pH 6.8, $I$ = 45 mA, 240 min | Degradation: 94% (graphite, $Na_2SO_4$), 96% (graphite, NaCl), 24% (Pt, $Na_2SO_4$), 38% (Pt, NaCl) | Zhu et al. (2019b) |
| Metribuzin | Beaker ($PbO_2$/$WO_3$, Ti) | 200 mL of 40 mg $L^{-1}$ herbicide, 0.050 M $Na_2SO_4$, pH 4.0, $I$ = 560 mA, 90 min | 100% degradation, $k_1$ = 0.040 $min^{-1}$, 76% COD reduction, ACE = 2.5%. By-products detected | Yang et al. (2019a) |
| *Urea* | | | | |
| Diuron | Cylindrical cell ($Co_3O_4$/graphite felt, Pt) | 300 mL of 20 mg $L^{-1}$ herbicide ($TOC_0$ = 50 mg $L^{-1}$), 0.050 M $Na_2SO_4$, pH 6.8, 25 °C, $I$ = 18 mA, 14 min | 100% degradation, 67% COD removal | Zhu et al. (2019a) |

**Table 1** (*continued*)

| Pollutant | System (anode, cathode) | Experimental remarks | Best results | Ref. |
|---|---|---|---|---|
| | Fig. 3d and e (Ti/$Ru_{0.36}Ti_{0.64}O_2$, SS) | 4 L of 215 mg $L^{-1}$ herbicide ($TOC_0$ = 100 mg $L^{-1}$), 0.050 M NaCl, pH 3.0, Flow rate = 50 L $h^{-1}$, 25 °C, $I$ = 7.8 A, 120 min | 30% TOC removal, MCE = 2.0%, $EC_{TOC}$ = 0.67 kWh (g TOC)$^{-1}$. By-products detected | de Matos et al. (2020) |
| Tebuthiuron | Fig. 3b (BDD, Pt) | 450 mL of 100 mg $L^{-1}$ herbicide ($TOC_0$ = 38 mg $L^{-1}$), 0.10 M $K_2SO_4$ + 0.10 M $H_2SO_4$, 20 °C, $I$ = 830 mA, 180 min | 90% degradation, $k_1$ = 0.031 $min^{-1}$, 82% TOCremoval, $EC_{TOC}$ = 2.9 kWh (g TOC)$^{-1}$. By-products detected | Alves et al. (2012) |
| | Flow plant with a cell like of Fig. 4d (BDD, Pt) | 1 L of 100 mg $L^{-1}$ herbicide, 0.10 M $Na_2SO_4$ and/or 25 mM NaCl, pH 3.0, Flow rate = 390 L $h^{-1}$, 25 °C, $I$ = 1.1 A, 240 min | 100% degradation ($Na_2SO_4$ and/or NaCl), 80% COD reduction ($Na_2SO_4$), 100% COD reduction ($Na_2SO_4$ + NaCl). By-products detected | Pereira et al. (2017) |
| **Anodic oxidation with electrogenerated $H_2O_2$** | | | | |
| *Chloroacetoanilide* | | | | |
| Alachlor | Cylindrical cell (Pt, air diffusion with $H_2O_2$ generation) | 100 mL of 0.60 mM herbicide ($TOC_0$ = 100 mg $L^{-1}$), 0.050 M $Na_2SO_4$, pH 3.0, $I$ = 100 mA, 25 °C, 360 min | 96% degradation, $k_1 = 1.38 \times 10^{-4}$ $s^{-1}$, 78% TOC removal, MCE = 15% | Pipi et al. (2014a) |
| Metolachlor | Cylindrical cell (BDD, air diffusion with $H_2O_2$ generation) | 100 mL of 0.55 mM herbicide ($TOC_0$ = 100 mg $L^{-1}$), 0.050 M $Na_2SO_4$, pH 3.0, $I$ = 150 mA, 360 min | 100% degradation, $k_1 = 1.47 \times 10^{-4}$ $s^{-1}$, $E_{EO}$ = 86,2 kWh $m^{-3}$ order$^{-1}$, 58% TOC removal, MCE = 7.1%, $EC_{TOC}$ = 2.32 kWh (g TOC)$^{-1}$ | Thiam and Salazar (2019) |
| *Triazine* | | | | |
| Metribuzin | Cylindrical cell (BDD, air diffusion with $H_2O_2$ generation) | 100 mL of 0.532 mM (112.0 mg $L^{-1}$) herbicide ($TOC_0$ = 50 mg $L^{-1}$), 0.050 M $Na_2SO_4$, pH 3.0, 25 °C, $I$ = 300 mA, 540 min | 100% degradation (180 min), $k_1$ = 0.0189 $min^{-1}$, 95% TOC removal, MCE = 2.6%. By-products detected | Guelfi et al. (2019b) |
| *Urea* | | | | |
| Diuron | Fig. 4c without photoreactor and with a flow cell like of Fig. 4d (BDD, air diffusion with $H_2O_2$ generation) | 2.5 L of 0.185 mM herbicide ($TOC_0$ = 20 mg $L^{-1}$), 0.050 M $Na_2SO_4$, pH 3.0, $I$ = 2 A, Flow rate = 200 L $h^{-1}$, 25 °C, 240 min | 67% degradation, $k_1 = 7.3 \times 10^{-5}$ $s^{-1}$, 21% TOC removal, MCE = 1.2%, $EC_{TOC}$ = 12.2 kWh (g TOC)$^{-1}$ | Pipi et al. (2014b) |

[a] $I$: current.
[b] SS: Stainless steel.
[c] $j$: current density.
[d] SDS: Sodium dodecyl sulfate.
[e] $Q$: Electric charge consumed.
[f] $E_{an}$: Anodic potential.
[g] DSA: Dimensionally stable anode.

followed by its hydrolytic disproportion to HClO by reaction (11), which is in equilibrium with $ClO^-$ by reaction (12). Different active chlorine species can oxidize organics as function of solution pH: $Cl_{2(aq)}$ ($E^\circ$ = 1.36 V/SHE) up to pH 3.0, HClO ($E^\circ$ = 1.49 V/SHE) in the pH interval 3.0–8.0 and $ClO^-$ ($E^\circ$ = 0.89 V/SHE) at pH > 8.0. The oxidation action of active chlorine is then more potent in acidic medium where organics are attacked by the strongest agent HClO (Martínez-Huitle and Brillas, 2009).

$$2\ Cl^- \rightarrow Cl_{2(aq)} + 2\ e^- \quad (10)$$

$$Cl_{2(aq)} + H_2O \leftrightarrows HClO + Cl^- + H^+ \quad (11)$$

$$HClO \leftrightarrows ClO^- + H^+ \quad pK_a = 7.55 \quad (12)$$

However, the oxidation with active chlorine is limited by its parasitic reactions. They include the consecutive oxidation to undesirable and toxic chlorite, chlorate and perchlorate ions, exemplified by reactions (13)–(15). Its cathodic reduction by reaction (16) is also feasible in an undivided cell (Souza et al., 2017).

$$ClO^- + H_2O \rightarrow ClO_2^- + 2H^+ + 2e^- \quad (13)$$

$$ClO_2^- + H_2O \rightarrow ClO_3^- + 2H^+ + 2e^- \quad (14)$$

$$ClO_3^- + H_2O \rightarrow ClO_4^- + 2H^+ + 2e^- \quad (15)$$

$$ClO^- + H_2O + 2e^- \rightarrow Cl^- + 2OH^- \quad (16)$$

It is noticeable that urban and industrial wastewaters usually contain high $Cl^-$ contents, reason for which the study of the AO performance in chloride medium is important to mimic the oxidation of organics in real matrices. The $RuO_2$ anodes (DSA-$Cl_2$) are preferable in such media because they originate larger amounts of active chlorine, even superior to that produced by BDD. Although these agents can oxidize sometimes more rapidly the target pollutant than M($^\bullet$OH), the production of highly recalcitrant chloroderivatives limits the mineralization power of AO. The experimental conditions have to be well selected to minimize both, the quantity of chloroderivatives formed and the rate of parasitic reactions like (13)–(16). A schematic mechanism of the different

processes occurring at the BDD surface to destroy organics by direct electron transfer and/or mediated oxidation with M(•OH) and other generated oxidants like active chlorine is presented in Fig. 6.

In the AO study of a herbicide wastewater, the concentration decay of the target pollutant and/or the abatement of COD and/or TOC are measured. The concentration decay typically obeys a pseudo-first-order kinetics, allowing determining the apparent rate constant $k_1$ as the corresponding slope of the $\ln(c_0/c)$-$t$ plot (Souza et al., 2016a). From the COD decay ($\triangle$COD, in mg $O_2$ $L^{-1}$) or TOC removal ($\triangle$TOC, in mg C $L^{-1}$) obtained at constant $I$ (in A) in batch mode, the percentage of COD or TOC removal can be determined by the following equations:

$$\%\text{COD removal} = \frac{\Delta \text{COD}}{\text{COD}_0} \times 100 \tag{17}$$

$$\%\text{TOC removal} = \frac{\Delta \text{TOC}}{\text{TOC}_0} \times 100 \tag{18}$$

where $\text{COD}_0$ and $\text{TOC}_0$ denote the initial values before treatment. These parameters allow obtaining the average current efficiency (ACE, in %) at time $t$ (in s) or the mineralization current efficiency (MCE, in %) at time $t$ (in h) according to Eqs. (19) and (20) (Brillas and Martínez-Huitle, 2015):

$$\text{ACE}(\%) = \frac{(\Delta \text{COD})FV}{8It} \times 100 \tag{19}$$

$$\text{MCE}(\%) = \frac{nFV(\Delta \text{TOC})}{4.32 \times 10^7 mIt} \times 100 \tag{20}$$

where $F$ is the Faraday constant (96,487 C $mol^{-1}$), $V$ is the solution volume (in L), the constant 8 is the oxygen equivalent mass (g $eq^{-1}$), $n$ is the number of electrons exchanged in the mineralization process, $4.32 \times 10^7$ is a conversion factor (= 3600 s $h^{-1}$ × 12,000 mg C $mol^{-1}$) and $m$ is the number of carbon atoms of the herbicide. For MCE estimation, the fate of the inorganic ions generated from the heteroatoms of the target herbicide needs to be determined for establishing the theoretical total mineralization reaction with the $n$-value (Moreira et al., 2017).

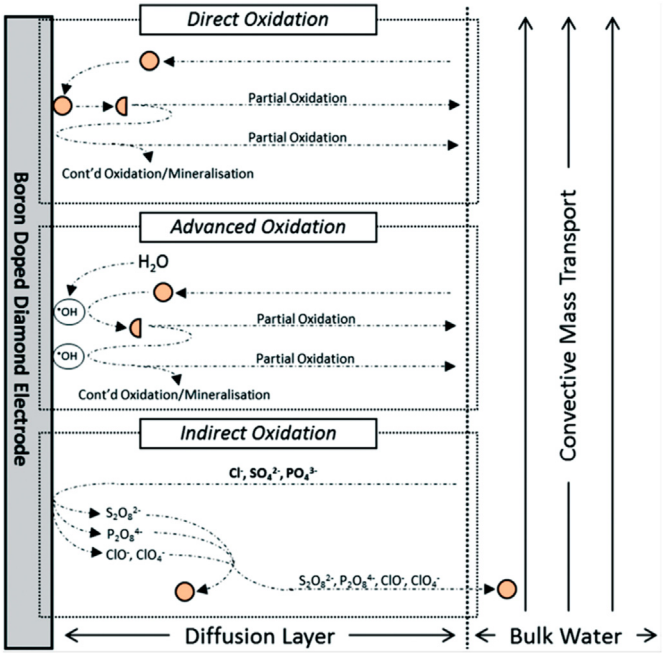


**Fig. 6.** Schematic mechanism of the direct electron transfer, advanced oxidation and indirect oxidation processes occurring at a BDD anode during AO. Adapted from McBeath et al. (2019).

Other figures of merit involve the evaluation of the electric consumption of the AO process, e.g., the electric energy per order ($E_{EO}$, in kWh $m^{-3}$ $order^{-1}$), the specific energy consumption (EC, in kWh $m^{-3}$) and the specific energy consumption by unit TOC mass ($EC_{TOC}$, in kWh (g TOC)$^{-1}$) at time $t$ (in h). The first term is related to the concentration decay and the two latter ones to the mineralization process, and they are calculated from Eq. (21)–(23) (Martínez-Huitle and Brillas, 2009):

$$E_{EO}\left(\text{kWhm}^{-3}\text{order}^{-1}\right) = \frac{E_{cell}It}{V\log(c_0/c)} = \frac{2.303E_{cell}I}{Vk_1} \tag{21}$$

$$EC\left(\text{kWhm}^{-3}\right) = \frac{E_{cell}It}{V} \tag{22}$$

$$EC_{TOC}\left(\text{kWh(gTOC)}^{-1}\right) = \frac{E_{cell}It}{V(\Delta \text{TOC})} \tag{23}$$

where $E_{cell}$ denotes the average cell voltage (in V) along the run.

It is note mentioning that the most important advantage claimed for AO is its ability to offer the complete mineralization of any organic pollutant, especially when the most powerful BDD anode is employed. However, this method presents several disadvantages including the high cost of this anode for industrial application and the very low efficiencies expected for the treatment of small concentrations of herbicides polluting groundwater or surface water (Rodrigo et al., 2014). This has propitiated the development of more powerful Fenton-based EAOPs, which will be analyzed below.

#### 4.1.2. Application to herbicide remediation

The results collected in Table 1 make in evidence the potentiality of the AO and AO-$H_2O_2$ processes for the removal of herbicides from wastewaters. AO-$H_2O_2$ differs from AO in the additional cathodic production of $H_2O_2$ that also oxidizes organics, but at much smaller extent than M(•OH) and/or active chlorine formed at the anode. In most cases, experimental conditions were set to attain overall degradation at acceptable short electrolysis times, but low COD and/or TOC abatements, with small MCE and high $EC_{TOC}$ values, were usually obtained as result of the large recalcitrance of the by-products formed to be slowly mineralized to $CO_2$. The influence of the anode over the herbicide removal, as well as the effect of pH, current density, herbicide content and the kind of electrolyte and its concentration, has been extensively studied to clarify the role of oxidizing agents generated and the best operating conditions.

The majority of AO studies on herbicide remediation have been made with small cylindrical, beaker or cubic tank reactors (see Table 1), operating in batch mode, upon magnetic stirring, and in some cases, jacketed to regulate the solution temperature with external water. Undivided reactors are preferred to avoid the extra voltage of the membrane or separator in divided ones, as in the case of Fig. 3a and c. A reduced number of studies have used flow systems similar to Fig. 3d, with cylindrical tank reactors or filter-press cells. Typically, two-electrode reactors are employed in monopolar connection under galvanostatic mode, i.e., by supplying a constant $I$ or $j$. Valenzuela et al. (2017) have reported the use of three-electrode cells under potentiostatic mode, i.e., by applying a constant $E_{an}$. The flow systems allow determining a better approach to a full-scale industrial application than simpler tank reactors, which

only inform about the potential oxidation ability of AO.

*4.1.2.1. Influence of the anode.* A crucial parameter analyzed by the authors is the nature of the anode regarding its active or non-active character. As an example, Fig. 7a shows the normalized atrazine concentration decay in sulfate medium at neutral pH by comparing the AO process of a non-active BDD anode (Oturan et al. (2012)) with active ones such as graphite and Pt (Zhu et al., 2019b), as well a DSA of $Ti/Ru_{0.3}Sn_{0.7}O_2$ (Malpass et al., 2010b), at analogous $j$ values of 7.5–10 mA $cm^{-2}$. This figure highlights that the degradation power of the anodes was upgraded in the sequence: DSA < Pt ≪ graphite ~BDD, related to the increasing reaction rate of atrazine with M(•OH) produced from reaction (1), which is the preponderant oxidant in sulfate medium. The large reactivity of the herbicide using active graphite can be ascribed to its adsorption over the anode, favoring the attack with physisorbed M(•OH) at similar rate to that of radicals originated by active BDD, where herbicide is not adsorbed. However, graphite is not recommended as anode because of its low stability since continuous material is released during prolonged electrolysis, especially at high $j$. Fig. 7b depicts the excellent linear profiles obtained for the above concentration decays assuming a pseudo-first-order kinetics for atrazine. This is the normal behavior observed for all herbicides in AO and other EAOPs, being related to the diffusion-convection control of the process and the production of small, but steady concentrations of oxidizing agents (Martínez-Huitle et al., 2015).

Note that Stirling et al. (2020) have recently proposed a techno-economic analysis for benchmarking AO against available commercial technologies for water treatment. These authors found that the $k_1$-value determined for the pseudo-first-order kinetics of atrazine, and the $E_{EO}$ calculated from Eq. (21) are relevant parameters that affect the operational expenses. They analyzed the $k_1$-values between $10^{-5}$ and $10^{-3}$ $s^{-1}$ reported for several electrodes and experimental conditions, including medium, pH and $j$, regarding the oxidants produced and scavengers, and concluded that $k_1 > 2.1 \times 10^{-5}$ $s^{-1}$ allowed achieving lower total costs of ownership for AO than classical carbon block used to extract the herbicide in private wells. This kind of techno-economic analysis should be extended to other herbicides and commercial removal techniques to demonstrate the interest of applying EAOPs at industrial level.

The greater mineralization ability of BDD over other non-active anodes like $PbO_2$ for the organophosphate chlorpyrifos (Samet et al., 2010a) and the pyridine picloram (Pereira et al., 2015), and active anodes like Pt for 2,4-D (García et al., 2014) and DSA of oxides of Ru-Sb (Santos et al., 2016) and Ru-Ti (Malpass et al., 2013) for atrazine and the benzoic acid clopyralid (Barbosa-Ferreira et al., 2020a) has been well-proven by AO in both, sulfate and chloride media. This is verified for herbicide degradation in sulfate medium but no in chloride one. As an example, Fig. 7c shows that using a cylindrical two-electrode cell with a DSA of $Ti/Ru_{0.3}Ti_{0.7}O_2$, atrazine was reduced by 30% in 0.033 mM $Na_2SO_4$ after 60 min of electrolysis at $j = 50$ mA $cm^{-2}$, whereas it was completely abated at about 30 min with 0.10 M NaCl (Malpass et al., 2013). It can be observed that the alternative use of BDD led to total removal of the herbicide in 60 and 30 min for the same sulfate and chloride media. These results illustrate the faster atrazine degradation with BDD in sulfate medium, where the predominant oxidant is M(•OH), which became more rapidly removed with the DSA anode in chloride medium, due to the quicker attack of the competitive active chlorine formed from reactions (10) and (11). In contrast, Fig. 7d and Table 1 corroborate a higher TOC removal at 60 min using the BDD (33%) than the DSA (13%) anode in 0.033 mM $Na_2SO_4$, whereas in 0.10 M NaCl, BDD (79%) also outperformed DSA (56%), conversely to its degradation behavior (see Fig. 7c). This can be accounted for by the quicker mineralization of the chloroderivatives (generated from the

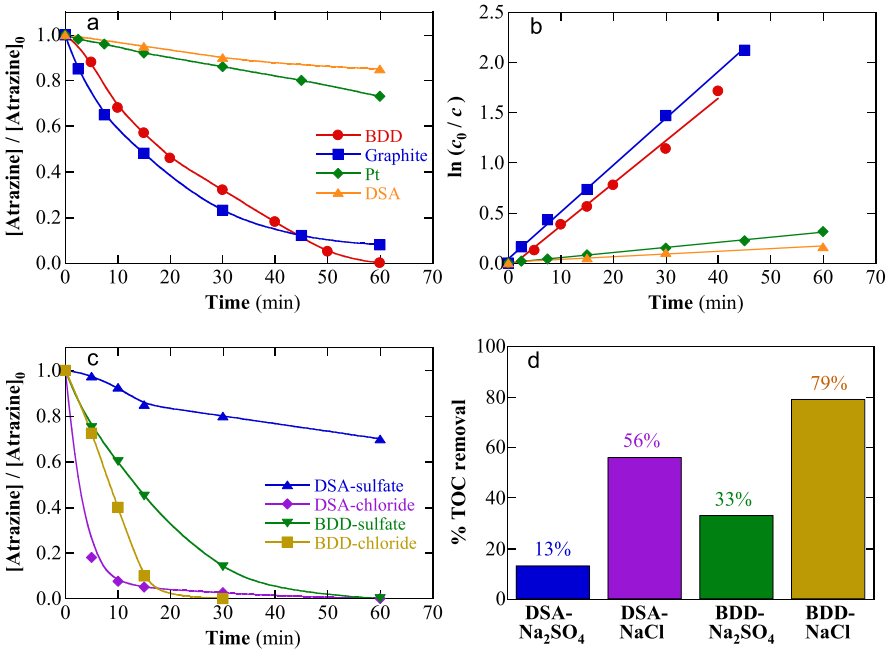


**Fig. 7.** (a) Normalized atrazine concentration and (b) pseudo-first-order kinetic analysis for the AO degradation of 220 mL of 0.10 mM herbicide in 0.10 M $Na_2SO_4$ at pH 6.7 using a cell like of Fig. 4a with a 25 $cm^2$ BDD anode at current density ($j$) = 10 mA $cm^{-2}$ (adapted from Oturan et al. (2012)), 300 mL of 10 mg $L^{-1}$ herbicide in 0.01 M $Na_2SO_4$ at pH 6.8 with a cylindrical cell with a 6 $cm^2$ graphite or Pt anode at $j = 7.5$ mA $cm^{-2}$ (adapted from Zhu et al., 2019b), and 250 mL of 20 mg $L^{-1}$ herbicide in 0.033 M $Na_2SO_4$ at pH 6.7 using a flow plant with a filter-press cell with a 14 $cm^2$ DSA ($Ti/Ru_{0.3}Sn_{0.7}O_2$) anode at $j = 10$ mA $cm^{-2}$ (adapted from Malpass et al. (2010b)). (c) Normalized atrazine concentration and (d) percentage of TOC removal at 60 min of the AO process of 50 mL of 20 mg $L^{-1}$ herbicide in 0.033 M $Na_2SO_4$ or 0.10 M NaCl with a cylindrical cell with a 0.78 $cm^2$ DSA ($Ti/Ru_{0.3}Ti_{0.7}O_2$) or 0.36 $cm^2$ BDD anode at $j = 50$ mA $cm^{-2}$. Adapted from Malpass et al. (2013).

oxidation with active chlorine) by the more rapid attack of the much greater amounts of M(•OH) produced at the non-active BDD as compared to the active DSA.

Despite the non-active BDD anodes offer the best option for the herbicide removal by AO, their high cost has motivated the synthesis of much cheaper active $RuO_2$-based DSA ones of large stability for their application in synthetic sulfate and chloride media. In this way, the following electrodes have been synthesized and checked with several herbicides: Ti/$Ru_xSn_{1-x}O_2$ (x = 0.10, 0.15, 0.20, 0.25 and 0.30) with atrazine (Malpass et al., 2010b), Ti/$Ru_{0.3}Ti_{0.7}O_2$ with atrazine (Malpass et al., 2013), the chloroacetonilide alachlor (de Mello et al., 2018) and 2,4-D (Forti et al., 2020), Ti/$Ru_xTi_{(1-x)}O_2$ and Ti/$Ir_xTi_{(1-x)}O_2$ (x = 0.3, 0.5 and 0.7) with diuron (Pipi et al., 2013), Ti/$(RuO_2)_{0.8}(MO_2)_{0.2}$ (M = Ce, Sn or Ir) with atrazine (Santos et al., 2015), Ti/$(RuO_2)_{0.5}$–$(Sb_2O_5)_{0.5}$ and Ti/$(RuO_2)_{0.8}$–$(Sb_2O_5)_{0.2}$ with atrazine (Santos et al., 2016), Ti/$RuO_2$-$IrO_2$ with the urea nicosulfuron (Zhao et al., 2019), Ti($Ru_{0.36}Ti_{0.64}O_2$ with the organophosphate glyphosate (Lima et al., 2019) and diuron (de Matos et al., 2020). The results collected in Table 1 confirm the excellent degradation of the herbicides in chloride medium as compared to the sulfate medium due to the quick oxidative action of the generated active chlorine, but with low mineralization in both matrices. Santos et al. (2015) prepared several oxides of Ru with different metals and found that the best anode of Ti/$(RuO_2)_{0.8}(IrO_2)_{0.2}$ (1.2 $cm^2$) led to overall removal of 10 mg $L^{-1}$ of atrazine in 40 mL of 0.10 M NaCl in a cylindrical tank reactor with a Pt cathode after 90 min of AO treatment at $j$ = 20 mA $cm^{-2}$. In further work of the same group, da Silva et al. (2018) reported that a non-active DSA anode of Ti/$Sn_{50}Sb_{40}Ce_{10}$ (2 $cm^2$) with high surface area, porosity and electrochemical conductivity gave 58% concentration removal of 10 mg $L^{-1}$ atrazine in 0.033 M $Na_2SO_4$ after 60 min at a $j$ value as low as 1.0 mA $cm^{-2}$, representing a substantial energy consumption reduction for AO.

Other authors have explored the use of cheap non-active anodes, like Ti/$SnO_2$ (Zaviska et al. (2011) and Ti/$SnO_2$-Sb (Wei et al., 2011). A very good performance has been described for diuron and the organochlorine pentachlorophenol using $Co_3O_4$/graphite felt (Zhu et al., 2019a) and Ti/$SnO_2$-Sb (Niu et al., 2013), where overall degradation was feasible in times as short as 14–15 min (see Table 1). The use of $PbO_2$ anodes has been a hot topic in this line. Samet et al. (2010b) prepared a Nb/$PbO_2$ anode by simple electrodeposition of 1 M $Pb^{2+}$ at $j$ = 10–50 mA $cm^{-2}$, which led to 40% COD reduction when treating 150 mL of 480 mg $L^{-1}$ of initial COD of chlorpyrifos in 1 M $H_2SO_4$ at 70 °C in a cylindrical cell at $I$ = 120 mA lasting 420 min, a value much smaller than 100% COD abatement found using BDD (see Table 1). The most important drawback of this $PbO_2$ anode was its large instability because it released large amounts of toxic $Pb^{2+}$ to the solution. To overcome this, more sophisticated methods have been developed to improve the stability and oxidation power of these anodes. It has been reported the treatment of picloram (Pereira et al., 2015) and 2,4-D (Dargahi et al., 2019) with β-$PbO_2$, glyphosate with Ti/$PbO_2$ (Tran et al., 2017), the triazine metribuzin with $PbO_2$/$WO_3$ (Yang et al., 2019a) and the triazine metamitron with $PbO_2$-$CeO_2$ (Yang et al., 2019b). For example, Yang et al. (2019a) described 100% degradation and 76% COD removal with ACE = 2.5% for the AO process of 200 mL of 40 mg $L^{-1}$ metribuzin in 0.050 M $Na_2SO_4$ at pH 4.0 in a beaker with a $PbO_2$/$WO_3$ anode at $I$ = 560 mA during 90 min (see Table 1).

Active anodes like graphite or Pt have been used to remove pentachlorophenol (Wu, 2010), the triazine atratone (González-Cadena, 2013), paraquat (Cartaxo et al., 2015), the triketones mesotrione and sulcotrione (Jović et al., 2015), diuron (Khongthon et al., 2016), 2,4-D (Samarghandi et al., 2019) and atrazine (Zhu et al., 2019b). The results shown in Table 1 make in evidence the good degradations obtained in these treatments, usually superior for graphite thanks to herbicide adsorption despite its instability.

The most used anodes in AO are the BDD electrodes. The studies have been centered in the remediation of atrazine (Borràs et al., 2010), glyphosate (Rubí-Juárez et al., 2016b), 2,4-D (Souza et al., 2016a) and the urea tebuthiuron (Pereira et al., 2017), whose main results are summarized in Table 1. Other works have considered the diphenyl ether bifenox (Zaouak et al., 2013), the imidazolinone imazapyr (Souza et al., 2014) and 2,4-D (Souza et al., 2016c). It should be noted that AO and AO-$H_2O_2$ present an analogous performance for herbicide destruction due to the very low oxidation power of $H_2O_2$ as compared to M(•OH). This point has been remarked in the work of Borràs et al. (2010), who found that 100 mL of 30 mg $L^{-1}$ atrazine in 0.050 M $Na_2SO_4$ at pH 3.0 by AO with a BDD/stainless steel cell and AO-$H_2O_2$ with a BDD/$O_2$-diffusion one using a cylindrical tank reactor at $I$ = 300 mA underwent total atrazine removal in the same time of 24 min, with $k_1$ = 0.168 $min^{-1}$, and an analogous TOC reduction of 90% at 360 min (see Table 1). Several examples of the application of the AO-$H_2O_2$ process with a Pt or BDD anode and an air-diffusion cathode to alachlor (Pipi et al., 2014a), diuron (Pipi et al., 2014b), metribuzin (Guelfi et al., 2019b) and the chloroacetoanilide metolachlor (Thiam and Salazar, 2019) are included at the end of Table 2. These results confirm again the large degradation and in some cases, large mineralization, with small MCE and high $E_{EO}$ and $EC_{TOC}$ values, achieved using a BDD anode.

Finally, it is worth noting the relevant role of the BDD composition expressed as the $sp^3/sp^2$ carbon ratio, i.e., the diamond/graphite structure ratio, over its oxidation power, since it determines the percentage of the electrochemical combustion/incineration of the AO process. This effect was clarified by Souza et al. (2016c) using a flow filter-press cell with BDD anodes doped with 500 ppm B and $sp^3/sp^2$ carbon ratio from 165 to 323 for the treatment of 600 mL of 100 mg $L^{-1}$ 2,4-D in 0.050 M NaCl at pH 3.5 and $j$ = 100 mA $cm^{-2}$. These authors showed a more rapid and efficient oxidative removal of 2,4-D and its intermediates with increasing the $sp^3/sp^2$ carbon ratio that favored the electrochemical combustion (Garcia-Segura et al., 2015). This explains the different oxidation power observed for various BDD electrodes in AO, thereby being recommendable to set materials with high $sp^3/sp^2$ carbon ratio (usually > 250) to ensure an efficient treatment.

*4.1.2.2. Effect of operation variables.* The oxidation ability of AO and AO-$H_2O_2$ processes has been assessed regarding several crucial operation variables including $j$, herbicide concentration, pH and the kind of background electrolyte. The $j$ value (or $I$ value) under galvanostatic conditions, or the $E_{an}$ value in potentiostatic mode, limits the amount of generated oxidizing agents in the electrolytic system. Generally, the rise of $j$ promotes the degradation and mineralization of herbicides by the acceleration of reaction (1) to form more amount of M(•OH) and/or of reactions (10) and (11) to give more active chlorine, as well as of $H_2O_2$ from $O_2$ reduction at the cathode in AO-$H_2O_2$ (Liu et al., 2019b) (see also subsection 4.2.1). The positive upgrading of the oxidation power of the system is usually observed up to a certain $j$, whereupon no greater oxidation rate of the herbicide occurs, due to the higher acceleration of parasitic reactions like (3)–(5) and (13)–(16). The existence of such parasitic reactions causes a progressive decay in ACE or MCE with the concomitant increase in energy consumption. Fig. 8a presents the effect of $j$ on the degradation of 30 mg $L^{-1}$ atrazine in 100 mL of 0.050 M $Na_2SO_4$ at pH 3.0 by AO using a BDD/stainless steel cell (Borràs et al., 2010). The herbicide disappeared completely at decreasing times of 100, 24 and 14 min for increasing $j$ of 33.3, 100 and 150 mA $cm^{-2}$, as expected from the gradual production of more quantity of M(•OH). The inset of Fig. 8a highlights the pseudo-first-order reaction followed by these assays with growing $k_1$-values of

**Table 2**
Selected results obtained for the homogeneous and heterogeneous electro-Fenton (EF) and photoelectro-Fenton (PEF) and solar PEF (SPEF) processes of several herbicide pollutants in synthetic aqueous matrices and real wastewaters.

| Pollutant | System (anode, cathode) | Experimental remarks | Best results | Ref. |
|---|---|---|---|---|
| **Synthetic wastewater** | | | | |
| **Homogeneous electro-Fenton** | | | | |
| *Benzoic acid* | | | | |
| Clopyralid | Fig. 4a (Pt, carbon felt) | 800 mL of 180 mg $L^{-1}$ herbicide in synthetic soil washing effluent, 0.10 mM $Fe^{2+}$, pH 3.0, 20 °C, $I$ = 200 mA, 480 min | 82% degradation, 31% TOC removal. By-products detected | Carboneras Contreras et al. (2019) |
| *Chloroacetoanilide* | | | | |
| Alachlor | Cylindrical cell (BDD, air diffusion) | 100 mL of 0.60 mM herbicide ($TOC_0$ = 100 mg $L^{-1}$), 0.050 M $Na_2SO_4$, 0.50 mM $Fe^{2+}$, pH 3.0, $I$ = 100 mA, 360 min | 100% degradation (120 min), $k_1$ = 0.0436 $min^{-1}$, 83% TOC removal, MCE = 17% | Pipi et al. (2014a) |
| | Cylindrical cell (Pt, RVC [a]) | 200 mL of 83.3 mg $L^{-1}$ herbicide ($COD_0$ = 172 mg $L^{-1}$), 0.050 M $Na_2SO_4$, 1 mM $Fe^{2+}$, pH 2.0, $E_{cat}$ [b] = −0.70 V/SCE, 75 min | 95% degradation, $k_1$ = 0.0213 $min^{-1}$, 93% TOC removal, ACE = 100% | Lizama-Baena et al., 2015 |
| Metolachlor | Cylindrical cell (BDD, air diffusion) | 100 mL of 0.55 mM herbicide ($TOC_0$ = 100 mg $L^{-1}$), 0.050 M $Na_2SO_4$, 0.50 mM $Fe^{2+}$, pH 3.0, $I$ = 150 mA, 360 min | 100% degradation (300 min), $k_1 = 2.60 \times 10^{-4}$ $s^{-1}$, $E_{EO}$ = 37.8 kWh $m^{-3}$ $order^{-1}$, 69% TOC removal, MCE = 8.4%, $EC_{TOC}$ = 1.97 kWh (g TOC)$^{-1}$ | Thiam and Salazar (2019) |
| Propachlor | Fig. 4a (Pt, carbon felt) | 175 mL of 0.25 mM herbicide ($TOC_0$ = 100 mg $L^{-1}$), 0.025 M $Na_2SO_4$, 0.20 mM $Fe^{3+}$, pH 3.0, $I$ = 300 mA, 360 min | 100% degradation (10 min), $k_2 = 3.6 \times 10^9$ $M^{-1}$ $s^{-1}$, 100% TOC removal, MCE = 4.5%. By-products detected | Gençten and Özcan (2015) |
| *Chlorophenoxy acid* | | | | |
| 2,4-D | Fig. 4c with the cell of Fig. 3d (Pt, air diffusion) | 2.5 L of 92 mg $L^{-1}$ herbicide ($TOC_0$ = 40 mg $L^{-1}$), 0.050 M $Na_2SO_4$, pH 3.0, 0.50 mM $Fe^{2+}$, Flow rate = 200 L $h^{-1}$, $I$ = 1 A, 300 min | 57% TOC removal, MCE = 10%, $EC_{TOC}$ = 0.63 kWh (g TOC)$^{-1}$. Carboxylic acids detected | García et al. (2014) |
| 2,4,5-T | Fig. 4a (BDD or Pt, carbon felt) | 230 mL of 0.10 mM herbicide, 0.050 M $Na_2SO_4$, 0.10 mM $Fe^{2+}$, pH 3.0, $I$ = 300 mA, 360 min | 100% degradation: 14 min (BDD), 8 min (Pt), $k_2 = 3.6 \times 10^9$ $M^{-1}$ $s^{-1}$, 95% TOC decay (BDD), 92% TOC decay (Pt). By-products detected | Zazou et al. (2017) |
| *Organophosphate* | | | | |
| Glyphosate | Beaker (Ti/$RuO_2$, ACF) | 400 mL of 1.0 mM herbicide, 0.10 M $Na_2SO_4$, 0.10 mM $Fe^{2+}$, pH 3.0, $I$ = 360 mA, 360 min. | 85% degradation (120 min), 48% TOC removal. By-products detected | Lan et al. (2016) |
| | Fig. 4a (Pt, carbon felt) | 200 mL of 0.1 mM herbicide, 0.050 M $Na_2SO_4$, 0.10 mM $Fe^{2+}$, pH 3.0, 25 °C, $I$ = 500 mA, 40 min | 92% degradation, $k_1$ = 0.063 $min^{-1}$, 82% TOC removal. By-products detected | Tran et al. (2019) |
| *Triazine* | | | | |
| Atrazine | Fig. 4a (BDD or Pt, carbon felt) | 220 mL of 0.10 mM herbicide, 0.050 M $Na_2SO_4$, 0.10 mM $Fe^{2+}$, pH 3.0, $I$ = 250 mA, 60 min | 100% degradation: (30 min, Pt), (20 min, BDD, with $k_1 = 2.8 \times 10^{-3}$ $s^{-1}$) | Oturan et al. (2012) |
| | Cylindrical cell (Pt, F-doped porous biomass carbon) | 30 mL of 30 mg $L^{-1}$ herbicide, 0.050 M $Na_2SO_4$, 2.0 mM $Fe^{2+}$, pH 2.0, $E_{cat}$ = −0.40 V/SCE, 60 min. | 100% degradation (30 min), $k_1$ = 0.18 $min^{-1}$, 67% TOC removal | Zhao et al. (2018) |
| Metribuzin | Cylindrical cell (BDD, air diffusion) | 100 mL of 0.532 mM (112.0 mg $L^{-1}$) herbicide ($TOC_0$ = 50 mg $L^{-1}$), 0.050 M $Na_2SO_4$, 0.50 mM | 100% degradation (90 min), 99% TOC removal, | Guelfi et al. (2019b) |

(*continued on next page*)

**Table 2** (*continued*)

| Pollutant | System (anode, cathode) | Experimental remarks | Best results | Ref. |
|---|---|---|---|---|
| | | $Fe^{2+}$, pH 3.0, 25 °C, $I$ = 300 mA, 540 min | MCE = 2.7%. By-products detected | |
| *Urea* | | | | |
| Diuron | Fig. 4a (Pt, carbon felt) | 125 mL of 0.17 mM herbicide, 0.20 mM $Fe^{3+}$, pH 3.0, $I$ = 100 mA, 180 min. | 100% degradation (12 min), $k_2 = 4.8 \times 10^9$ $M^{-1}$ $s^{-1}$, 92% TOC removal, ACE = 11%. By-products detected | Oturan et al. (2010) |
| | Fig. 4c without photoreactor and a flow cell like of Fig. 3d (BDD, air diffusion) | 2.5 L of 0.185 mM herbicide ($TOC_0$ = 20 mg $L^{-1}$), 0.050 M $Na_2SO_4$, 0.50 mM $Fe^{2+}$, pH 3.0, $I$ = 2 A, Flow rate = 200 L $h^{-1}$, 25 °C, 240 min | 100% degradation (6 min), $k_1 = 1.3 \times 10^{-2}$ $s^{-1}$, 70% TOC removal, MCE = 3.9%, $EC_{TOC}$ = 3.7 kWh (g TOC)$^{-1}$ | Pipi et al. (2014b) |
| Fenuron | Fig. 4a (Pt, carbon felt) | 125 mL of 0.20 mM herbicide, 0.20 mM $Fe^{3+}$, pH 3.0, $I$ = 100 mA, 180 min. | 100% degradation (12 min), $k_2 = 1.2 \times 10^{10}$ $M^{-1}$ $s^{-1}$, 94% TOC removal, ACE = 13%. By-products detected | Oturan et al. (2010) |
| Fluometuron | Fig. 4a (Pt or BDD, carbon felt) | 230 mL of 0.17 mM herbicide, 0.050 M $Na_2SO_4$, 0.10 mM $Fe^{3+}$, pH 3.0, $I$ = 300 mA (Pt) or 200 mA (BDD), 480 min. | 100% degradation: (20 min, Pt), (10 min, BDD, with $k_2 = 4.44 \times 10^9$ $M^{-1}$ $s^{-1}$), 54% TOC decay (Pt), MCE = 0.48% $EC_{TOC}$ = 4.6 kWh (g TOC)$^{-1}$, 88% TOC decay (BDD), MCE = 1.9%. By-products detected | Diaw et al. (2017) |
| Monuron | Fig. 4a (Pt, carbon felt) | 125 mL of 0.25 mM herbicide, 0.20 mM $Fe^{3+}$, pH 3.0, $I$ = 100 mA, 180 min. | 100% degradation (10 min), $k_2 = 7.3 \times 10^9$ $M^{-1}$ $s^{-1}$, 93% TOC removal, ACE = 13%. | Oturan et al. (2010) |
| **Heterogeneous electro-Fenton** | | | | |
| *Triazine* | | | | |
| Atrazine | Cylindrical cell (Pt, allophane supported with $Fe_2O_3$) | 30 mL of 46 mM herbicide, 90% 0.10 M $Na_2SO_4$ + 10% methanol, pH 3.0–6.0, $E_{cat}$ = −1.04 V/Ag\|AgCl, 480 min | Degradation: 94% (pH 3.0), 89% (pH 4.0), 76% (pH 6.0). By-products detected | Garrido-Ramírez et al. (2013) |
| *Urea* | | | | |
| Diuron | Cylindrical cell with suspended AC + PTFE [c] + $Fe_3O_4$ (Pt, graphite felt) | 300 mL of 10 mg $L^{-1}$ herbicide, 0.050 M $Na_2SO_4$, 3 g $L^{-1}$ catalyst, pH 3.0–6.7, $I$ = 100 mA, 120 min | 100% degradation (30 min, pH 3.0), 95% degradation (pH 6.7) | Wang et al. (2018) |
| **Photoelectro-Fenton** | | | | |
| *Benzoic acid* | | | | |
| Chloramben | Cylindrical cell with a 6 W UVA light over solution ($IrO_2$, $RuO_2$, $PbO_2$ or BDD, air diffusion) | 100 mL of 1.19 mM herbicide ($TOC_0$ = 100 mg $L^{-1}$), 0.050 M $Na_2SO_4$, 0.50 mM $Fe^{2+}$, natural pH 3.4, $I$ = 300 mA, 300 min | 100% degradation (15 min, all anodes), $k_1 = 0.47$ $min^{-1}$, 96% TOC decay (all anodes except $RuO_2$), MCE = 5.0%. By-products detected | Thiam et al. (2018) |
| *Chloroacetoanilide* | | | | |
| Alachlor | Cylindrical cell with a 6 W UVA light over solution (Pt, air diffusion) | 100 mL of 0.60 mM herbicide ($TOC_0$ = 100 mg $L^{-1}$), 0.050 M $Na_2SO_4$, 0.50 mM $Fe^{2+}$, pH 3.0, $I$ = 100 mA, 360 min | 100% degradation (60 min), $k_1$ = 0.061 min-1, 93% TOC removal, MCE = 19%. Products detected | Pipi et al. (2014a) |
| Metolachlor | Cylindrical cell with a 6 W UVA light over solution (BDD, air diffusion) | 100 mL of 0.55 mM herbicide ($TOC_0$ = 100 mg $L^{-1}$), 0.050 M $Na_2SO_4$, 0.50 mM $Fe^{2+}$, pH 3.0, $I$ = 150 mA, 360 min | 100% degradation (180 min), $k_1 = 2.91 \times 10^{-4}$ $s^{-1}$, $E_{EO}$ = 33.4 kWh $m^{-3}$ $order^{-1}$, 94% TOC removal, MCE = 12%, $EC_{TOC}$ = 1.69 kWh (g TOC)$^{-1}$. By-products detected | Thiam and Salazar (2019) |

**Table 2** (*continued*)

| Pollutant | System (anode, cathode) | Experimental remarks | Best results | Ref. |
|---|---|---|---|---|
| *Triazine* | | | | |
| Metribuzin | Cylindrical cell with a 4 W UVA light over solution (BDD, air diffusion) | 100 mL of 0.532 mM (112.0 mg $L^{-1}$) herbicide ($TOC_0$ = 50 mg $L^{-1}$), 0.050 M $Na_2SO_4$, 0.50 mM $Fe^{2+}$, pH 3.0, 25 °C, $I$ = 300 mA, 420 min | 100% degradation (90–105 min), 100% TOC removal, MCE = 3.5% | Guelfi et al. (2019b) |
| **Solar photoelectro-Fenton** | | | | |
| *Chlorophenoxy acid* | | | | |
| 4-chloro-2-methylphenoxyacetic acid | Fig. 4c with the cell of Fig. 4d (Pt, air diffusion) | 10 L of 186 mg $L^{-1}$ herbicide ($TOC_0$ = 100 mg $L^{-1}$), 0.050 M $Na_2SO_4$, 1.00 mM $Fe^{2+}$, pH 3.0, $I$ = 5.0 A, Flow rate = 180 L $h^{-1}$, 35 °C, 120 min | 100% degradation (60 min), $k_1 = 1.25 \times 10^{-3}$ $s^{-1}$, 75% TOC removal, MCE = 71%, $EC_{TOC}$ = 0.088 kWh (g TOC)$^{-1}$. By-products detected | Garcia-Segura et al. (2011) |
| *Triazine* | | | | |
| Ametryn | Fig. 4c with a planar photoreactor and a flow cell like of Fig. 4d (Pt, air diffusion) | 2.5 L of 0.18 mM herbicide ($TOC_0$ = 20 mg $L^{-1}$), 0.050 M $Na_2SO_4$, 0.50 mM $Fe^{2+}$, pH 3.0, $I$ = 1 A, Flow rate = 200 L $h^{-1}$, 35 °C, 360 min | 100% degradation (90 min), 52% TOC removal, MCE = 11%, $EC_{TOC}$ = 2.61 kWh (g TOC)$^{-1}$. By-products detected | Gozzi et al. (2017) |
| *Urea* | | | | |
| Diuron | Fig. 4c with a planar photoreactor and a flow cell like of Fig. 4d (BDD, air diffusion) | 2.5 L of 0.185 mM herbicide ($TOC_0$ = 20 mg $L^{-1}$), 0.050 M $Na_2SO_4$, 0.50 mM $Fe^{2+}$, pH 3.0, $I$ = 2 A, Flow rate = 200 L $h^{-1}$, 25 °C, 240 min | 100% degradation (6 min), $k_1 = 1.3 \times 10^{-2}$ $s^{-1}$, 42% TOC removal, MCE = 2.3%, $EC_{TOC}$ = 6.1 kWh (g TOC)$^{-1}$. By-products detected | Pipi et al. (2014b) |
| Tebuthiuron | Fig. 4c with a planar photoreactor and a flow cell like of Fig. 4d (BDD, air diffusion) | 2.5 L of 0.18 mM herbicide ($TOC_0$ = 20 mg $L^{-1}$), 0.050 M $Na_2SO_4$, 0.50 mM $Fe^{2+}$, pH 3.0, $I$ = 1 A, Flow rate = 200 L $h^{-1}$, 35 °C, 360 min | 100% degradation (180 min), 70% TOC removal, MCE = 11%, $EC_{TOC}$ = 2.23 kWh (g TOC)$^{-1}$. By-products detected | Gozzi et al. (2017) |
| **Real wastewater Photoelectro-Fenton** | | | | |
| *Benzoic acid* | | | | |
| Chloramben | Cylindrical cell with a 6 W UVA light over solution ($IrO_2$ or BDD, air diffusion) | 100 mL of 1.19 mM herbicide in a real urban wastewater ($TOC_0$ = 115 mg $L^{-1}$), 0.50 mM $Fe^{2+}$, natural pH 3.4, $I$ = 100 mA, 300 min | 100% degradation (40 min, all anodes), $k_1$ = 0.13 $min^{-1}$, 74% TOC decay ($IrO_2$), 82% TOC decay (BDD) | Thiam et al. (2018) |
| *Chloroacetonilide* | | | | |
| Metolachlor | Cylindrical cell with a 6 W UVA light over solution (BDD, air diffusion) | 100 mL of 0.55 mM herbicide spiked into a real wastewater of winery industry ($TOC_0$ = 120 mg $L^{-1}$), 0.50 mM $Fe^{2+}$, pH 3.0, $I$ = 112 mA, 360 min | 100% degradation (120 min), $k_1 = 2.65 \times 10^{-4}$ $s^{-1}$, 84% TOC removal, $EC_{TOC}$ = 1.40 kWh (g TOC)$^{-1}$ | Thiam and Salazar (2019) |

[a] RVC: Reticulated vitreous carbon.
[b] $E_{cat}$: Cathodic potential.
[c] PTFE: Polytetrafluoroethylene.

0.038, 0.168 and 0.292 $min^{-1}$. However, the content of herbicide removed/$k_1$ ratio dropped down as $j$ was raised due to the larger preponderance of the parasitic reactions of M(•OH). This effect was clearer when the TOC abatement was measured. Fig. 8b shows the change of this parameter under the same conditions by applying AO-$H_2O_2$ with a BDD/$O_2$-diffusion cell, which was reduced by 90–92% after 540 min at 100 mA and 240 min at 300 and 450 mA. The enhancement of the parasitic reactions is then reflected by the achievement of the maximum oxidation power at 300 mA and the progressive decay of the MCE value with increasing $j$, as can be seen in the inset of Fig. 8b. The profiles of the MCE curves showed a maximal followed by a strong decay at longer time, which can be ascribed to the loss of organic matter with formation of more recalcitrant products (Panizza and Cerisola, 2009). According to this, in AO the $j$-value has to be modulated to attain the maximum degradation rate and mineralization degree with acceptable MCE.

The influence of parasitic reaction was also observed by varying the herbicide content at constant $j$, as reported by the degradation

of the herbicide bifenox with BDD (Zaouak et al., 2013), atrazine with Pt (Liu et al., 2019b) or with graphite (Zhu et al., 2019b) and metribuzin with a $PbO_2/WO_3$ composite (Yang et al., 2019b). Upgrading this parameter, the degradation and mineralization rates seem decelerated because similar amounts of oxidizing agents attack greater quantities of herbicide, and a gradual decrease of $k_1$-value and percentage of TOC removal are determined. Nevertheless, the oxidation ability of the system is progressively raised regarding that the concentration of herbicide removed/$k_1$ ratio and the MCE value undergone a gradual increase. This results of the preferential attack of oxidants over the higher amounts of organics present in the medium that reduce the impact of parasitic reactions. This behavior limits the application of AO to real wastewaters with very low herbicide contents, since the process becomes so slow that too many long time is needed to reach a large removal, even applying a high $j$ value, with the consequent loss of great electric energy, making it more expensive. However, the problem regarding the great electric energy required could be reduced by the use of renewable energies (Ganiyu and Martínez-Huitle, 2020).

Another important operation variable is the pH since it determines the oxidation power of the generated oxidants depending on the herbicide adsorption at the anode. For the AO treatment of 250 mL of 40 mg $L^{-1}$ metribuzin in 0.050 M $Na_2SO_4$ using a stirred beaker equipped with a $PbO_2/WO_3$ anode and a Ti cathode after 90 min at $j$ = 60 mA $cm^{-2}$, Yang et al. (2019a) reported herbicide and COD reductions of 99.6% and 83.7% at pH 2.0, which regularly dropped down up to 83.0% and 68.6% at pH 10.0. This effect can be explained by the concomitant loss of the oxidation power of M(•OH) at higher pH. In contrast, Pereira et al. (2015) did not found any significant pH influence between 3 and 10 over the degradation and TOC removal of 100 mg $L^{-1}$ of picloram in 0.10 M $Na_2SO_4$ using a flow filter-press cell with a β-$PbO_2$ anode at $j$ = 30 mA $cm^{-2}$. Zhao et al. (2019) have described a quicker degradation in alkaline medium. This can also be observed in Fig. 8c that shows a faster removal rate of metribuzin at pH 9.0 than at pH 3.0, with greater $k_1$-value (0.023 vs. 0.019 $min^{-1}$, see inset) for the AO-$H_2O_2$ process of 100 mL of 112.0 mg $L^{-1}$ herbicide in 0.050 M $Na_2SO_4$ using a cylindrical BDD/air-diffusion cell at 100 mA $cm^{-2}$ (Guelfi et al., 2019b). This tendency can be associated to a larger adsorption of the herbicide at the BDD surface that enhances its reaction with M(•OH). Nevertheless, it is much less apparent for the TOC abatement and MCE evolution (see Fig. 8d), probably because of the weak adsorption of by-products formed. A different trend with varying pH is found in chloride medium where the generated active chlorine oxidizes in the bulk. Wu (2010) described the overall abatement of 14 mg $L^{-1}$ pentachlorophenol in 50 mL of 0.50 M KCl after 20 min at pH 3.9, 60 min at pH 7.8 and >120 min at pH 10.0 of AO using a cylindrical cell with a Pt/Pt cell at $E_{an}$ = +1.50 V/Ag|AgCl (see Table 1). This loss of oxidation power is accounted for by the change of active chlorine (see reactions (10)–(13)): at pH 3.9 the main oxidant is the more powerful HClO and at pH 10.0 it is the weaker $ClO^-$, whereas at pH 7.8 a mixture near 50% of both species acts as oxidant. The decay in degradation rate with increasing pH in NaCl has also been reported for picloram (Pereira et al., 2015) and diuron (Khongthon et al., 2016).

The kind of electrolyte and its concentration influence the performance of AO. In the studies carried out with metribuzin with a $PbO_2/WO_3$ anode (Yang et al., 2019a) and metamitron with a Ti/$PbO_2$-$CeO_2$ one (Yang et l., 2019b) at pH 4.0, an increase up to a 25% of the degradation rate when the $Na_2SO_4$ content grew from 0.05 to 0.20 M was detailed. This is attributable to a greater production of $S_2O_8^{2-}$ by reaction (7), producing more quantity of the intermediate strong oxidant $SO_4^{\bullet-}$ that accelerates the herbicide removal. On the other hand, the addition of more NaCl to the medium led to faster degradation of the herbicide due to the larger formation of active chlorine by the rise in rate of reactions (10)–(12) (Khongthon et al., 2016). Several works have described a greater degradation and mineralization in chloride than in sulfate medium, as stated above. Using a filter-press cell with a BDD/stainless steel cell, Rubí-Juárez et al. (2016b) found that the AO process during 180 min of 600 mL of 100 mg $L^{-1}$ glyphosate at $I$ = 7.8 A led to 38%, 80% and 100% COD reduction for 3 g $L^{-1}$ of $Na_2CO_3$, $Na_2SO_4$ and NaCl, (see Table 1), showing the scavenging effect of the $CO_3^{2-}$ ion over M(•OH).

Several papers focused the optimization of the AO treatment of herbicide wastewaters by response surface technology (RSM). This analytical tool is useful to minimize the number of experiments required for optimization by means of a central composite design (CCD) test, in which independent operating variables within given value intervals are selected, and the obtained results are expressed as a quadratic-function of them and minimized using the ANOVA program. Samarghandi et al. (2019) established a number of 20 experiments to apply the RSM to the degradation of 50 or 100 mg $L^{-1}$ 2,4-D in 0.10 M $Na_2SO_4$ with a graphite/stainless steel cell. For each concentration, the percentage of 2,4-D removal was determined for pH (3.0–11.0), $j$ (1.0–5.0 mA $cm^{-2}$) and electrolysis time (20–80 min) set as independent variables. The optimum conditions were found for 50 mg $L^{-1}$ at pH 7.0, $j$ = 3.0 mA $cm^{-2}$ and 50 min, yielding 70% 2,4-D removal (see Table 1).

Few papers have considered the removal of herbicides spiked into real wastewaters. Jović et al. (2015) determined that the overall removal of 100 mg $L^{-1}$ mesotrione in 0.050 M $Na_2SO_4$ and spiked into Danube river water was achieved after 60 min and a longer time of 80 min, operating at pH 3.0 using a cylindrical cell with a Ti/Pt anode at $j$ = 55.3 mA $cm^{-2}$. Similarly, Zhu et al. (2019a) reported that the total decay of 20 mg $L^{-1}$ diuron in an unspecified real wastewater with 0.050 M $Na_2SO_4$ at pH 6.8 in a $Co_3O_4$/graphite felt cell at $j$ = 3.0 mA $cm^{-2}$ was reached in 16 min, a time longer than 14 min required in 0.050 M $Na_2SO_4$ (see Table 1). The fact that a slower degradation occurs in real wastewater is explained by the competitive oxidation of its organic compounds, e.g., natural organic matter (NOM), thereby diminishing the amount of generated oxidants with ability to attack the herbicide. The same behavior was also observed when using a commercial herbicide (with organic impurities) instead of pure compound (see Lima et al. (2019) in Table 1).

Soils accumulate the herbicides disseminated over them in crops. The remediation of synthetic contaminated soils has been investigated by the Rodrigo's group using a soil-washing effluent contaminated with atrazine (dos Santos et al., 2015), chlopyralid (Carboneras et al., 2018) and organochlorinated products (Barbosa Ferreira et al., 2020b). The approach consisted in the mixing of a model kaolinite soil with the herbicide dissolved in acetonitrile or hexane, followed by its extraction, once the organic solvent was evaporated, with an aqueous solubilizing solution containing 500 mg $L^{-1}$ of $NaHCO_3$ and sodium dodecyl sulfate (SDS) as surfactant. The separated effluent was then electrolyzed in a flow filter-press plant with a BDD/stainless steel cell. Table 1 shows the overall disappearance of 100 mg $L^{-1}$ of oxyfluorfen in the soil-washing effluent, alongside 98% of SDS removal with an initial dosage of 5.0 g $kg^{-1}$, after an electric charge consumed ($Q$) of 20 Ah $L^{-1}$ at $j$ = 30 mA $cm^{-2}$ (dos Santos et al., 2016), evidencing the large effectiveness of the treatment.

The detection of by-products is detailed in many articles, as remarked in Table 1. Reversed-phase high-performance liquid chromatography (HPLC) (Samarghandi et al., 2019), HPLC-mass spectrometry (MS) (Guelfi et al., 2019b) and gas chromatography (GC)-MS (Guelfi et al., 2019b) are commonly used to identify the initial by-products formed, whereas ion-exclusion HPLC allows the detection of the final carboxylic acids (García et al., 2014). Inorganic ions ($Cl^-$, $NO_3^-$, $NH_4^+$) released from the heteroatoms are quantified

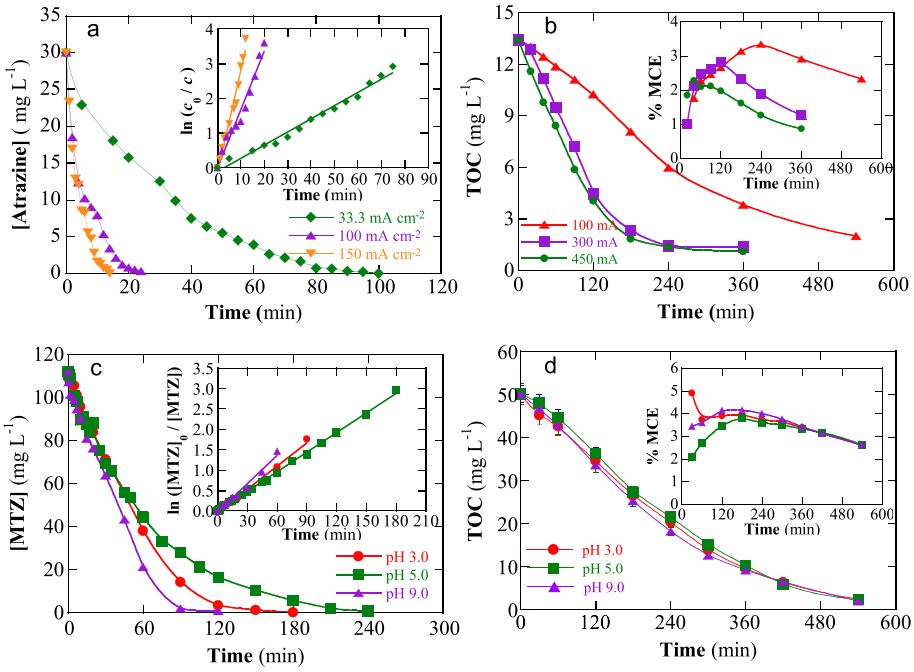


**Fig. 8.** (a) Effect of *j* over atrazine concentration (pseudo-first-order kinetics in the inset) and vs. electrolysis time for AO with a BDD/stainless steel (SS) cell of 100 mL of 30 mg $L^{-1}$ herbicide in 0.050 M $Na_2SO_4$ at pH 3.0. The area of each electrode was 3 $cm^2$. (b) Effect of *I* on TOC (mineralization current efficiency in the inset) by AO-$H_2O_2$ with a BDD/$O_2$-diffusion cell upon the same conditions. Adapted from Borràs et al. (2010). Influence of pH on the change of (c) metribuzin (MTZ) concentration (pseudo-first-order kinetics in the inset) and (d) TOC (mineralization current efficiency in the inset) with electrolysis time for the AO-$H_2O_2$ treatment of 100 mL of 112.0 mg $L^{-1}$ herbicide in 0.050 M $Na_2SO_4$ with a BDD/air-diffusion cell (each electrode with 3 $cm^2$ area) at $j = 100$ mA $cm^{-2}$. Adapted from Guelfi et al. (2019b).

by ion chromatography (Rubí-Juárez et al., 2016a,b). From these compounds, a reaction sequence can be proposed for the herbicide mineralization. The same reactions routes are expected for AO, AO-$H_2O_2$, EF, PEF and SPEF because the same kinds of oxidants act in all them. Some examples will be given in next sections 4.2-4.4.

Finally, the Rodrigo's group explored new sustainable AO treatments without electric cost, directly powered by a wind turbine for 2,4-D (Souza et al., 2015a) or photovoltaic panels for 2,4-D (Souza et al., 2015c) and for clopyralid (Millán et al., 2019). The development of these systems seems necessary for the construction of electrochemical systems to be operative in remote regions without electricity. In the case of 2,4-D, the assays were made with 4 L of 100 mg $L^{-1}$ herbicide in 3 g $L^{-1}$ NaCl at pH 3.5 using a flow plant like of Fig. 3d with a Diacell® 401 BDD/BDD cell. When a wind turbine was checked, fluctuating *I* values up to 18 A were provided to the cell, depending on the wing velocity, and overall degradation and mineralization were attained after 20 h with an electric consumption of 19 Ah $L^{-1}$ (Souza et al., 2015a). With the photovoltaic panels, the *I* value varied from about 6 A (maximal at midday) to 0 A at the night and about 25 h were required to achieve a $Q = 19$ Ah $L^{-1}$ for complete degradation and mineralization (Souza et al., 2015c). A similar performance was obtained by providing the same *Q* value with a constant *I* from a power supply. These findings demonstrate the effectiveness of renewable free and green energies to power the AO treatments, a research field that should be potentiated and widely explored in the next years for their possible industrial application (Ganiyu et al., 2020).

### 4.2. Homogeneous and heterogeneous electro-Fenton

The homo-EF process has been proposed to take advantage over AO from the oxidation power of $H_2O_2$ generated at the cathode of the electrolytic cell upon the catalytic action of soluble iron ions to remove organics in conjunction with the oxidation action of the species produced at the anode. This dual technique presents as major advantages (Martínez-Huitle and Brillas, 2009):

(i) Prevention of the hazardous transport and storage of $H_2O_2$ because it is in situ electrogenerated,
(ii) faster degradation of organics than in conventional Fenton treatment, with much smaller quantity of added $Fe^{2+}$ because it is regenerated at the cathode, and
(iii) achievement of potential total mineralization with relatively low electric consumption.

However, the following important drawbacks for homo-EF have been emphasized:

(i) Limitation to acidic wastewaters, typically in the pH interval 2–4,
(ii) spent of high amount of chemicals for effluent acidification before treatment and/or neutralization of treated solution before disposal, and
(iii) sludge treatment after neutralization with the consequent rise in operation cost.

To solve these problems, the hetero-EF has been recently developed to operate at neutral pH using insoluble iron catalysts or cathodic materials with iron (Ganiyu et al., 2018). An increasing research of both, homo- and hetero-EF to show their viability over herbicide remediation at lab scale has been developed in the last decade, as described in this subsection. Table 2 collects the main results obtained for both electrochemical Fenton-based processes.

#### 4.2.1. Fundamentals

$H_2O_2$ is a green chemical and weak oxidant that gives $O_2$ and $H_2O$ as by-products. It can be activated in acidic matrices by some catalytic metallic ions (El-Ghenymy et al., 2014). The most popular

combination is $H_2O_2 + Fe^{2+}$, known as Fenton's reagent, that produces $Fe^{3+}$ and homogenous $^{\bullet}OH$ as strong oxidant of organics from the classical Fenton's reaction (24), optimal at pH near 3 with absolute rate constant $k_2 = 63\ M^{-1}\ s^{-1}$ (Brillas and Garcia-Segura, 2020):

$$Fe^{2+} + H_2O_2 \rightarrow Fe^{3+} + {}^{\bullet}OH + OH^- \quad (24)$$

Unlike the conventional Fenton treatment where both added reagents are quickly consumed, the homo-EF is more powerful because $H_2O_2$, as well as added $Fe^{2+}$, are continuously generated at a carbonaceous cathode with high surface area. $O_2$ is reduced to $H_2O_2$ by the following two-electron reaction with $E^{\circ} = 0.68$ V/SHE (Sirés et al., 2014):

$$O_{2(g)} + 2H^+ + 2e^- \rightarrow H_2O_2 \quad (25)$$

This reaction occurs at the surface of immersed cathodes in solution such as carbon felt (Carboneras-Contreras et al., 2019), reticulated vitreous carbon (RVC) (Lizama-Baena et al., 2015), activated carbon fiber (ACF) (Lan et al., 2016) and BDD (García et al., 2013), where pure $O_2$ or air is continuously dissolved to keep an $O_2$-saturated solution. In contrast, when a gas ($O_2$ or air) -diffusion cathode is employed, the gas is provided on its dry face and then, it crosses the material to be reduced to $H_2O_2$ when enters in contact with the solution and carbon (Sirés et al., 2014). The generation and stability of $H_2O_2$ rely not only on the cathode used but also of the cell configuration and operation conditions. Its parasitic reactions include the cathodic reduction to $OH^-$ and the chemical disproportion to $O_2$ and $H_2O$. Parallel reduction of $H^+$ to $H_2$ also causes a lowering of current efficiency for $H_2O_2$ production. The use of air-diffusion cathodes yields the greater generation of this compound (Brillas, 2020). However, in an undivided cell, the concentration of accumulated $H_2O_2$ decreases by its oxidation to $O_2$ at the anode producing $HO_2^{\bullet}$ as intermediate as follows (Martínez-Huitle and Brillas, 2009):

$$H_2O_2 \rightarrow HO_2^{\bullet} + H^+ + e^- \quad (26)$$

$$HO_2^{\bullet} \rightarrow O_{2(g)} + H^+ + e^- \quad (27)$$

In the homo-EF process, $Fe^{2+}$ is regenerated pre-eminently from the continuous cathodic reduction of $Fe^{3+}$ by reaction (28) with $E^{\circ} = 0.77$ V/SHE (Ganiyu et al., 2018). Much slower $Fe^{3+}$ reduction takes place in the medium from Fenton-like reaction (29) with $k_2 = 8.4 \times 10^{-6}\ M^{-1}\ s^{-1}$ and from organic radical intermediates $R^{\bullet}$ by reaction (30) (Monteil et al., 2019):

$$Fe^{3+} + e^- \rightarrow Fe^{2+} \quad (28)$$

$$Fe^{3+} + H_2O_2 \rightarrow Fe^{2+} + H^+ + HO_2^{\bullet} \quad (29)$$

$$Fe^{3+} + R^{\bullet} \rightarrow Fe^{2+} + R^+ \quad (30)$$

The efficient $Fe^{2+}$ regeneration by reaction (28) allows the direct $Fe^{3+}$ addition as catalyst to the wastewater because this does not affect significantly the rate of Fenton's reaction (24). However, the electrogenerated Fenton's reagent loses efficiency by several parasitic reactions. For example, the homogeneous $^{\bullet}OH$ formed from Fenton's reaction (24) is partially spent by reactions like (4) and (5), as well as by the attack of $Fe^{2+}$ from reaction (31) with $k_2 = 3.2 \times 10^8\ M^{-1}\ s^{-1}$. The soluble $Fe^{2+}$ content can also be reduced by its oxidation at the anode from reaction (32) if an undivided cell is utilized (Monteil et al., 2019).

$$Fe^{2+} + {}^{\bullet}OH \rightarrow Fe^{3+} + OH^- \quad (31)$$

$$Fe^{2+} \rightarrow Fe^{3+} + e^- \quad (32)$$

The homo-EF treatment in an undivided electrolytic cell involves the parallel concurrence of ROS (mainly M($^{\bullet}$OH)) and other oxidants formed at the anode and that of homogeneous $^{\bullet}OH$ formed in the bulk from Fenton's reaction (24) (Coria et al., 2016). Unfortunately, many authors disregard the role of the anode because of the more powerful oxidation achieved by homogeneous $^{\bullet}OH$. A drawback in the mineralization of aromatic herbicides is the generation of final short-linear carboxylic acids that are complexed with $Fe^{3+}$. The difficult attack of such Fe(III)-carboxylate species by $^{\bullet}OH$ enlarges the electrolysis time and eventually prevents total mineralization. A schematic representation of the generation of $^{\bullet}OH$ in homo-EF and its attack to yield the dehydrogenation of an unsaturated compound RH and the hydroxylation of an aromatic Ar is shown in Fig. 9a.

The hetero-EF process is performed under similar operating conditions to the homo-EF one, but differs from the use of insoluble iron ions, either as solid catalyst or contained in the cathode (Ganiyu et al., 2018). The surface $Fe^{II}$ ion (represented as $\equiv Fe^{II}$) is usually hydroxylated with $-OH$ and originates the same oxidants as in homo-EF upon similar surface reactions. Reaction (33) represents the heterogeneous Fenton's reaction between the surface $\equiv Fe^{II}$ and generated $H_2O_2$ to originate surface $\equiv Fe^{III}$ and heterogeneous $^{\bullet}OH$ (Brillas, 2020):

$$\equiv Fe^{II} + H_2O_2 \rightarrow \equiv Fe^{III} + {}^{\bullet}OH + OH^- \quad (33)$$

This reaction taking place at the catalyst surface generates heterogeneous $^{\bullet}OH$ at pH near 7, with release of very low quantities of iron ions to the treated solution, preventing sludge formation. Fig. 9b presents a schematic mechanism of the main processes that are produced during a hetero-Fenton treatment of an organic pollutant with a solid iron catalyst. Despite these advantages with respect to homo-EF, most catalysts are slowly inactivated by the deposition of organic by-products and need of careful cleaning for reuse.

#### 4.2.2. Application to herbicide remediation

The same electrochemical systems used for AO and AO-$H_2O_2$ are utilized in homo-EF and hetero-EF, allowing the benchmarking between them. When the cathode is immersed in the solution, simple cylindrical or beaker two-electrode cells with parallel electrodes are usually employed. If a 3D carbon-felt cathode is utilized, it is positioned in the inner side of the cell, like in Fig. 4a. They operate by providing a constant $I$ o $j$ with a power supply. Table 2 highlights that in homo-EF, the former arrangement has been applied to the treatment of glyphosate with a Ti/$RuO_2$ anode and an ACF cathode (Lan et al., 2016). The latter arrangement has been proposed and developed by the Oturan's group and has been utilized for the remediation of diuron and monuron (Oturan et al., 2010), the chloroacetoanilide propachlor (Gençten and Özcan, 2015) and glyphosate (Tran et al., 2019) using a Pt anode, and of atrazine (Oturan et al., 2012), the urea fluometuron (Diaw et al., 2017) and the chlorophenoxy acid 2,4,5-T (Zazou et al., 2017), also using comparatively a BDD anode (see Table 2). A lower number of the studies have been devoted to cylindrical three-electrodes cells, as in the case of the azole sulfentrazone with a Pt/carbon felt cell (Lima et al., 2010), alachlor with a Pt/RVC cell (Lizama-Baena et al., 2015), and atrazine with a Pt/F-doped porous biomass carbon (Zhao et al., 2018). In these three-electrode systems, a constant $E_{cat}$ was applied to the cathode to obtain the maximum $H_2O_2$ production from reaction (25). A crucial experimental point in all these

electrochemical system is the need of a continuous vigorous bubbling of pure $O_2$ or air into the wastewater to obtain an $O_2$-saturated solution for ensuring the maximum rate of reaction (25). The effect of the injected gas flow rate on the homo-EF performance has been analyzed for glyphosate with a Ti/$RuO_2$ anode and an ACF cathode (Lan et al., 2016) and for 2,4-D with a BDD/sulfur-doped carbon (Kamaraj and Vasudevan, 2019).

A second approach for homo-EF is the use of an $O_2$- or air-diffusion cathode. The most popular electrodes are those composed of carbon-polytetrafluoroethylene (PTFE). These electrodes can be easily coupled to an anode in a cylindrical tank reactor or a flow filter-press cell, like that of Fig. 4d, and are characterized by a gas chamber in contact with its inner face where pure $O_2$ or air is injected to generate $H_2O_2$ at its external face in contact with the carbon and wastewater (Sirés et al., 2014). Cylindrical undivided two-electrode cells have been checked for alachlor (Pipi et al., 2014a) with a Pt anode, and metribuzin (Guelfi et al., 2019b) and metolachlor (Thiam and Salazar, 2019) with a BDD one, as can be seen in Table 2. This table also collects the results obtained for 2,4-D (García et al., 2014) and diuron (Pipi et al., 2014b) using a flow system like of Fig. 4c with a two-electrode cell with a Pt or BDD anode. In these systems, the pressure of the injected gas has to be regulated to avoid the percolation of the solution through the cathode that inhibits the $H_2O_2$ generation.

The immersed and gas-diffusion cathodes differ from their ability to produce $H_2O_2$ from reaction (25) and to regenerate $Fe^{2+}$ from reaction (28) in homo-EF. The $H_2O_2$ concentration formed from the former cathodes is very small because of the low solubility of dissolved $O_2$ that is transported to them, but conversely, $Fe^{2+}$ is quickly regenerated at their surface. For this reason, $Fe^{3+}$ can be added as catalyst in homo-EF. In contrast, the gas-diffusion cathodes originate much higher $H_2O_2$ concentrations, but with low $Fe^{2+}$ regeneration. Due to this different behavior, it has been established that the optimum $Fe^{2+}$ content is 0.10 and 0.50 mM for the immerse and gas-diffusion cathodes (Brillas, 2020). Fe(II)-carboxylate complexes are predominantly formed as final products in the former case, which are more easily destroyed by •OH than final Fe(III)-carboxylate ones produced preferentially in the second case. This explains the slightly superior mineralization achieved with immersed cathodes, especially with carbon felt, as can be inferred by comparing the data of some examples given in Table 2. Despite this, an excellent performance is obtained with both approaches, with the peculiarity that the gas-diffusion cathodes have been checked at much larger scale in pre-pilot flow plants that inform more reliably about the homo-EF applicability at industrial level.

Many studies have shown that the homo-EF process in an undivided cell outperforms the homologous AO-$H_2O_2$ one. This results of the quicker attack of organics by homogeneous •OH formed from Fenton's reaction (24) than by M(•OH) formed from reaction (1). The action of the latter radical is more apparent when non-active anodes are employed. This fact has been confirmed for sulcotrione (Murati et al., 2012) and mesotrione (Murati et al., 2014), 2,4,5-T (Zazou et al., 2017) and the urea monolinuron (Diaw et al., 2020) with a Pt or BDD/carbon felt cell, glyphosate with a Ti/$Ru_{0.36}Ti_{0.64}O_2$/carbon felt cell (Barbosa et al., 2018), alachlor (Pipi et al., 2014a) and tebuthiuron (Gozzi et al., 2018) with a Pt or BDD/air-diffusion cell (Pipi et al., 2014a), and metribuzin with a BDD/air-diffusion cell (Guelfi et al., 2019b).

Fig. 10 depicts the comparison of the AO-$H_2O_2$ and homo-EF with 0.10 mM $Fe^{2+}$ for 0.10 mM 2,4,5-T in 0.050 M $Na_2SO_4$ at pH 3.0 using a Pt/carbon felt or BDD/carbon felt cell at $I$ = 300 mA (Zazou et al., 2017). The degradation of this chlorophenoxy acid in AO-$H_2O_2$ is slightly faster using BDD (Fig. 10d) than Pt (Fig. 10a), yielding total removal in 70 vs. 80 min, according to the higher oxidation of M(•OH) produced by BDD. A much quicker herbicide

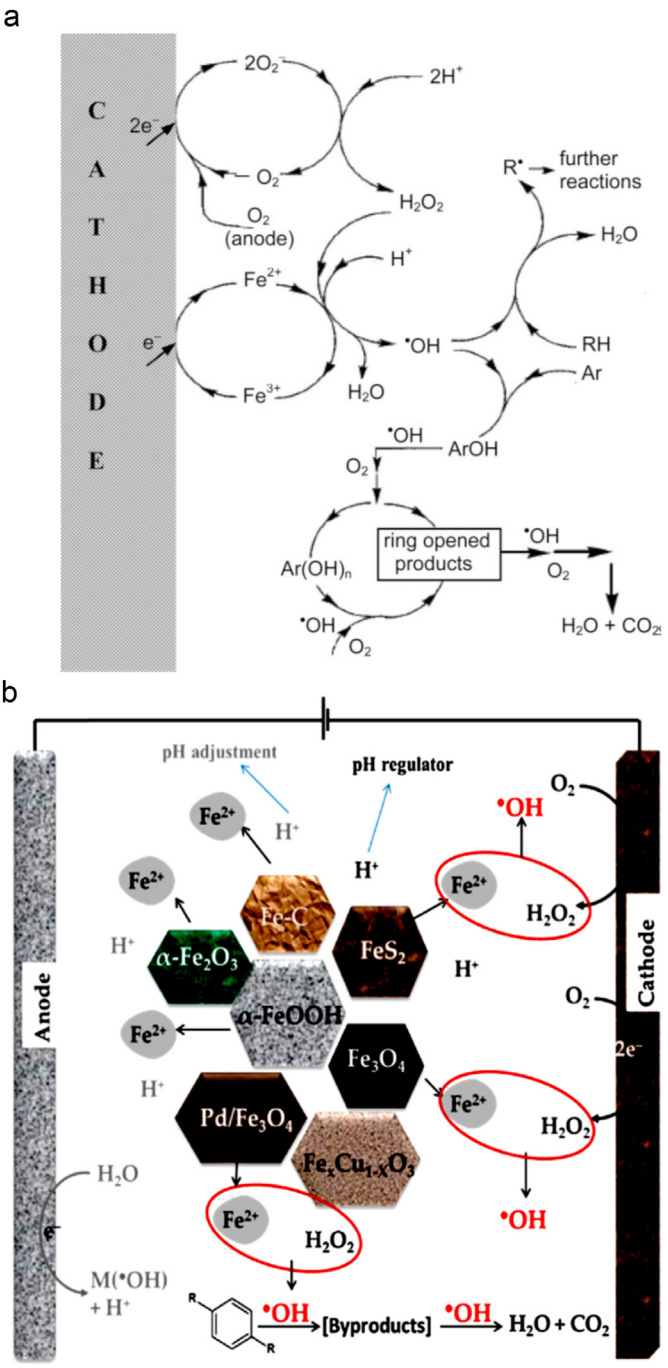


**Fig. 9.** (a) Schematic representation of the main reactions involved in the homo-EF process in a divided cell. RH is an unsaturated compound that undergoes dehydrogenation and Ar is an aromatic pollutant that is hydroxylated. Adapted from Brillas et al. (2009). (b) Schematic mechanism of the hetero-EF process in an undivided cell with different solid catalysts, in which electrogenerated $H_2O_2$ reacts with their surface $Fe^{2+}$ ions. Adapted from Ganiyu et al. (2018).

decay can be observed in homo-EF because of the more rapid concurrent oxidation with homogeneous •OH, which surprisingly led to a faster disappearance with Pt (8 min) than with BDD (14 min). The superiority of BDD over Pt in AO-$H_2O_2$ was clearer by comparing the TOC abatement, which was reduced by 89% with the former anode in 360 min but only by 48% with the latter one (see Fig. 8b–e). The oxidative ability of homogeneous •OH in homo-EF became much more significant with Pt that yielded a final TOC

reduction of 92%, a value slightly lower than 95% obtained with BDD (see Table 2). The different mineralization behavior of these anodes can be better visualized from the evolution of the final carboxylic detected during 2,4,5-T oxidation that are formed with loss of $Cl^-$ ion and breaking of the benzene ring. Fig. 8c–f shows the time course of glyoxylic, glycolic and maleic acids, which are oxidized to the predominant oxalic acid that is directly converted into $CO_2$. These acids were more rapidly removed by BDD due to the quicker attack of the stronger oxidant M(•OH) formed at its surface over the iron complexes of carboxylic acids, explaining the slightly higher oxidation power of the BDD/carbon felt cell in homo-EF. Fig. 11 presents the mineralization route proposed for 2,4,5-T by homo-EF based on the primary byproduct identified by GC-MS and final carboxylic acids detected by ion-exclusion HPLC. The oxidative action of •OH originates the breaking and loss of the lateral acetic group and the dechlorination and hydroxylation of the benzene ring, followed by its breaking to form carboxylic acids that finally yield $CO_2$. It is also noticeable the decrease of solution toxicity monitored by Microtox (by *Vibrio Fisheri*) with the mineralization progress. This is an important fact that ensures the effectiveness of the EAOPs for herbicide remediation. Reaction sequences for herbicides involving the formation of consecutive primary aromatic, heteroaromatic or cyclic byproducts, followed by their transformation into carboxylic acids is general for these treatment. Fig. 12 exemplifies the mineralization route proposed by Oturan et al. (2011) for the homo-EF treatment of diuron in acidic sulfate medium, with loss of $Cl^-$ and $NO_3^-$ ions, using a BDD/carbon felt cell.

The superiority of homo-EF over AO-$H_2O_2$, better using BDD instead of Pt, has been confirmed by using gas-diffusion cathodes as well. This can be seen in Fig. 13a–e for the degradation of 0.60 mM alachlor in 0.050 M $Na_2SO_4$ at pH 3.0, where 69% and 98% herbicide removal were attained after 360 min of AO-$H_2O_2$ at $j$ = 33.3. mA $cm^{-2}$ using a Pt and BDD anode (Pipi et al., 2014a). These figures highlight the quicker destruction of alachlor by homo-EF with a BDD anode, with overall disappearance in 120 min, whereas that occurs after 360 min with a Pt one. From the pseudo-first-order kinetic analysis illustrated in Fig. 13b–f, increasing $k_1$-values of $3.2 \times 10^{-3}$ $min^{-1}$ (AO-$H_2O_2$ with Pt), $8.6 \times 10^{-3}$ $min^{-1}$ (AO-$H_2O_2$ with BDD), 0.0139 $min^{-1}$ (EF with Pt) and 0.0436 $min^{-1}$ (EF with BDD) were determined. The TOC decays shown in Figs. 13c–11g make in evidence the larger mineralization achieved by homo-EF with a BDD anode (83%), slightly higher than 78% found for the homologous AO-$H_2O_2$ process. That corroborates the high oxidation power of M(•OH) formed by BDD, along with the positive oxidative role of homogeneous •OH originated from Fenton's reaction (24). According to this trend, Figs. 13d–h highlight that greater MCE values were calculated using the BDD anode in both EAOPs, with values dropping down from about 38% to 17% due to the continuous loss of organic matter and production of more recalcitrant byproducts, as pointed out above. These authors identified the by-products originated during alachlor mineralization and proposed the reaction sequence of Fig. 14. The herbicide underwent initially a complex pathway with partial loss of the lateral group with N, cyclization, demethylation and hydroxylation of lateral chain and benzenic ring, followed by oxidation of the by-products formed to acetic and chloroacetic acids, whereas the heteroatoms were released as $Cl^-$, $NO_3^-$ and $NH_4^+$ ions.

The optimum pH for homo-EF is 3.0, near to the optimal of Fenton's reaction (24), as has been confirmed for the urea chlortoluron and the thiadiazine bentazon with a BDD/carbon felt cell (Abdessalem et al., 2010) and atrazine with a BDD/$O_2$-diffusion one (Borràs et al., 2010). At lower pH, the rate of Fenton's reaction (24) decreases because the inactive protonated $H_2O_2$ ($H_3O_2^+$) is formed, whereas at higher pH, it is slowed down by the loss of catalyst content because of the precipitation of iron hydroxides. Other crucial parameter is the optimum catalyst content, which has been found to be of 0.10 mM for a carbon felt cathode from the degradation of 2,4,5-T (Zazou et al., 2017) and monolinuron (Diaw et al., 2020), and 0.50 mM using a gas-diffusion cathode. Fig. 15a–b shows that operating within the interval of 0.10–1.50 mM $Fe^{2+}$ content, 0.50 mM offers the quicker degradation and mineralization of 100 mL of 0.523 mM metribuzin in 0.050 M $Na_2SO_4$ at pH 3.0 with a BDD/air-diffusion cell at $j$ = 100 mA $cm^{-2}$. Total removal of the herbicide and 99% TOC reduction, with 2.7% MCE, were achieved in 90 and 540 min (see Table 2).

Like in the case of AO and AO-$H_2O_2$, the rise of $I$, $j$ or $E_{cat}$ in homo-EF provokes faster herbicide concentration decay and larger mineralization. This influence is due to the acceleration of reactions (1) and (25), with the consequent upgrading of M(•OH) and $H_2O_2$ contents, which in turn accelerates the production of homogeneous •OH from Fenton's reaction (24). The rate of this reaction is also enhanced by the faster $Fe^{2+}$ regeneration from reaction (28). However, the corresponding MCE values dropped down by the concomitant increase in rate of parasitic reactions like (3)–(5), (13)–(16) and (31) and (32). These tendencies have been corroborated for the homo-EF treatment of 2,4-D with a BDD/BDD cell (García et al., 2013), propachlor with a Pt/carbon felt cell (Gençten and Özcan, 2015), metribuzin with a BDD/air-diffusion cell (Guelfi et al., 2019b) and the uracil bromacil with a BDD/carbon felt cell (Moraleda et al., 2020). Figs. 15c–d illustrate the growing herbicide concentration removal and TOC decay for 0.523 mM metribuzin in 0.050 M $Na_2SO_4$ with 0.50 mM $Fe^{2+}$ at pH 3.0 with a BDD/air-diffusion cell by increasing $j$ from 33.3 to 100 mA $cm^{-2}$ (Guelfi et al., 2019b). In contrast, the inset panel of Fig. 15d illustrates the opposite trend for the MCE values, which progressively dropped down from 7.9% at $j$ = 33.3 mA $cm^{-2}$ to 2.7% at $j$ = 100 mA $cm^{-2}$ after 540 min owing to the larger enhancement of the parasitic reactions of hydroxyl radicals, as pointed out above.

The influence of herbicide concentration as operation parameter has been widely studied, showing the same characteristics as described above for the AO and AO-$H_2O_2$ processes. For the homo-EF treatment of metribuzin solution in sulfate medium with 0.50 mM $Fe^{2+}$ at pH 3.0 and $j$ = 100 mA $cm^{-2}$, Guelfi et al. (2019b) reported a lower normalized concentration and TOC decays when the herbicide content grew from 0.262 to 1.046 mM, as can be seen in Fig. 15e–f. Nevertheless, the MCE value (see the inset of Fig. 15f) underwent a progressive upgrading from 1.3% at 0.262 mM to 5.4% at 1.046 mM owing to the preferential attack of hydroxyl radicals over greater amounts of organics in the medium with deceleration of their parasitic reactions. That means that the homo-EF becomes more efficient for the treatment of concentrated herbicide wastewater.

Scarce information has been provided over soil remediation with homo-EF. Only one work of Carboneras Contreras et al. (2019) focused on the preparation of a synthetic soil-washing effluent composed of salts of $Cl^-$, $SO_4^{2-}$, $I^-$ and $CO_3^{2-}$ and the spiking of clopyralid for homo-EF treatment with a Pt/carbon fell cell. The optimum $Fe^{2+}$ content was 0.10 mM and $I^-$ ion had a negative impact over the process because it consumed generated $H_2O_2$ to form $I_3^-$. For this the treatment was slow leading to 83% clopyralid decay with 31% TOC removal after 480 min of electrolysis at $I$ = 200 mA of 800 mL of 180 mg $L^{-1}$ of herbicide at pH 3.0 (see Table 2).

A reduced number of papers have been devoted to the remediation of herbicide wastewaters by hetero-EF aiming to develop an efficient process at neutral pH. Insoluble iron catalysts like Fe@$Fe_2O_3$ for atrazine (Ding et al., 2017) and suspended AC + PTFE + $Fe_3O_4$ for diuron (Wang et al., 2018), as well as iron-modified cathodes like allophane supported with $Fe_2O_3$ for atrazine (Garrido-Ramírez et al., 2013), martite-graphite for paraquat

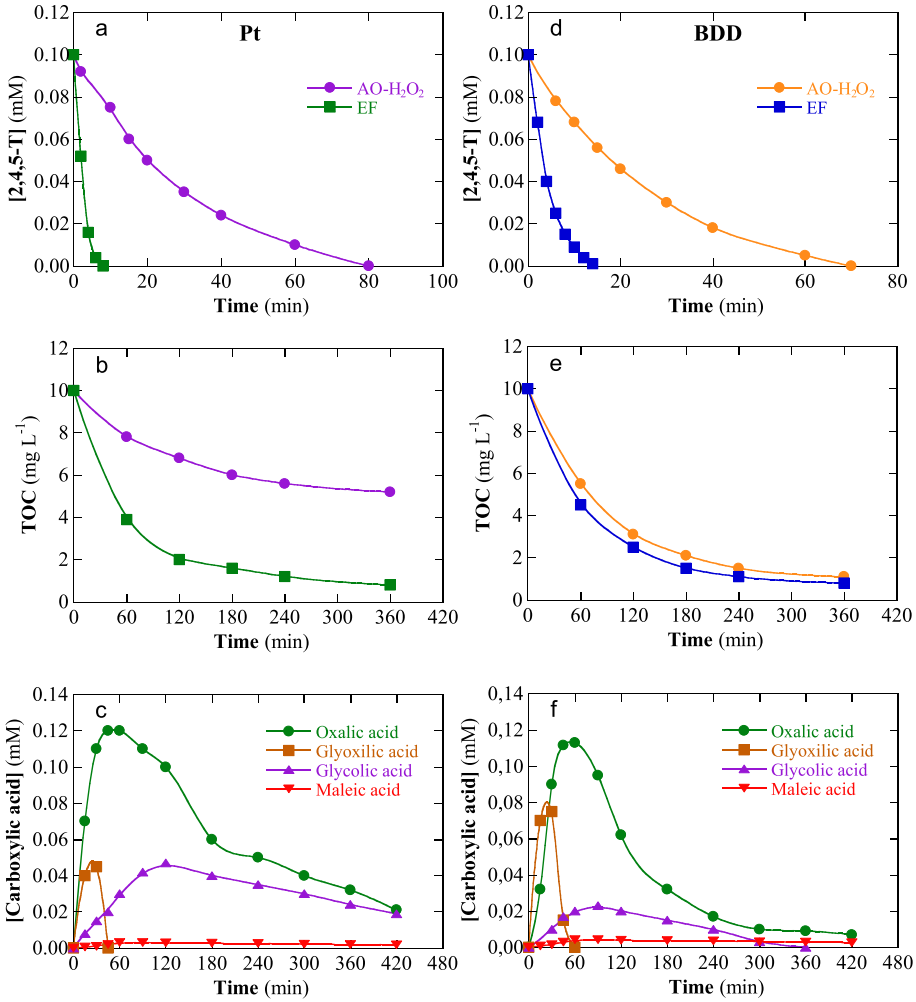


**Fig. 10.** Time course of (a,d) 2,4,5-T concentration and (b,e) TOC under AO-$H_2O_2$ and homo-EF with 0.10 mM $Fe^{2+}$, and (c,f) carboxylic acids generated upon homo-EF for 230 mL of an $O_2$-saturated 0.10 mM herbicide solution in 0.050 M $Na_2SO_4$ at pH 3.0 using an undivided stirred tank reactor like of Fig. 4a with a (a,b,c) Pt or (d,e,f) BDD anode and a large carbon-felt cathode at current ($I$) = 300 mA. Adapted from Zazou et al. (2017).

(Khataee et al., 2017) and metal organic frameworks for the amide napropamide (Liu et al., 2019a), have been considered. These studies assessed the performance of hetero-EF in a pH range from 3.0 to 6.7. The examples of Table 2 using a Pt anode by applying either an $E_{cat} = -1.04$ V/Ag|AgCl, for 480 min (Garrido-Ramírez et al., 2013) or an $I = 100$ mA for 120 min (Wang et al., 2018) highlight a quick herbicide abatement at pH 3.0 that gradually decreased up to pH 6.0–7.0. This is a general behavior observed in all the cases checked with the advantage of a larger stability of the catalysts and cathodes near neutral pH, with very low release of iron to the wastewater (Khataee et al., 2017). This research line needs to be potentiated in the next future, searching novel materials with higher catalytic properties to enhance the hetero-EF process at pH 7.0, avoiding the cumbersome procedure of acidification before homo-EF application and the subsequent neutralization before disposal.

### 4.3. Photoelectro-Fenton and solar photoelectro-Fenton

The PEF process is a photo-assisted EF treatment, more powerful in acidic matrices. In PEF, the wastewater upon EF process is submitted to light illumination with artificial lamps. Although UVA light (λ = 315–400 nm) is the most frequently radiation used, UVB (λ = 280–315 nm) or UVC (λ = 100–280 nm) lights are employed as well (Brillas, 2020). The PEF treatment has the advantage to upgrade the mineralization process of EF, regardless of the exciting light utilized. The action of UVA and UVB lights is accounted for by Thiam and Salazar (2019):

(i) The additional fast $Fe^{2+}$ regeneration from the photoreduction of hydrolyzed Fe(III) ions that accelerates Fenton's reaction (24). At pH 2.8–3.5, the predominant species is $Fe(OH)^{2+}$ that is photolyzed according to reaction (34), yielding extra $^{\bullet}OH$, and

(ii) the photodecomposition of photoactive Fe(III) complexes with organic intermediates and final carboxylic acids when the mineralization progresses. The general reaction (35) gives the photolysis of Fe(III)-carboxylate complexes that also regenerates $Fe^{2+}$.

$$Fe(OH)^{2+} + h\nu \rightarrow Fe^{2+} + {}^{\bullet}OH \quad (34)$$

$$Fe(OOCR)^{2+} + h\nu \rightarrow Fe^{2+} + CO_2 + R^{\bullet} \quad (35)$$

Apart from the above reactions, an UVC light enhances $^{\bullet}OH$ generation from the photohomolysis of $H_2O_2$ by reaction (36), although it is less utilized in practice (Brillas, 2020).

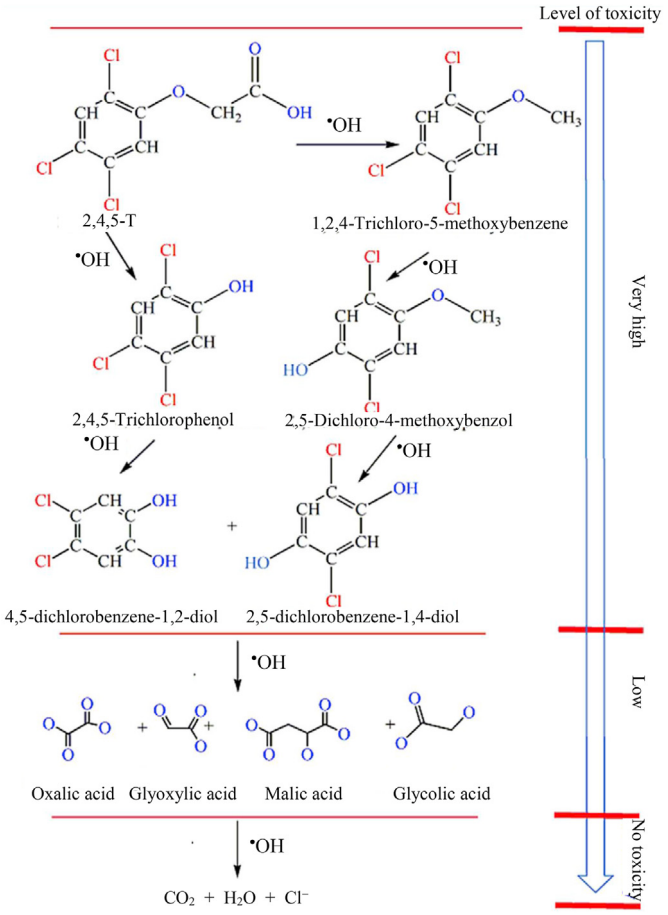


**Fig. 11.** Proposed mineralization route for 2,4,5-T in acidic sulfate medium by homo-EF with Pt/carbon felt and BDD/carbon felt cells. Adapted from Zazou et al. (2017).

$$H_2O_2 + h\nu \rightarrow 2^{\bullet}OH \quad (36)$$

The main disadvantage for PEF application at industrial scale is the high electric cost of the UV lamp, much superior to that of the electrochemical cell. To overcome this drawback, the SPEF process has been developed. In this method, the solution is irradiated with photons from free sunlight ($\lambda > 300$ nm) and it is much more cost-effective and even more powerful than PEF because of the higher UV irradiance and the possibility of extent the reaction (35) to $\lambda > 400$ nm (Garcia-Segura et al., 2014). However, the main disadvantage of SPEF is that it is restricted to a few daily hours of sun, relied on the geographic area and its climatology. One can then envisage a combined process involving SPEF upon sunlight and EF with UV light in its absence for industrial application. The electric consumption of this combined treatment could be free if the input current is directly supplied from solar photovoltaic panels and accumulated in batteries to power the electrochemical cell and the UV lamp.

The PEF and SPEF processes have been mainly developed by the Brillas' group with gas-diffusion electrodes upon homogeneous conditions. Large amounts of photoactive Fe(III) complexes are found to be formed, which can be much more rapidly photodecomposed than the homologous Fe(II) complexes, predominantly produced using immersed carbonaceous cathodes. Stirred cylindrical two-electrodes tank reactors are commonly used in PEF with exposition of the solution to an UVA lamp placed over it. Some articles have described the PEF treatment with flow plants with either a cylindrical two electrode cell like of Fig. 3e with an inner

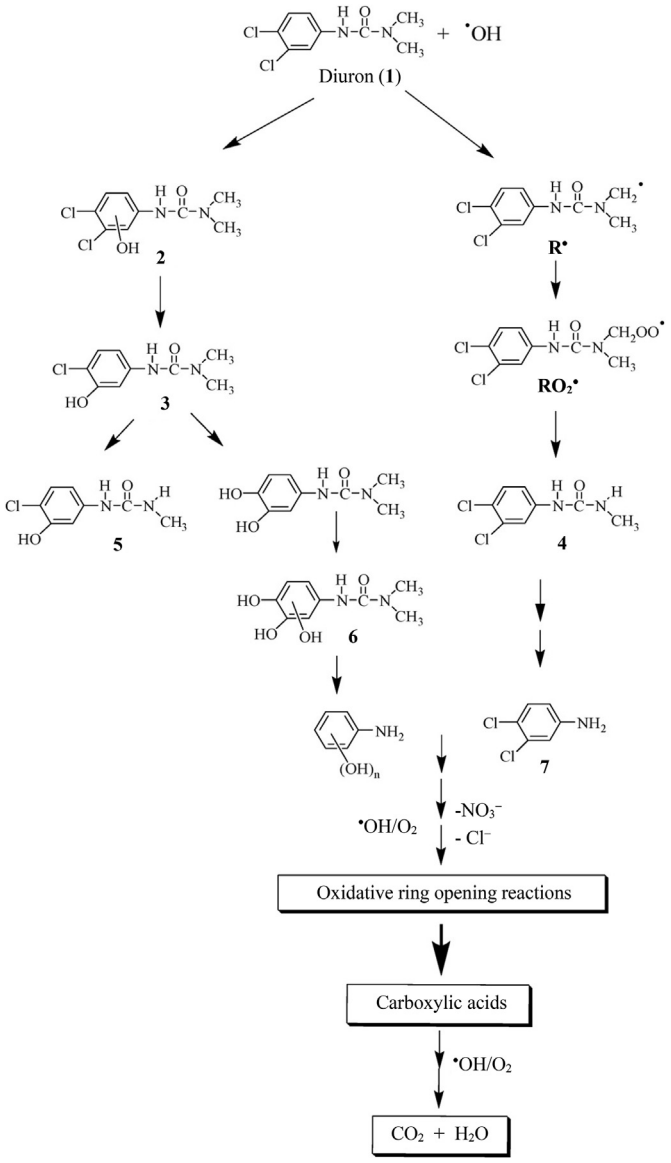


**Fig. 12.** Proposed mineralization pathway for diuron in acidic sulfate medium by homo-EF with a BDD/carbon felt cell. Adapted from Oturan et al. (2011).

UV lamp (Komtchou et al., 2017) or a filter-press two-electrode one like of Fig. 4d either with the UV light into an annular recipient (Alcaide et al., 2020) or immersed into the reservoir (Souza et al., 2019). Flow plants like of Fig. 4c with a solar CPC photoreactor are the best options to assess the SPEF process, although sometimes a simpler solar planar photoreactor has been employed (Gozzi et al., 2017). Cylindrical cells directly illuminated with sunlight have also been applied to the SPEF process (Guelfi et al., 2018; 2019a). Note that only the viability of the PEF and SPEF processes and their comparative oxidation power with other EAOPs are considered in these studies, without any optimization of the electrochemical system and light caption. This should be a hot topic in the next years for their feasible scale-up at industrial level, with the development of autonomous systems directly powered by solar panel photovoltaics in order to provide free electric energy for the system performance including that needed for running the UVA lamps, as stated above.

Table 2 shows the good results obtained for the remediation of several herbicides by PEF and SPEF. Comparison of the data

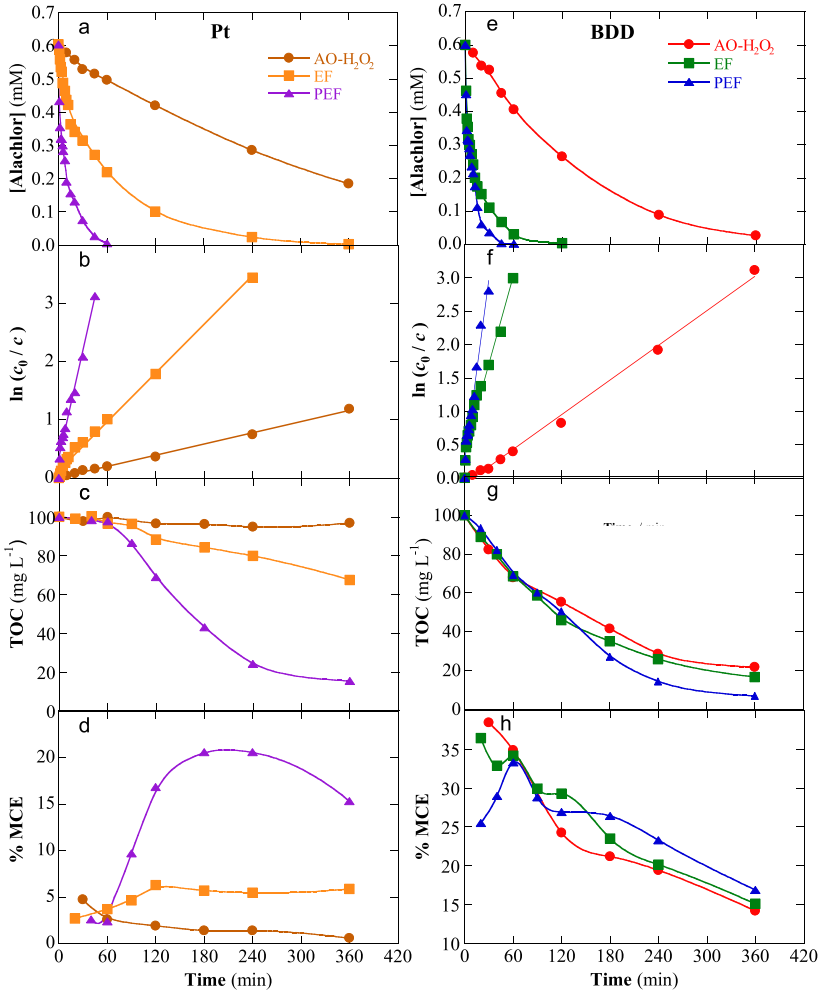


**Fig. 13.** Time course of (a,e) alachlor concentration, (b,f) pseudo-first-order kinetic analysis, (c,g) TOC and (d,h) mineralization current efficiency for the treatment of 100 mL of 0.60 mM herbicide solution in 0.050 M $Na_2SO_4$ at pH 3.0 by AO-$H_2O_2$, as well as homo-EF and photoelectro-Fenton (PEF) with 0.50 mM $Fe^{2+}$, using an undivided stirred cylindrical tank reactor with a (a,b,c,d) Pt or (e,f,g,h) BDD anode and an air-diffusion cathode (3 $cm^2$ electrode area) at $j$ = 33.3 mA $cm^{-2}$. Adapted from Pipi et al. (2014a).

collected in this table and Table 1 for alachlor (Pipi et al., 2014a) and metolachlor (Thiam and Salazar, 2019) using Pt and/or BDD anodes, allows inferring a rise in the oxidation power of EAOPs in the order: AO-$H_2O_2$ < homo-EF < PEF. This tendency can be clearly observed in Fig. 13 for the treatment by these three methods of 0.60 mM alachlor solutions in 0.050 M $Na_2SO_4$ at pH 3.0 with Pt/air-diffusion and BDD/air-diffusion cells at $j$ = 33.3 mA $cm^{-2}$ (Pipi et al., 2014a). That has been reported for other herbicides like atrazine (Borràs et al., 2010), the triazines desmetryne (Borràs et al., 2011) and cyanazine (Borràs et al., 2013), and tebuthiuron (Gozzi et al., 2018) using BDD/gas-diffusion cells. Fig. 13 discloses a smaller influence of the anode over the degradation and mineralization in PEF as compared to AO-$H_2O_2$ and homo-EF. This is indicative of a large production of $^{\bullet}$OH from the photolytic reaction (34) and a rapid photodecomposition of final Fe(III)-carboxylate species from reaction (35). The non-active BDD usually outperforms active anodes in all EAOPs because of the much higher oxidation ability of M($^{\bullet}$OH) that it generates from reaction (1). For example, the $k_1$-value of alachlor with BDD (0.091 $min^{-1}$) was greater than with Pt (0.062 $min^{-1}$) (see Fig. 13b–f), as well as the corresponding MCE values (see Fig. 13d–h). In contrast, Thiam et al. (2018) showed a similar performance for the benzoic acid chloramben with an $IrO_2$, $RuO_2$, $PbO_2$ or BDD anode (see Table 2), opening the door to the use of cheaper active anodes than BDD. This feature is even better verified by SPEF, which possesses greater oxidation power than PEF due to the incidence of a higher number of photons from sunlight over the solution, accelerating reactions (34) and (35), as found for diuron (Pipi et al., 204b) and bentazon (Guelfi et al., 2019a).

The optimum pH for PEF and SPEF is 3.0, the same value as in homo-EF, because the processes are controlled by homogeneous $^{\bullet}$OH originated from Fenton's reaction (24). This has been discussed in the studies made for atrazine (Borràs et al., 2010) and desmetryne (Borràs et al., 2011). Similarly, the same effects of $Fe^{2+}$ and herbicide concentrations, as well as of $I$ or $j$, over the herbicide performance have been described for all these EAOPs. Garcia-Segura et al. (2011) optimized the SPEF process of 4-chloro-2-methylphenoxyacetic acid by RSM using the plant of Fig. 4c with the Pt/air-diffusion cell of Fig. 4d. Values of current from 1.6 to 8.4 A, $Fe^{2+}$ content from 0.41 to 2.09 mM and pH from 1.32 to 4.68 were chosen as independent variables to calculate second-order models for the percentage of TOC and MCE decays and $EC_{TOC}$ through 17 trials designed from a CCD test. The best conditions were found for $I$ = 5.0 A, 1.00 mM $Fe^{2+}$ and pH 3.0. Fig. 16a shows the fast degradation achieved for the herbicide, obeying a pseudo-first-order kinetics with $k_1 = 1.25 \times 10^{-3}$ $s^{-1}$. Fig. 16b–d shows the time course of the determined optimized parameters, whose their excellent achievements obtained after 120 min of electrolysis are collected in Table 2. The three main aromatic products detected,

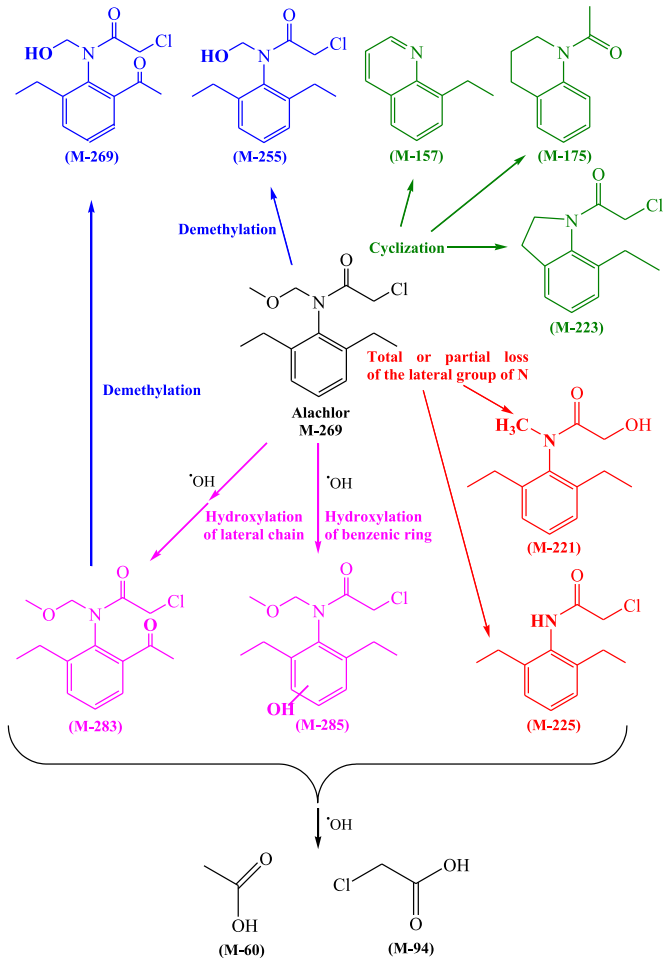


**Fig. 14.** Proposed reaction pathways for alachlor mineralization in acidic sulfate medium by AO-$H_2O_2$, homo-EF and PEF with a BDD anode and an air-diffusion cathode. Adapted from Pipi et al. (2014a).

namely 4-chloro-2-methylphenol, 2-methylhydroquinone and 2-methylbenzoquinone, were rapidly accumulated and destroyed in 50–70 min, a time similar to that of the parent herbicide (see Fig. 16e). This demonstrates the large effectiveness of SPEF to remove aromatics. Eight final carboxylic acids were identified and quantified by ion-exclusion HPLC, which were accumulated and disappeared completely in 120 min (see Fig. 16f) due to the quick photolysis of their Fe(III) complexes from reaction (35). From these by-products, the reaction sequence of Fig. 17 was proposed, showing the transformation of aromatics into carboxylic acids, being oxalic and formic acids the ultimate by-products that are directly mineralized to $CO_2$. The Cl atom of the herbicide was released as $Cl^-$ ion.

The PEF process and particularly the SPEF one are the best methods for herbicide remediation, at least upon the sulfate media tested. Less is known about the performance of these processes in complex aqueous matrices, a field that needs to be investigated in the next future. Only two papers referred the treatment of chloramben spiked into an urban wastewater (Thiam et al., 2018) and metolachlor spiked into a real wastewater of winery industry (Thiam and Salazar, 2019) by the most potent SPEF process have been reported. The data of Table 2 reveal a total degradation of these herbicides with a large mineralization, showing a good performance using an active $IrO_2$ anode, although slightly lower than for the non-active BDD.

### 4.4. Photoelectrocatalysis

PEC is an electrochemical variant of photocatalysis (PC), involving a photoanode submitted to an UVA, visible or sunlight irradiation that is connected to a cathode in an electrochemical cell in order to enhance the production of oxidizing agents for removing more rapidly herbicides from wastewaters. This method is usually performed with lower herbicide concentrations than in the above EAOPs since lower $I$ values can be applied to preserve the photoanode stability due to its low conductivity. This subsection describes the fundamentals of this technique and its application to treat synthetic solutions with herbicides. Main results reported in the literature are summarized in Table 3.

#### 4.4.1. Fundamentals

The PC process generates oxidants at the surface of a photocatalyst like a semiconductor material upon light absorption of photons of energy higher or equal to its band gap energy ($E_g$), which promotes an electron from its valence band (VB) to its conductive band (CB) in aqueous medium (Garcia-Segura and Brillas, 2017). The semiconductor photoactivation originates a charge carriers' separation in its surface, with formation of a positively vacancy or hole in the VB ($h^+_{VB}$) and an electron in the CB ($e^-_{CB}$), according to reaction (37). These separated species are able to generate ROS like $^\bullet OH$ and $O_2^{\bullet-}$ from reactions (38) and (39). It is also feasible the direct attack of organics by the strong oxidant $h^+_{VB}$, However, the most important drawback of PC is the strong fall in efficiency owing to the fast recombination of the photogenerated $e^-_{CB}/h^+_{VB}$ pair via reaction (40).

$$\text{Semiconductor} + h\nu \rightarrow e^-_{CB} + h^+_{VB} \quad (37)$$

$$h^+_{VB} + H_2O \rightarrow {}^\bullet OH + H^+ \quad (38)$$

$$e^-_{CB} + O_2 \rightarrow O_2^{\bullet-} \quad (39)$$

$$e^-_{CB} + h^+_{VB} \rightarrow \text{Semiconductor} + \text{heat} \quad (40)$$

The PEC technique is advantageous due to the coupling of a photocatalyst upon light irradiation as photoanode to an electrochemical system to pass the photoinduced $e^-_{CB}$ to the cathode. This decreases the amount of these species at the photoanode surface and drops down drastically the recombination rate of reaction (40). The lifetime of $h^+_{VB}$ is then raised giving rise to more opportunities for the enhancement of $^\bullet OH$ generation from reaction (38), as well as its direct attack over organic pollutants (Garcia-Segura and Brillas, 2017). Fig. 18 shows a schematic illustration of the PEC mechanism using a $TiO_2$ photoanode with the corresponding photooxidation and photoreduction processes. In contrast, Fig. 19a exemplifies the PEC process with a Ti/$IrO_2$-Pt-$WO_3$ or Ti/$IrO_2$-Pt-$Ag_3PO_4$ photoanode upon simulated sunlight (Guo et al., 2017), where the organics can be oxidized and reduced at the photoanode and cathode.

Note that the photoanode is constructed by deposition of a semiconductor photocatalyst onto a conductive substrate, like indium tin oxide (ITO), to improve its conductivity. PEC runs are made either at constant $E_{anod}$ or at constant $I$ or $j$. This extracts the $e^-_{CB}$ toward the cathode, largely preventing the recombination of the $e^-_{CB}/h^+_{VB}$ pair and accelerating the production of more $h^+_{VB}$ with higher oxidation power to destroy the organics, as stated above. Non-aggressive operation conditions are used in PEC in order to facilitate the easy recovering of the photocatalyst after usage to be further consecutively recycled.

The crystalline anatase form of $TiO_2$ is the most ubiquitous semiconductor photocatalyst used in PC and PEC. This highly stable,

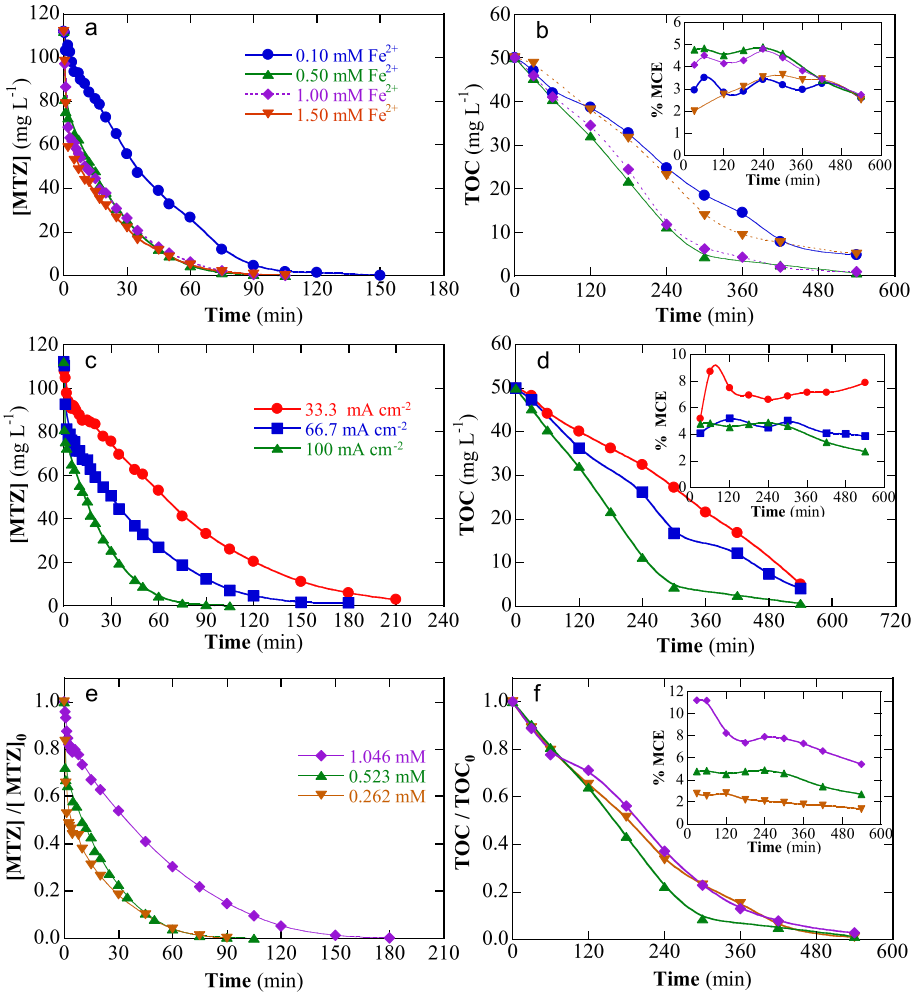


**Fig. 15.** Effect of operation variables on the change of (a,c,e) (normalized) MTZ content and (b,d,f) (normalized) TOC and mineralization current efficiency with electrolysis time for the homo-EF process of 100 mL of herbicide solutions in 0.050 M $Na_2SO_4$ at pH 3.0 using a BDD/air-diffusion cell (each electrode of 3 $cm^2$ area). (a,b) 0.523 mM MTZ at different $Fe^{2+}$ contents at $j = 100$ mA $cm^{-2}$. (c,d) 0.523 mM MTZ with 0.50 mM $Fe^{2+}$ at different $j$ values. (e,f) different MTZ concentrations with 0.50 mM $Fe^{2+}$ at $j = 100$ mA $cm^{-2}$. Adapted from Guelfi et al. (2019b).

cheap and low toxic material has a wide $E_g = 3.22$ eV ($\lambda = 385$ nm), which can be easily overcome by photons of UVA light to photogenerate the $e^-_{CB}/h^+_{VB}$ pair. In many works, the $TiO_2$ photocatalyst is modified, e.g., producing nanotubes (NTs) (Xin et al., 2011) or by doping with other elements or oxides (Wang et al., 2019), to take advantage of the solar light as energy source. Fig. 19b illustrates the photoexcitation of a 2D microporous $SnO_2$ assembled into $TiO_2$ NTs upon UVA light (Li et al., 2012). The light irradiation produces the $e^-_{CB}/h^+_{VB}$ pair in both semiconductors, the $TiO_2$ NTs and $SnO_2$ with $E_g$ values of 3.22 and 3.88 ($\lambda = 319$ nm) eV. As the potentials of the VB and CB of $SnO_2$ are lower than those of $TiO_2$ NTs, more $h^+_{VB}$ reach the surface of the latter semiconductor, whereas more $e^-_{CB}$ are delivered to the former one. On the whole, the system behaves as a semiconductor with a lower $E_g = 2.96$ eV ($\lambda = 418$ nm), meaning that it can absorb visible light.

The low conductivity of photoanodes employed in PEC only allows the use of relatively small $E_{an}$ and $j$ values. This is the main disadvantage of this technique for the treatment of relatively high herbicide contents from industrial wastewaters. Since it behaves as an active anode, this entails a very weak M(•OH) production from reaction (1), which gives a poor degradation and mineralization of herbicides. This AO process takes place in parallel with the oxidative action originated by $h^+_{VB}$. So, it is very difficult to separate the AO contribution in the total process. To clarify this point, many studies present a comparison of the AO, PC and PEC treatments of the herbicide. It is found that the sum of the AO and PC contributions can be either equal or lower than the overall PEC, meaning that the latter behaves as an additive or synergistic process, i.e., the oxidizing agents of the two former act independently or in cooperation.

### 4.4.2. *Application to herbicide remediation*

The PEC process of herbicides in wastewaters has been mainly focused to the preparation and characterization of new photoanodes with $E_g$ values low enough to make feasible the organic oxidation upon illumination with visible light,. This has been confirmed by applying potent Xe lamps that mimic the radiation of sunlight. Small stirred cylindrical or similar undivided tank reactors have been usually employed in order to check the PEC performance (see Table 3). Glass or quartz cells have been used to permit the photoanode illumination from an external lamp placed near and in front of it. Only Long et al. (2019) have degraded atrazine in a phosphate medium of pH 7 with a $TiO_2$ NTs/$TiO_2$-Pt photoanode under a 500 W Xe irradiation using a small divided cell. The application of larger systems needs to be developed in the next future to show more clearly if PEC is viable for herbicide treatment

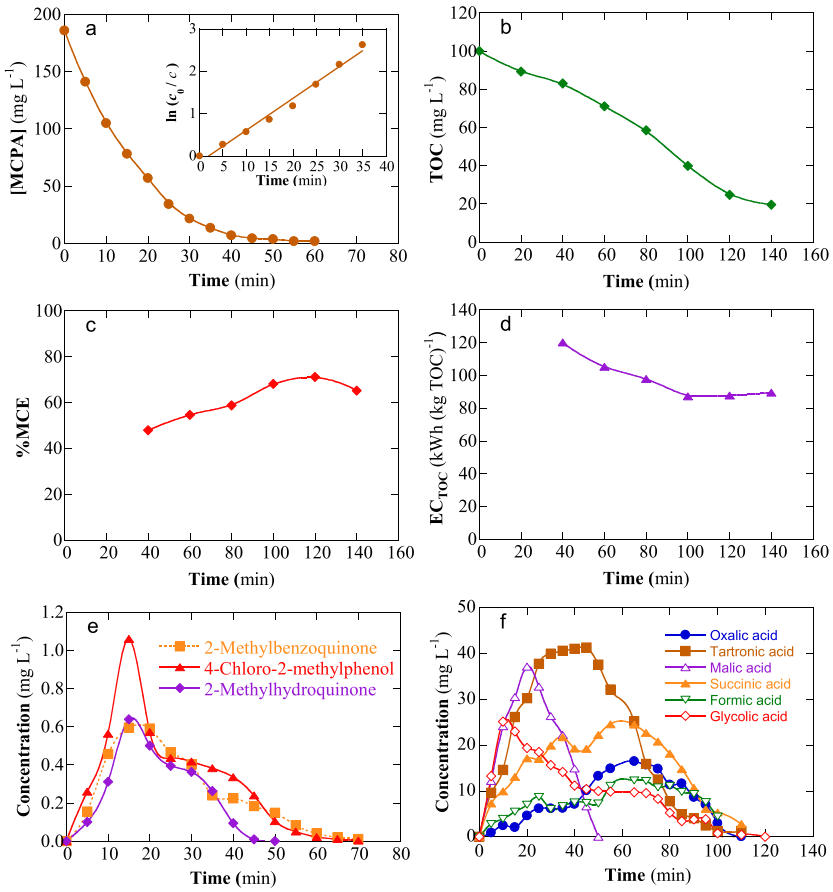


**Fig. 16.** Time course of (a) 4-chloro-2-methylphenoxyacetic acid with pseudo-first-order kinetic analysis, (b) TOC, (c) mineralization current efficiency, (d) energy consumption per unit TOC mass, (e) aromatic intermediates and (f) final carboxylic acids for the SPEF process of 10 L of 186 mg $L^{-1}$ herbicide in 0.050 M $Na_2SO_4$ under optimum conditions of 1.00 mM $Fe^{2+}$, pH 3.0 and 35 °C, using the flow plant of Fig. 4c with a Pt/air-diffusion cell (100 $cm^2$ electrode area) like of Fig. 4d and a CPC solar photoreactor (32 W $m^{-2}$ of average UV irradiation intensity) at 5 A and liquid flow rate of 180 L $h^{-1}$. Adapted from Garcia-Segura et al. (2011).

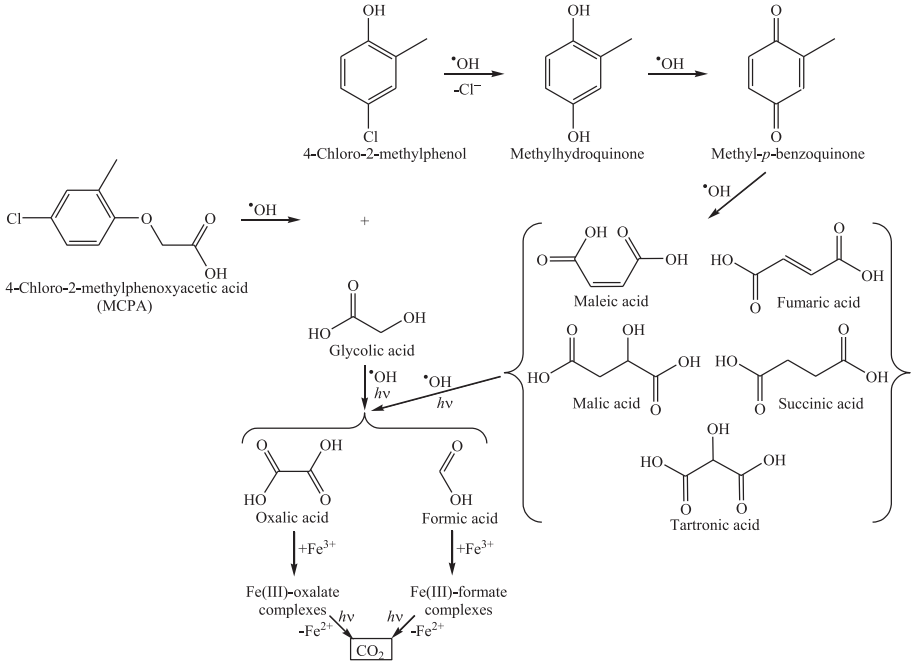


**Fig. 17.** Mineralization route proposed for 4-chloro-2-methylphenoxyacetic acid by SPEF with the flow plant of Fig. 4d with a Pt/air-diffusion filter-press cell and a CPC solar photoreactor. Adapted from Garcia-Segura et al. (2011).

in practice.

Modified $TiO_2$ anodes such as Ti/$TiO_2$ NTs for alachlor (Xin et al., 2011), 2D macroporous $SnO_2$/$TiO_2$ NTs for 2,4-D (Li et al., 2012), Ti/$TiO_{2-x}$ for atrazine (Komtchou et al., 2016), graphene oxide (GO)/$TiO_2$ NTs for pentachlorophenol (Rajput et al., 2018b), $CuInS_2$/$TiO_2$ NTs for 2,4-D (Liu et al., 2011) and B,F/$TiO_2$ NTs for atrazine (Wang et al., 2019) among others, have been checked as photoanodes. $WO_3$ nanosheets with $E_g = 2.6$ eV ($\lambda = 477$ nm) have also been tested for the degradation of diuron (Fernández-Domene et al., 2018a), atrazine (Fernández-Domene et al., 2018b) and bromacil (Roselló-Márquez et al., 2019). In these articles and after the description of the synthesis of the photoanode, its morphological, structural, electrochemical and photoelectrochemical characteristics are reported and discussed. For example, Fig. 20a–b shows scanning electron microscopy (SEM) images of as-prepared 2D macroporous $SnO_2$/$TiO_2$ NTs at two different magnifications. The $SnO_2$ grew in an orderly 2D periodic nanoholes with circular orifices of diameter from 150 to 400 nm (Li et al., 2012). Fig. 20c presents the comparison of the X-ray diffraction (XRD) patterns for a typical $SnO_2$/$TiO_2$ NTs and a 2D macroporous $SnO_2$/$TiO_2$ NTs material As can be observed, the diffraction peak of $SnO_2$ rutile in the latter material was enhanced, being determined a smaller particle size and surface area alongside a high degree of dispersion that improved the PEC performance (Li et al., 2012). Fig. 21a–b shows the field emission SEM (FE-SEM) images of synthesized $TiO_2$ NTs and GO/$TiO_2$ NTs, by Rajput et al. (2018a). The GO particles covered most of the $TiO_2$ NTs and coexisted with the rest of uncovered region, increasing the oxidation sites for PEC.

Table 3 illustrates the excellent degradation, and in some cases mineralization, reached during the PEC treatment of selected herbicides with a variety of photoanodes illuminated with UVA light or simulated sunlight with Xe lamps. The comparative herbicide concentration removal was also assessed by AO (without light irradiation) and PC (without current). Results of Table 3 reveal a quite poor degradation by these processes, being the sum of both herbicide decays lower than that of PEC. This evidence the synergism with cooperation of the oxidants formed from the two individual processes in PEC. In contrast, a quite additive behavior can be seen in Figs. 20d–e for the concentration and COD profiles, obtained for several treatments of 100 mg $L^{-1}$ of 2,4-D in 0.10 M $Na_2SO_4$ at pH 3.0 with $SnO_2$/$TiO_2$ NTs and 2D macroporous $SnO_2$/$TiO_2$ NTs under a 300 W UVA light. In both cases, the oxidation power increased in the sequence: PC < AO ≪ PEC, always with better abatements for the latter photoanode. The PC process with $TiO_2$ NTs yielded much smaller performance. Fig. 20f highlights that for the most powerful PEC treatment with the 2D macroporous $SnO_2$/$TiO_2$ NTs photoanode, the instantaneous current efficiency (ICE), calculated considering the term d(COD)/d$t$ instead of ($\triangle$COD)/$t$ in Eq. (19), attained its maximum value of 100%, indicating that all the electric charge supplied to the electrolytic system was spent in organic oxidation.

Aqueous sulfate media have been tested aiming to assess the role of ROS generated by the photoanode. Rajput et al. (2018a) analyzed the scavenging of 20 mg $L^{-1}$ pentachlorophenol in 0.010 M $Na_2SO_4$ at pH 3.14 with a GO/$TiO_2$ NTs photoanode upon a 3.2 W $cm^{-2}$ UVA exposition at $I = 10.28$ mA for 93 min. Isopropyl alcohol (IPA), disodium ethylenediaminetetraacetate (EDTA) and L-ascorbic acid were employed as $^{\bullet}OH$, $h^+_{VB}$ and $O_2^{\bullet-}$ scavengers. As can be seen in Fig. 21c, $^{\bullet}OH$ formed from reactions (1) and (38) was the most pre-eminent oxidizing agent (47% degradation), with preponderance of that produced from $h^+_{VB}$ (38% degradation), whereas the participation of $O_2^{\bullet-}$generated from reaction (39) only accounted for by a 23% degradation since the photoexcited $e^-_{CB}$ were pre-eminently extracted and sent to the cathode. The authors proposed the reaction sequence of Fig. 22 that includes 6 aromatic and 2 aliphatic by-products identified by HPLC-MS analysis of the treated pentachlorophenol solution. The Cl atoms were lost in the form of $Cl^-$ ion.

Low $E_{an}$ (<+1.5 V) or $I$ (<30 mA) values were selected for the PEC trials to preserve the structure and oxidation power of the photoanode (see Table 3). For the degradation of 100 mL of 50 mg $L^{-1}$ of the chlorophenoxy acid (S)-dichlorprop in 0.10 M $Na_2SO_4$ with a Ti/$TiO_2$ photoanode upon a 300 W Xe lamp, Zhang et al. (2017) found that the herbicide underwent a 92% concentration reduction after 6 h at $E_{an} = +0.9$ V/SCE, with a small loss of performance after reuse in three consecutive cycles. In contrast, Özcan et al. (2018) reported that the degradation of 150 mL of 37.4 μM paraquat in 0.10 M $Na_2SO_4$ with a Ti/$TiO_2$ NTs-Pt photoanaode upon a 48 W UVA light at an optimum $E_{an} = +1.0$ V/Ag|AgCl for 180 min decayed from 64% to 42% after 25 consecutive reuses, probably due to the adsorption of by-products at the photoanode surface, diminishing the number of active sites for organic oxidation.

Similar effects of applied $I$ and herbicide concentration to those of precedent EAOPs have been described for the PEC process as result of the enhancement or inhibition of the parasitic reactions of the radical oxidants M($^{\bullet}OH$) and $^{\bullet}OH$, as explained above (Wang et al., 2019). However, the influence of pH on herbicide abatement is not so clear. While several authors describe a progressive loss of herbicide performance from pH 3 to alkaline medium, in agreement with the decrease of the oxidation power of M($^{\bullet}OH$) and $^{\bullet}OH$ (Liu et al., 2011), in the case of atrazine, an optimum degradation at pH 6 has been described, related to its adsorption characteristics on the $TiO_2$ surface (Komtchou et al., 2016).

### 4.5. Combined treatments

Hybrid and sequential treatments of recalcitrant herbicide wastewaters have been developed aiming the acceleration of the removal of organic pollutants and cost reducing. Hybrid processes are performed by direct combination of the electrochemical system with additional oxidation techniques or adsorption over carbonaceous materials. Light irradiation in PE and/or US in SE have been proposed pre-eminently by the Rodrigo's group for the remediation of effluents extracted from soils contaminated with herbicides and surfactants. Less attention has been paid over sequential processes, where biological pre- or post-treatments or pre-bioadsorption of pollutants are coupled to the electrochemical one. Table 4 collects relevant results obtained for combined techniques for selected herbicide removals, which are discussed in this subsection.

#### 4.5.1. Hybrid processes

The majority of hybrid processes are focused to the enhancement of the AO treatment of herbicide wastewaters by combination with light irradiation or US. For the first arrangement, UVC lamps immersed or over the solution of a cylindrical cell or illuminating the quartz cover of a filter-press cell coupled to a flow system like of Fig, 3d are employed. The UVC irradiation photodegrades many organic pollutants and additionally, it can produced extra oxidant radicals. So, in sulfate medium, the $S_2O_8^{2-}$ ion formed from anodic oxidation of $SO_4^{2-}$ via reaction (7) is photolyzed to $SO_4^{\bullet-}$, improving the oxidation ability of the system (Souza et al., 2020). More notable is the photoexcitation of active chlorine produced from reactions (10)–(12) in chloride medium, since HClO is photodecomposed in chlorine radical ($Cl^{\bullet}$) and $^{\bullet}OH$, and further, $Cl^{\bullet}$ can react with $Cl^-$ to yield the strong oxidant dichlorine radical anion ($Cl_2^{\bullet-}$) (Santos et al., 2020a). When an US horn is coupled, systems like of Fig. 5a–d are utilized. A double action of US is expected, involving the acceleration of the transport of reactants toward the anode alongside the extra production of the above oxidant radicals formed in sulfate and chloride media, upgrading their oxidation

**Table 3**
Selected results obtained for the photoelectrocatalysis (PEC) treatment of several herbicides in synthetic aqueous matrices with different photoelectrochemical systems.

| Pollutant | System (photoanode, cathode) | Experimental remarks | Best results | Ref. |
|---|---|---|---|---|
| *Chloroacetoanilide* | | | | |
| Alachlor | Cylindrical quartz cell upon a 75 W Xe lamp (Ti/$TiO_2$ NTs, Pt) | 30 mL of 5 mg $L^{-1}$ herbicide, 0.50 M $Na_2SO_4$, natural pH, $E_{an}$ = +1.50 V/SCE, 120 min | 12% degradation (AO), 60% degradation (PC[a]), 94% degradation (PEC). By-products detected | Xin et al. (2011) |
| *Chlorophenoxy acid* | | | | |
| 2,4-D | Quartz beaker upon a 500 W Xe lamp ($CuInS_2$/$TiO_2$ NTs, Pt) | 60 mL of 10 mg $L^{-1}$ herbicide, 0.050 M $Na_2SO_4$, pH 3.0, $E_{an}$ = +0.50 V/SCE, 160 min | 6% degradation (AO) $k_1$ = 0.0121 $min^{-1}$, 93% degradation (PC) $k_1$ = 0.0660 $min^{-1}$, 100% degradation (PEC) $k_1$ = 0.1011 $min^{-1}$ | Liu et al. (2011) |
| | Round reaction pool upon a 300 W UVA light ($SnO_2$/$TiO_2$ NTs, Ti) | 100 mL of 100 mg $L^{-1}$ herbicide, 0.10 M $Na_2SO_4$,natural pH, 25 °C, $I$ = 30 mA, 180 min | 100% degradation (120 min), 90% COD removal, ICE[c] = 100%. By-products detected | Li et al. (2012) |
| *Organochlorine* | | | | |
| Pentachlorophenol | Cylindrical glass cell upon two 36 W UVA light (GO[b]/$TiO_2$ NTs, Cu) | 250 mL of 15 mg $L^{-1}$ herbicide, 0.010 M $Na_2SO_4$, pH 3.14, $I$ = 20.68 mA, 93 min | 92% degradation, EC = 2.72 kWh $m^{-3}$. By-products detected | Rajput et al. (2018a) |
| *Triazine* | | | | |
| Atrazine | Similar to Fig. 4b with a 5.4 mW $cm^{-2}$ UVC light (Ti/$TiO_{2-x}$, graphite) | 1 L of 0.10 mg $L^{-1}$ herbicide, 0.050 M $Na_2SO_4$, pH 6.0, Flow rate = 10 L $h^{-1}$, $I$ = 100 mA, 120 min | 55% degradation (AO), 100% degradation (PC), 100% degradation at 60 min (PEC), $k_1$ = 0.146 $min^{-1}$. By-products detected | Komtchou et al. (2016) |
| | Cylindrical quartz cell upon a 1000 W Xe light at λ = 360 nm ($WO_3$, Pt) | 14 mL of 20 mg $L^{-1}$ herbicide (TOC$_0$ = 8.9 mg $L^{-1}$), 0.10 M $H_2SO_4$, $E_{an}$ = +1 V/Ag\|AgCl, 1320 min | 100% degradation (180 min), $k_1$ = 0.0233 $min^{-1}$, 72% TOC removal. By-products detected | Fernández-Domene et al. (2018b) |
| | Cylindrical quartz cell upon a 500 W Xe light (B,F-$TiO_2$ NTs, Ag) | 5 mg $L^{-1}$ herbicide, 0.10 M $Na_2SO_4$, pH 6, $I$ = 20 mA, 120 min | 21% degradation (AO), 30% degradation (PC), 76% degradation (PEC) | Wang et al. (2019) |
| *Urea* | | | | |
| Diuron | Cylindrical quartz cell upon a 1000 W Xe light at λ = 420 nm ($WO_3$, Pt) | 14 mL of 20 mg $L^{-1}$ herbicide, 0.10 M $H_2SO_4$, $E_{an}$ = +1 V/Ag\|AgCl, 360 min | 73% degradation, $k_1$ = 0.0035 $min^{-1}$, $Cl^-$ and $NO_3^-$ detected | Fernández-Domene et al. (2018a) |

[a] PC: Photocatalysis (no current).
[b] GO: Graphene oxide.
[c] Instantaneous current efficiency.

rate (dos Santos et al., 2017b). The main drawback of PE and SE is the enormous electric energy spent by the UVC lamps and US horns, then being necessary the development of systems powered with free and renewable energies for their practical use.

Similar effects of solution pH, applied current and herbicide concentrations to AO and AO-$H_2O_2$ have been described for the PE and SE treatments of synthetic herbicide solutions as well. In these studies, it is remarkable the influence of the supporting electrolyte and the nature of the anode. The PE process has been examined in sulfate medium for atrazine with a DSA anode (Malpass et al., 2010b), 2,4-D with a BDD anode (Souza et al., 2020), the triazine deethylatrazine with a Pt or BDD anode (Frangos et al., 2016) and the dinitroaniline trifluralin with a Pt anode (Hasanzadeh et al., 2018). In the two latter cases, an $O_2$-diffusion cathode to electrogenerate $H_2O_2$ was utilized, so that, the oxidation power of the system was upgraded by the extra generation of $^{\bullet}OH$ from the photolytic homolysis of $H_2O_2$, apart from other photogenerated radicals like $SO_4^{\bullet-}$, as stated above. Under these conditions, the PE process was synergistic as compared to the photocatalysis and AO (or AO-$H_2O_2$), which was more apparent for active anodes than for the more powerful non-active BDD. Malpass et al. (2010a) reported a concentration reduction of 55% by direct photolysis, 10% by AO and 88% by PE after 90 min of treatment of 22 L of 20 mg $L^{-1}$ atrazine in 0.10 M $Na_2SO_4$ at pH 3.0 in a flow plant like of Fig. 3d with a cylindrical cell equipped with a Ti/$Ir_{0.3}Ti_{0.7}O_2$ anode and a Ti cathode and an inner 36 W UVC lamp, by applying a $I$ = 108 A for the two latter treatments. The PE process was so powerful that yielded a small $E_{EO}$ value of 31 kWh $m^{-3}$ $order^{-1}$ and a high TOC removal of 90% (see Table 4).

Other important features have been detailed when using chloride media. Atrazine (Malpass et al., 2012), a real effluent of atrazine manufacturing process (Aquino et al., 2017) and tebuthiuron (Montes et al., 2017) with a DSA anode, 2,4-D (Souza et al., 2016b) and clopyralid (Santos et al., 2020a) with a BDD anode, and glyphosate (Sánchez-Montes et al., 2020) and clopyralid (Santos et al., 2020b) with a DSA or BDD anode, have been treated by PE. The results of Table 4 show a large enhancement of this process for DSA electrodes. While 100% degradation with 43% TOC removal were achieved for clopyralid with a BDD anode, a slight lower degradation of 89% with higher TOC decay of 47% were reached

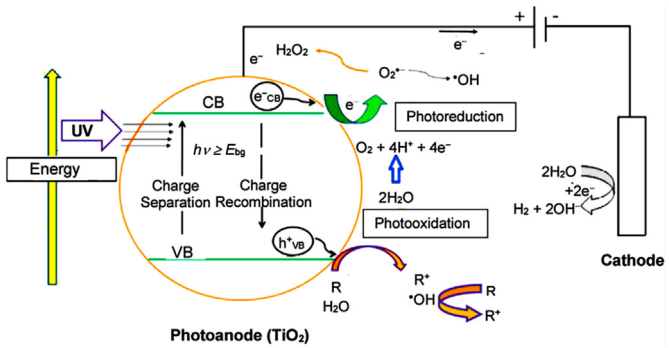


**Fig. 18.** Schematic mechanism of the processes taking place in a $TiO_2$ photoanode upon PEC. Adapted from Garcia-Segura and Brillas (2017).

with a $RuO_2TiO_2$ anode (Santos et al., 2020b). In the case of glyphosate, Sánchez-Montes et al. (2020) reported even a higher TOC reduction with a $Ti/Ir_{0.3}Ti_{0.7}O_2$ anode than a BDD one (100% vs. 67%). This behavior results of the large photogeneration of $^{\bullet}OH$, $Cl^{\bullet}$ and $Cl_2^{\bullet -}$ that destroy the organic pollutants at high rate, practically regardless of the ROS produced from the simple AO process. The relevance of these oxidizing agents can be deduced from the work of Rubí-Juárez et al. (2016a), who checked the PE treatment of 600 mL of 100 mg $L^{-1}$ glyphosate in different electrolytes at natural pH with a BDD anode at 0.78 A lasting 180 min. As can be seen in Table 4, TOC was reduced by 100% in 3.0 g $L^{-1}$ $Na_2SO_4$ and largely, up to 92% in 3.0 g $L^{-1}$ NaCl, whereas a good mineralization of 78% was achieved in 3.0 g $L^{-1}$ $Na_2CO_3$. The latter positive finding was found despite the scavenging effect of $CO_3^{2-}$ ion over generated ROS, owing to the potent oxidative action of photoproduced $Cl^{\bullet}$ and $Cl_2^{\bullet -}$.

The Rodrigo's group extended their initial research on the treatment of 100 mg $L^{-1}$ of oxyfluorfen in a soil-washing effluent with SDS as surfactant by AO (see section 4.1.2.2 and Table 1) to the PE process with a 15 W UVC irradiation (dos Santos et al., 2017a) and the SE one with an US of 24 kHz and 200 W (dos Santos et al., 2017b). In both cases, faster degradation of the herbicide and SDS was detected, with the accumulation of more quantities of released $SO_4^{2-}$ ion, an indirect measurement of SDS mineralization. Table 4 highlights that after consuming a $Q = 30–40$ Ah $L^{-1}$ in SE, 100% of COD and TOC removal were found, making in evidence the potentiality of this technique for soil remediation.

Table 4 shows the good performance of the SE process, superior to the homologous AO one, for the cases of diuron in 10 g $L^{-1}$ $Na_2SO_4$ with the BDD/BDD cell of Fig. 5a (Bringas et al., 2011) and 2,4-D in 3.0 g $L^{-1}$ NaCl with a flow Diacell® 401 cell of 3 compartments with bipolar BDD electrodes (Souza et al., 2015b). In the former case, the expected increase of the rate constant for TOC removal ($k_{TOC}$) with temperature, from 0.305 $h^{-1}$ at 10 °C to 0.416 $h^{-1}$ at 40 °C, related to a very low activation energy of 7.7 kJ $mol^{-1}$, was reported.

The PE and SE processes have been compared for the treatment of the urea chlorsulfuron in 0.050 M $Na_2SO_4$ or 0.050 M NaCl using a flow filter-press BDD/BDD cell (Souza et al., 2017) and atrazine in 1.73 M NaCl pH 7.0 with a plant like of Fig. 3d with a $Ti/Ru_{0.3}Ti_{0.4}O_2$ anode, a Ti cathode and a reservoir with a 9 W UVC light and a 60 W US (Pinto et al., 2019). The latter authors optimized the process by RSM and determined that the best results were obtained at $I = 200$ mA, with total herbicide removal at 50 min for PE or SE and only 30 min for the combined PE/SE process, where 98% of TOC was reduced in 240 min with a low EC of 3.36 kWh $m^{-3}$, only consumed by the electrolytic cell (see Table 4). More research should be made to confirm the benefits of combining PE and SE instead of each single process.

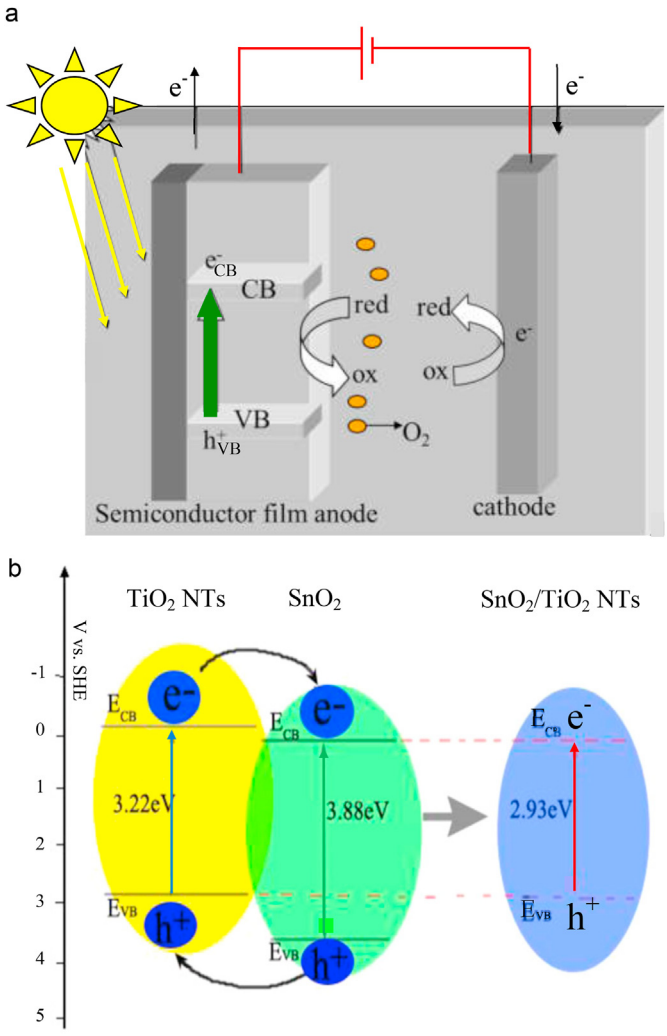


**Fig. 19.** Mechanism of the PEC process with different photoanodes for the degradation of herbicide solutions. (a) $Ti/IrO_2$-Pt-$WO_3$ or $Ti/IrO_2$-Pt-$Ag_3PO_4$ under simulated solar light. Adapted from Guo et al. (2017). (b) 2D microporous $SnO_2$ assembled into $TiO_2$ NTs upon UVA light. Adapted from Li et al. (2012).

It has been described the PE or SE treatments, compared to sonolysis, photolysis and AO, of soil-washing effluents with SDS surfactant contaminated with the dinitroaniline pendimethalin (Almazán-Sánchez et al., 2017) and atrazine (dos Santos et al., 2018), with a flow plant like of Fig. 5d with a filter-press BDD/SS cell with a quartz cover for illumination with a 4 W and 15 W UVC, and an US of 24 kHz and 200 W. Fig. 23 depicts the change of atrazine concentration, TOC and COD with time for 100 and 5000 mg $L^{-1}$ of SDS contents at $j = 30$ mA $cm^{-2}$. While the herbicide decayed more rapidly with the higher SDS content, the opposite behavior can be observed for TOC and COD removal due to the presence of more quantities of organic matter. The oxidation power of treatments increased as: sonolysis < photolysis ≪ AO < SE < PE, indicating a greater enhancement of the destruction rate of organics by UVC photolysis and oxidation with photogenerated oxidants in PE (see Table 4).

Other hybrid processes have considered the combination of AO with ozonation to destroy atrazine in phosphate + $Na_2SO_4$ with a cylindrical BDD/SS reactor (Saylor et al., 2018) and diuron in 0.050 M $Na_2SO_4$ using a cylindrical Pt/RVC cell (Bavasso et al., 2020). In the latter system, $H_2O_2$ was electrogenerated in the cathode, which reacted with $O_3$ at pH 10 to produce additional ROS

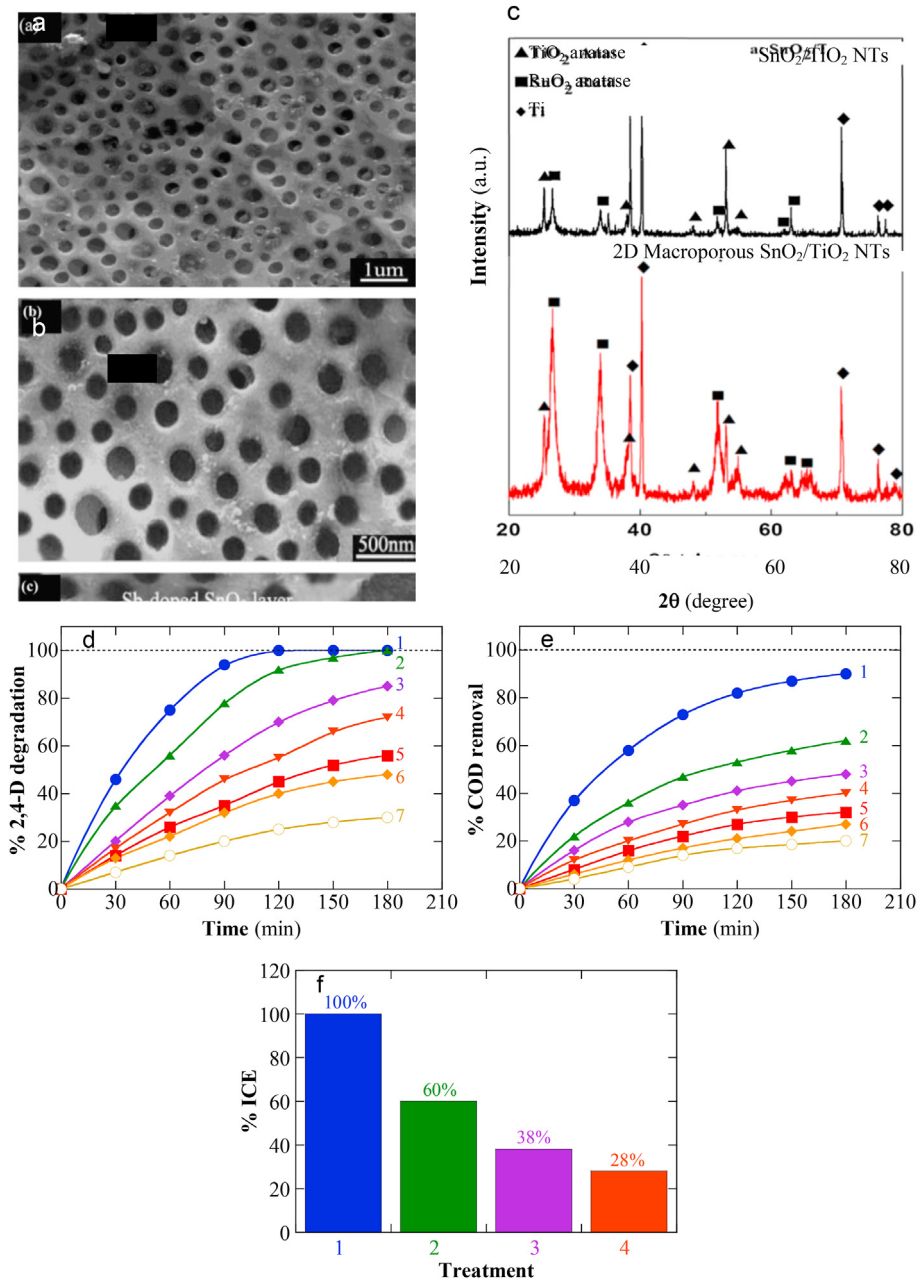


**Fig. 20.** SEM images of synthesized (a) and (b) 2D macroporous $SnO_2/TiO_2$ NTs electrodes or photocatalysts. (c) XRD patterns for $SnO_2/TiO_2$ NTs and 2D macroporous $SnO_2/TiO_2$ NTs. Variation of (d) percentage of 2,4-D degradation and (e) percentage of COD removal for the treatment of 100 mL of 100 mg $L^{-1}$ herbicide in 0.10 M $Na_2SO_4$ at pH 3.0 using a stirred cylindrical tank reactor with a 3 $cm^2$ electrode or photocatalyst and a 3 $cm^2$ Ti cathode. Treatments with: 2D macroporous $SnO_2/TiO_2$ NTs using (1) photoelectrocatalysis (PEC), (3) AO and (5) photocatalysis (PC); $SnO_2/TiO_2$ NTs using (2) PEC, (4) AO and (6) PC. In PEC, the electrodes acted as photoanodes upon a 300 W UVA illumination. In PEC and AO, a $j = 10$ mA $cm^{-2}$ was applied. (7) $TiO_2$ NTs/UVA photocatalysis (PC). (f) Instantaneous current efficiency for PEC and AO processes at 30 min. Adapted from Li et al. (2012).

($^{\bullet}OH$, $HO_2^{\bullet}$, $O_3^{\bullet-}$) that largely contribute to organic removal. This process is known as electro-peroxone. Table 4 shows the rapid diuron degradation and almost total mineralization achieved operating with this procedure.

Variable effectiveness has been reported for other less explored hybrid methods. Raschitor et al. (2017) and Llanos et al. (2018) conditioned an electrodialysis cell with an anionic and a cationic membrane to concentrate a 2,4-D effluent for subsequent oxidation at a DSA or BDD anode. However, similar performance was obtained operating without both membranes, i.e., by only AO, particularly for the most potent BDD, making such combination unviable. More positive results have been described by Dargahi et al. (2018) for 2,4-D and by Pedersen et al. (2019) for other chlorophenoxy acids using the BDD/SS and β-$PbO_2$/SS cells like of Fig. 5a, with simultaneous adsorption on GAC and AO. For 2,4-D, Table 4 reveals that the presence of the adsorbent enhances its removal from 72% to 93% at pH 3.0 after 100 min at 36 mA. Xu et al. (2019) also detailed a positive upgrading of sodium pentachlorophenate by adsorption/AO with a dual CNT/$PbO_2$ anode. The hybrid adsorption/AO treatment could then be useful for ionic herbicides like 2,4-D and pentachlorophenate ion, easily adsorbed onto high-surface carbonaceous materials. Other articles have been devoted to the combination of AO with $MnO_2$ for glyphosate removal with a DSA/DSA cell (Lan et al., 2013) and that of AO with PEC for the urea fenuron

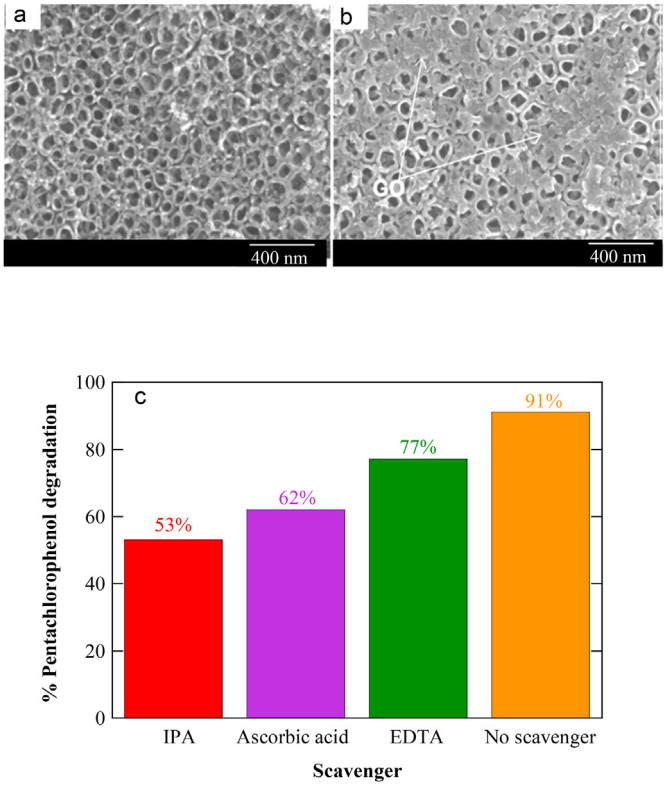


**Fig. 21.** FE-SEM images of (a) $TiO_2$ NTs and (b) graphene oxide (GO)/$TiO_2$ NTs photoanodes used for the PEC treatment of 250 mL of 20 mg $L^{-1}$ pentachlorophenol in 0.010 M $Na_2SO_4$ in a cylindrical glass reactor upon a 3.2 W $cm^{-2}$ UVA exposition. (c) Effect of different scavengers (isopropyl alcohol (IPA) as $^{\bullet}OH$ scavenger, disodium ethylenediaminetetraacetate (EDTA) as $h^+_{VB}$ scavenger and L-ascorbic acid as $O_2^{\bullet-}$ scavenger) on the percentage of pentachlorophenol degradation with a GO/$TiO_2$ NTs photoanode at applied $I$ of 20.68 mA; pH 3.14 and degradation time of 93 min. Adapted from Rajput et al. (2018a).

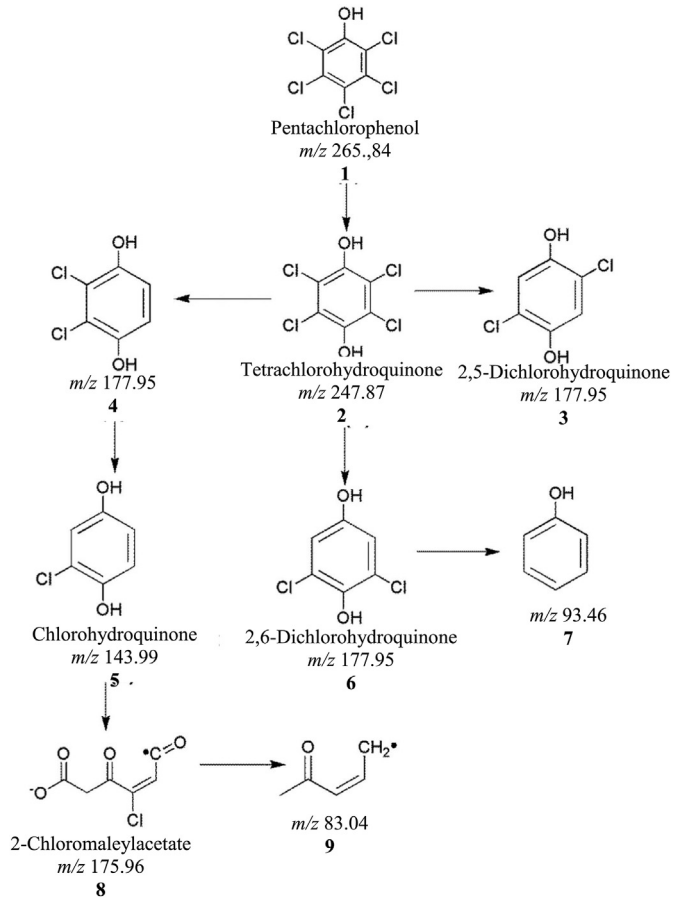


**Fig. 22.** Degradation route for pentachlorophenol in acidic sulfate medium by PEC with a GO/$TiO_2$ nanotube arrays photoanode upon UVA illumination. Adapted from Rajput et al. (2018a).

with a dual $PbO_2/SnO_2$-$Sb_2O_3$/Ti//Ti/$TiO_2$ anode/photoanode (Barbari et al., 2018).

It is remarkable the work of Garza-Campos et al. (2014) who studied 200 mL of 20 mg $L^{-1}$ atrazine in 0.050 M $Na_2SO_4$ at pH 3.0 with the BDD/BDD cell of Fig. 5b by individual SPC, AO, EF and SPEF alongside the hybrid SPC/SPEF. The SPC process was performed with 0.3 g $L^{-1}$ of $TiO_2$ onto glass spheres and the electrolytic trials were made at 100 mA. Fig. 24a–c disclose an increasing oxidation ability in the sequence: SPC ≪ AO ≪ EF < SPEF < SPEC/SPEF, as expected by the greater production of $^{\bullet}OH$ from reactions (38), (1), (24) and (34), with photodecomposition of final Fe(III)-carboxylate complexes by reaction (35). All these reactions occur simultaneously in SPEC/SPEF. Fig. 24b presents the increasing accumulation of cyanuric acid, the major aromatic by-product of atrazine, in the same oxidation power order. Figs. 24d–e shows that the higher MCE and lower $EC_{TOC}$ values corresponded to the combined SPEC/SPEF. The results obtained at 300 min are collected in Table 4.

### 4.5.2. Sequential processes

A reduced number of studies have reported the coupling of AO followed by a biological treatment of the resulting wastewater initially contaminated with a herbicide. Feng et al. (2013) pretreated an actual wastewater of a clomazone factory by AO with a flow tubular three-dimensional Ti/$SnO_2$ cell, whereas the AO pretreatment with a flow cell with a graphite cell anode has been checked for the treatment of 2,4-D (Fontmorin et al., 2013) and the commercial herbicide U46D® solution (Fontmorin et al., 2014). These articles show a notable enhancement of the biodegradability of the resulting wastewater after the AO pre-treatment, reducing significantly the time needed for total mineralization by subsequent biological treatment. In contrast, Carboneras et al. (2020) carried out a biological pre-treatment followed by an AO process. In the biological pre-treatment, 500 mg $L^{-1}$ oxyfluorfen were degraded in 500 mL bioreactors with a bacterial culture during 70 h at 30 °C, giving rise to an 88% degradation of the herbicide. The further AO process was made with a flow plant like of Fig. 3d with a Diacell® 101 BDD/SS cell, and overall degradation and mineralization were achieved after consumption of 26 Ah $L^{-1}$ (see Table 4). It was also found that addition of 0.035 M $Na_2SO_4$ yielded a more cost-effective AO post-treatment since total decontamination was reached at only $Q$ = 18 Ah $L^{-1}$ with an EC reduction from 360 to 122 kWh $m^{-3}$.

Sequential biosorption-electrochemical treatments have been reported for the remediation of soil-washing effluents spiked with 2.4-D (Chair et al., 2017a) and oxyfluorfen (Chair et al., 2017b) with SDS as surfactant. Fig. 25a illustrates the drastic abatement of 60 mg $L^{-1}$ oxyfluorfen with raising the biomass/herbicide ratio (BHR) upon biosorption with an activated sludge, whereas the corresponding COD underwent a continuous increase due to the accumulation of organics. Figs. 25b–c depict the change of normalized oxyfluorfen concentration and TOC with $Q$ by different treatments in a flow plant like of Fig. 5d with a filter-press BDD/stainless steel cell at $j$ = 30 mA $cm^{-2}$. A similar decay can be

**Table 4**
Selected results obtained for hybrid and sequential treatments of several herbicides pollutants in synthetic aqueous matrices.

| Pollutant | System (anode, cathode) | Experimental remarks | Best results | Ref. |
|---|---|---|---|---|
| **Hybrid process** | | | | |
| **Anodic oxidation/UV (Photoelectrolysis, PE)** | | | | |
| *Benzoic acid* | | | | |
| Clopyralid | Cylindrical cell under a 9 W UVC light (MMO-$RuO_2TiO_2$ or BDD, Pt) | 150 mL of 100 mg $L^{-1}$ herbicide, ($COD_0$ = 130 mg $L^{-1}$), 3.7 g $L^{-1}$ NaCl, natural pH 3.4, $I$ = 120 mA, 480 min | 100% degradation (BDD), 43% COD removal (BDD), 89% degradation (MMO), 47% COD removal (MMO) | Santos et al. (2020b) |
| *Chlorophenoxy acid* | | | | |
| 2,4-D | Fig, 3d with a filter-press cell with a quartz site upon a 15 W UVC light (BDD, SS) | 1.2 L of 100 mg $L^{-1}$ herbicide, 0.050 M $Na_2SO_4$ or NaCl, Flow rate: 26.4 L $h^{-1}$, natural pH, $I$ = 7.8 A, $Q$ = 18 Ah $L^{-1}$ | $k_1$ = 0.62 $h^{-1}$ ($Na_2SO_4$), $k_1$ = 0.72 $h^{-1}$ (NaCl), 100% TOC removal ($Na_2SO_4$) 78% TOC decay (NaCl) By-products detected Inorganic ions detected | Souza et al. (2016b) |
| *Diphenyl ether* | | | | |
| Oxyfluorfen | Fig. 3d with a filter-press cell upon a 15 W UVC light (BDD, SS) | 1 L of 100 mg $L^{-1}$ herbicide spiked in a soil washing effluent with SDS surfactant (dosage from 100 to 5000 mg $L^{-1}$), Flow rate = 200 L $h^{-1}$, $Q$ = 20 Ah $L^{-1}$ | 100% degradation, 100% SDS removal. 1.2 g $L^{-1}$ $SO_4^{2-}$ released | dos Santos et al. (2017a) |
| Glyphosate | Fig. 3d with a filter-press cell upon a 4 W UVC light (BDD, SS) | 600 mL of 100 mg $L^{-1}$ herbicide, 3.0 g $L^{-1}$ $Na_2CO_3$, $Na_2SO_4$ or NaCl, natural pH, $I$ = 0.78 A, 180 min. | TOC reduction: 78% ($Na_2CO_3$), 92% (NaCl), 100% ($Na_2SO_4$). Inorganic ions detected | Rubí-Juárez et al. (2016a) |
| | Fig. 3d with a filter-press cell and an immersed 9 W UVC light (DSA-Ti/$Ir_{0.3}Ti_{0.7}O_2$ or BDD, SS) | 1.5 L of 50 mg $L^{-1}$ herbicide, 3.0 g $L^{-1}$ NaCl, pH 4–5, Flow rate = 29.1 L $h^{-1}$, 25 °C, $I$ = 0.78 A, 60 min. | TOC reduction: 100% (DSA) with MCE = 18%, 67% (BDD) with MCE = 13%. By-products detected Inorganic ions detected | Sánchez-Montes et al. (2020) |
| *Triazine* | | | | |
| Atrazine | Fig. 3d with a 36 W UVC light immersed in the cylindrical cell (Ti/$Ir_{0.3}Ti_{0.7}O_2$, Ti) | 22 L of 20 mg $L^{-1}$ herbicide, 0.10 M $Na_2SO_4$, pH 3.0, Flow rate = 3000 L $h^{-1}$, 20 °C, $I$ = 108 A, 90 min. | 10% (AO) 55% (photolysis) 88% degradation, (PE) with $E_{EO}$ = 31 kWh $m^{-3}$ $order^{-1}$, 90% TOC removal | Malpass et al. (2010a) |
| *Urea* | | | | |
| Tebuthiuron | Fig. 3d with a filter-press cell upon a 125 W UVC light (Ti/$Ir_{0.3}Ti_{0.7}O_2$, SS) | 1 L of 100 mg $L^{-1}$ herbicide, 0.10 M $Na_2SO_4$ + 2.0 g $L^{-1}$ NaCl, pH 3.0, Flow rate = 420 L $h^{-1}$, $I$ = 250 mA, 360 min. | 100% degradation (90 min), 95% TOC removal, MCE = 6%, $EC_{TOC}$ = 6 kWh (g TOC)$^{-1}$. By-products detected | Montes et al. (2017) |
| **Anodic oxidation/US (Sonoelectrolysis, SE)** | | | | |
| *Chlorophenoxy acid* | | | | |
| 2,4-D | Fig. 5d with a Diacell® 401 cell up to 3 compartments, US of 24 kHz and 200 W (BDD, BDD) | 1.2 L of 100 mg $L^{-1}$ herbicide, 3.0 g $L^{-1}$ NaCl, natural pH 3.4, Flow rate = 26.4 L $h^{-1}$, 25 °C, $I$ = 10 A, 72 min | For 3 compartments: 100% degradation, 100% COD removal, 100% TOC removal. By-products detected | Souza et al. (2015b) |
| *Diphenyl ether* | | | | |
| Oxyfluorfen | Fig. 5d, US of 24 kHz and 200 W (BDD, SS) | 1 L of 90 mg $L^{-1}$ herbicide spiked in a soil washing effluent with SDS surfactant (dosage 400 mg $L^{-1}$), Flow rate = 200 L $h^{-1}$, $I$ = 2.1 A, $Q$ = 30–40 Ah $L^{-1}$ | 100% degradation, 100% COD removal, 100% TOC removal. 900 mg $L^{-1}$ $SO_4^{2-}$ released | dos Santos et al. (2017b) |
| *Urea* | | | | |
| Diuron | Fig. 5a, US of 20 kHz and 750 W (BDD, BDD) | 250 mL of 20 mg $L^{-1}$ herbicide, 10 g $L^{-1}$ $Na_2SO_4$, pH 12, 10 °C, $I$ = 700 mA, 360 min | 100% degradation, $k_1$ = 0.712 $h^{-1}$, 92% TOC removal, $k_{TOC}$ [a] = 0.305 $h^{-1}$, $k_{TOC}$ = 0.416 $h^{-1}$ (40 °C) | Bringas et al. (2011) |
| **Photoelectrolysis, Sonoelectrolysis** | | | | |
| *Triazine* | | | | |
| Atrazine | Fig. 5d with a filter-press cell upon a 15 W UVC light, US of 24 kHz and 200 W (BDD, SS) | 700 mL of 100 mg $L^{-1}$ herbicide spiked in a soil-washing effluent with SDS surfactant (dosage 100 mg $L^{-1}$), Flow rate = 160 L $h^{-1}$, $I$ = 2.34 A, 420 min | 100% degradation: 420 min (AO or SE) 300 min (PE), 100% TOC removal: 360 min (AO) 300 min (SE) 180 min (PE) | dos Santos et al. (2018) |
| | Fig. 3d with a reservoir with a 9 W UVC light and a 60 W US (Ti/$Ru_{0.3}Ti_{0.4}O_2$, Ti) | 15 mg $L^{-1}$ herbicide, 1.73 M NaCl, pH 7.0, Flow rate = 26.3 L $h^{-1}$, 25 °C, $I$ = 200 mA, 240 min | 100% degradation: 50 min (PE or SE) 30 min (PE/SE) | Pinto et al. (2019) |

**Table 4** (*continued*)

| Pollutant | System (anode, cathode) | Experimental remarks | Best results | Ref. |
|---|---|---|---|---|
| | | | 98% TOC removal (PE/SE)<br>EC = 3.36 kWh $m^{-3}$ | |
| **Other hybrid treatments** | | | | |
| *Chlorophenoxy acid* | | | | |
| 2,4-D | Fig. 5c with 40 g $L^{-1}$ GAC [b] ($\beta$-$PbO_2$, SS) | 250 mL of 200 mg $L^{-1}$ herbicide, 4.0 g $L^{-1}$ $Na_2SO_4$, pH 3.0–10.0, $I$ = 36 mA, 100 min | 72% degradation (pH 3.0, no GAC)<br>92% degradation (pH 3.0, with GAC).<br>By-products detected | Dargahi et al. (2018) |
| *Triazine* | | | | |
| Atrazine | Fig. 5b, SPEF/SPC with 180 $TiO_2$ glass spheres (BDD, BDD) | 200 mL of 20 mg $L^{-1}$ herbicide, 0.050 M $Na_2SO_4$, 0.10 mM $Fe^{2+}$, pH 3.0, $I$ = 100 mA, 300 min | 100% degradation (120 min)<br>$k_1$ = 0.034 $s^{-1}$,<br>80% TOC removal,<br>MCE = 9%<br>$EC_{TOC}$ = 1.93 kWh $(g\ TOC)^{-1}$<br>By-products detected | Garza-Campos et al. (2014) |
| *Urea* | | | | |
| Diuron | Cylindrical cell, $O_3$+$H_2O_2$, electro-peroxone (Pt, RVC with $H_2O_2$ electrogeneration) | 100 mL of 40 mg $L^{-1}$ herbicide, 0.050 M $Na_2SO_4$, pH 10, $O_3$ flow rate = 260 mg $L^{-1}$ $h^{-1}$, 24 °C, $I$ = 50 mA, 180 min | 100% degradation (30 min),<br>92% TOC removal,<br>MCE = 9% | Bavasso et al. (2020) |
| **Sequential process** | | | | |
| *Diphenyl ether* | | | | |
| Oxyflourfen | Biological treatment followed by AO with a flow system like of Fig. 3d with a Diacell® 101 cell (BDD, SS) | Biological: 500 mg $L^{-1}$ herbicide with a culture after 70 h at 30 °C. AO: resulting wastewater, pH 7.2, Flow rate = 54 L $h^{-1}$, $I$ = 2.34 A | 88% degradation after biological treatment.100% degradation and 100% TOC removal after AO at $Q$ = 26 Ah $L^{-1}$,100% TOC removal after AO by adding 0.035 M $Na_2SO_4$ at 18 Ah $L^{-1}$ | Carboneras et al. (2020) |
| | Biosorption followed by AO with a flow system like of Fig. 5d with a filter-press cell (BDD, SS) | Biosorption: active sludge on 60 mg $L^{-1}$ herbicide spiked in a soil washing effluent with SDS surfactant with a biomass load of 20. AO: 2 L of the resulting wastewater, Flow rate = 200 L $h^{-1}$, $I$ = 2.34 A, $Q$ = 80–120 Ah $L^{-1}$ | 100% degradation (50 Ah $L^{-1}$),<br>100% TOC removal.<br>Inorganic ions detected | Chair et al. (2017b) |

[a] $k_{TOC}$: Rate constant for TOC removal.
[b] GAC: Granular activated carbon.

observed in Fig. 25b using AO, PE with a 4 UVC light, high frequency-SE (HF-SE) with US of 100 MHz and low frequency–SE (LF-SE) with US of 24 Hz. This indicates that the main oxidant is always M(•OH) formed at the BDD anode. In contrast, the photolytic action of UVC irradiation favored the overall TOC removal by PE at $Q$ = 80 Ah $L^{-1}$, whereas the other three methods required near $Q$ = 120 Ah $L^{-1}$ (see Table 4). Again, the PE treatment became superior to AO and SE, as stated above (see Fig. 23). The oxidation of $Cl^-$ present in the effluent with conversion into toxic $ClO_3^-$ and $ClO_4^-$ and the accumulation of $NO_3^-$ and $NH_4^+$ from the destruction of nitrogenated organics during the PE process, are shown in Fig. 25d–e.

Some sequential electrochemical-electrochemical processes have been explored as well. So, alachlor dechlorination with a Ni/Ag cathode was performed to accelerate the subsequent EF with a Pt/graphite felt cell (Lou et al., 2020). Electrocoagulation was applied to concentrate oxyfluorfen in sulfate medium, which was further degraded more quickly by EF than by AO using a flow plant with a BDD/BDD cell (Raschitor et al., 2019).

## 5. Future challenges

The information available over herbicide remediation by EAOPs has been pre-eminently obtained with synthetic solutions at lab-scale using cylindrical cells and flow plants with small wastewater volumes and small electrodes. Then, there is a lack of knowledge over the electrochemical behavior of real agricultural wastewaters and contaminated soils with complex organic and inorganic matrices. This is a first important challenge to be solved because large discrepancies exist between real environmental concentrations of herbicides in agricultural wastewaters and those tested in lab settings, even of several orders of magnitude (Garcia-Segura et al., 2020). The influence of the matrix (other organics, natural organic matter, inorganic ion composition) should be clearly elucidated to better understand the consequences of competitive reactions and generation of different oxidizing agents (ROS, active chlorine) on the degradation and mineralization processes of the herbicide. In this way, the treatment of soil-washing effluents should be extended to real soils to confront their performance with that reported at present for kaolinite (dos Santos et al., 2018). A second challenge is the development of stable electrodes at industrial level with the establishment of steady conditions for long-time operation. Up to now, most research has been conducted in batch reactors during short-time periods rather than in continuous flow reactors. For this reason, there exist a lack of understanding of the mechanisms of electrode scaling and fouling that can be detrimentally influenced by the solutes and bacteria present in real agricultural wastewaters when passing by the electrode surfaces. These aims should be considered in future research to make the EAOPs viable at industrial level. As third challenge, the design and easily scalable efficient electrochemical plants with optimum cells and exciting systems (light radiation, US) should be made for their implementation if necessary. Autonomous electrochemical systems powered by free renewable energy (wind, solar

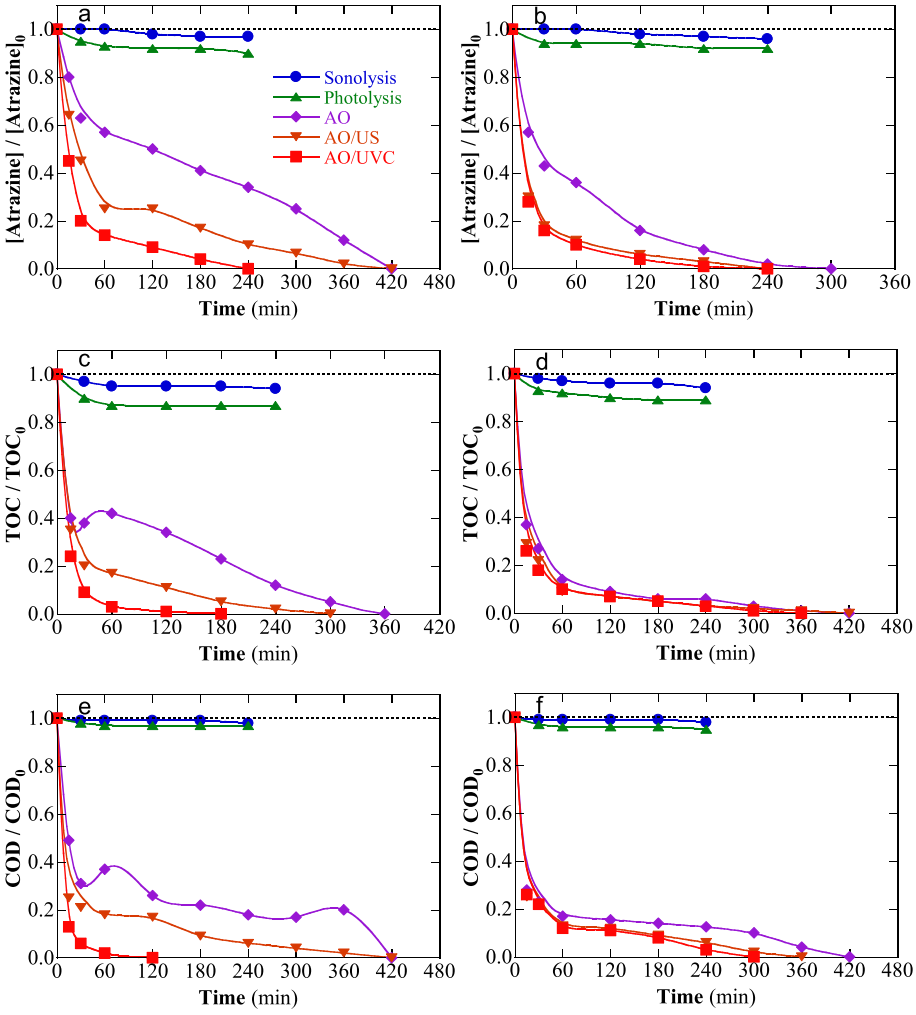


**Fig. 23.** Change of (a,b) normalized atrazine concentration, (c,d) normalized TOC and (e,f) normalized COD with time for different treatments (sonolysis, photolysis, AO, AO/US (or SE) and AO/UVC (or photoelectrolysis, PE)) of 700 mL of 100 mg $L^{-1}$ herbicide with (a,c,e) 100 and (b,d,f) 5000 mg $L^{-1}$ sodium dodecyl sulfate (SDS) using a flow electrochemical plant with a filter-press BDD/stainless steel reactor (78 $cm^2$ electrode area) with an US generator (24 kHz, 200 W). For the photolytic trials, a 15 W UVC light was irradiated through a quartz cover of the cell. The liquid flow rate was 160 L $h^{-1}$ and a $j$ = 30 mA $cm^{-2}$ was applied for the electrolytic experiments. Adapted from dos Santos et al. (2018).

photovoltaic panels) with low maintenance should be developed to make the EAOPs more attractive for their industrial use, even in remote regions. Finally, as fourth challenge, it is encouraged to the researchers to perform a techno-economic analysis for each process studied in order to demonstrate the competitive interest of applying EAOPs for treating wastewaters and soils contaminated with herbicides.

## 6. Conclusions

Nine kinds of treatments with EAOPs have been identified for herbicide remediation from synthetic wastewaters and soil-washing effluents in the last decade. Atrazine, 2,4-D and diuron are the major herbicides studied. The major part of electrochemical systems utilize undivided cylindrical tank reactors or flow cells with two- or three-electrodes. AO and AO-$H_2O_2$ present an analogous performance due to the very low oxidation power of $H_2O_2$ as compared to M(•OH). Non-active BDD is the more powerful anode because it produces larger amounts of M(•OH). In chloride medium, cheaper active $RuO_2$ anodes generate more quantity of active chlorine that can oxidize more rapidly the target herbicide than M(•OH). However, the BDD anode can mineralize more rapidly the solution since it can remove more easily the recalcitrant chloroderivatives formed. Good performance was also achieved using non-active anodes like $PbO_2$, $Co_3O_4$/graphite felt and Ti/$SnO_2$-Sb. Herbicide adsorption favors its removal with graphite. The degradation of herbicides in AO and AO-$H_2O_2$ obeys a pseudo-first-order kinetics, but their mineralization evolves with low COD and/or TOC decays, with small MCE and high $EC_{TOC}$ values, as result of the recalcitrant by-products generated. Techno-economic analysis based on $k_1$-values and $E_{EO}$ results valuable for benchmarking AO against available commercial technologies for water treatment. The rise of $j$ promotes the degradation and mineralization processes, but with a progressive decay in ACE or MCE alongside with greater energy consumption due to the acceleration of parasitic reactions. A similar behavior is found by decreasing the herbicide content in the wastewater. In chloride medium, the oxidation power of AO decreases at greater pH due to the change of active chlorine species. Optimum conditions for AO can be obtained by means of RSM. The competitive oxidation with other organic compounds accounts for by the slower degradation of herbicides in real wastewaters. AO is useful for the remediation of soil-washing effluents prepared from kaolinite as simulated soil. Preliminary studies have shown that the electrochemical systems can be powered by wind turbines or

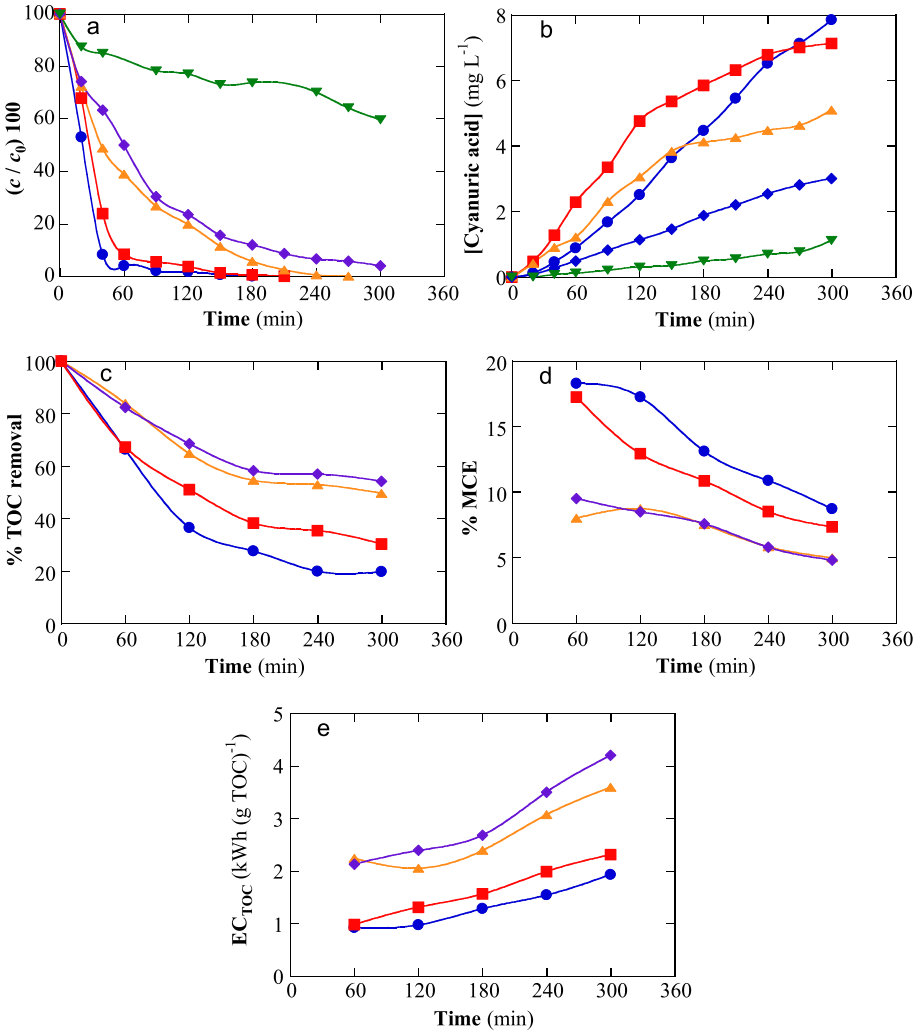


**Fig. 24.** Time course of (a) normalized atrazine concentration, (b) cyanuric acid concentration, (c) percentage of TOC removal, (d) mineralization current efficiency and (e) energy consumption per unit TOC mass for 200 mL of 20 mg $L^{-1}$ atrazine in 0.050 M $Na_2SO_4$ at pH 3.0 using the system of Fig. 5b. Method: (▼) SPC, (◆) AO with a Pt mesh cathode, (▲) EF, (■) SPEF and (●) hybrid SPC/SPEF. In the three latter processes, a BDD cathode was used and 0.10 mM $Fe^{2+}$ was added to the solution. The electrochemical treatments were made with a BDD anode at 100 mA. SPC was performed with 180 spheres of $TiO_2$-coated glass (0.3 g $L^{-1}$ of $TiO_2$). Adapted from Garza-Campos et al. (2014).

photovoltaic panels as renewable free and green energies. In many studies, a mineralization route for the target herbicide is proposed from the by-products detected.

Two kinds of homo-EF system are used for $H_2O_2$ electrogeneration: cylindrical two- or three electrodes tank reactors with an immersed carbonaceous cathode and cylindrical or flow filter-press cells with an anode and a gas ($O_2$ or air)-diffusion cathode. The homo-EF process in an undivided cell outperforms the homologous AO-$H_2O_2$ because of the quicker attack of organics by homogeneous •OH formed from Fenton's reaction. The herbicide mineralization is better enhanced with BDD than with Pt due to the more rapid attack of final iron-carboxylate complexes with M(•OH) originated by the former more potent anode. The optimum pH of homo-EF is 3.0, near to the optimum pH of Fenton's reaction, and the best $Fe^{2+}$ content depends on the kind of cathode utilized. Less information is known for hetero-EF using insoluble iron catalysts like Fe@$Fe_2O_3$ or iron-modified cathodes like allophane supported with $Fe_2O_3$ that offer a good performance at neutral pH with large stability.

The PEF process with UVA light outperforms the EF 1 at pH 3.0 by the formation of more •OH from the photolysis of $Fe(OH)^{2+}$ and the photodecomposition of final Fe(III)-carboxylate species. The SPEF process leads even to faster degradation and more rapid overall mineralization due to the higher UV irradiance of sunlight. This method is the EAOP with higher oxidation power for herbicide remediation. Flow plants with a solar CPC photoreactor are the best options to assess the SPEF process. Cheaper active anodes than non-active BDD can be used in SPEF because they yield similar herbicide performance. Good degradation and mineralization results were found for the PEF treatment of real wastewaters, e.g., chloramben spiked into an urban wastewater and metolachlor spiked into a real wastewater of winery industry. The PEC process of herbicides in wastewaters has been mainly focused to the preparation and characterization of new photoanodes like modified $TiO_2$ and $WO_3$ nanosheets, with $E_g$ values low enough to absorb visible light simulated with Xe lamps. Lower herbicide concentrations than the above EAOPs were usually treated by PEC due to the low stability of the photocatalyst. Low $E_{an}$ or $I$ values were applied to the PEC cell to preserve the photoanode stability. Under comparable conditions, the oxidation power is risen in the order: AO < PC < PEC, so that, PEC can follow an additive or synergistic process of the other two methods.

The major part of hybrid processes are focused to the enhancement of the AO treatment of herbicide wastewaters by PE

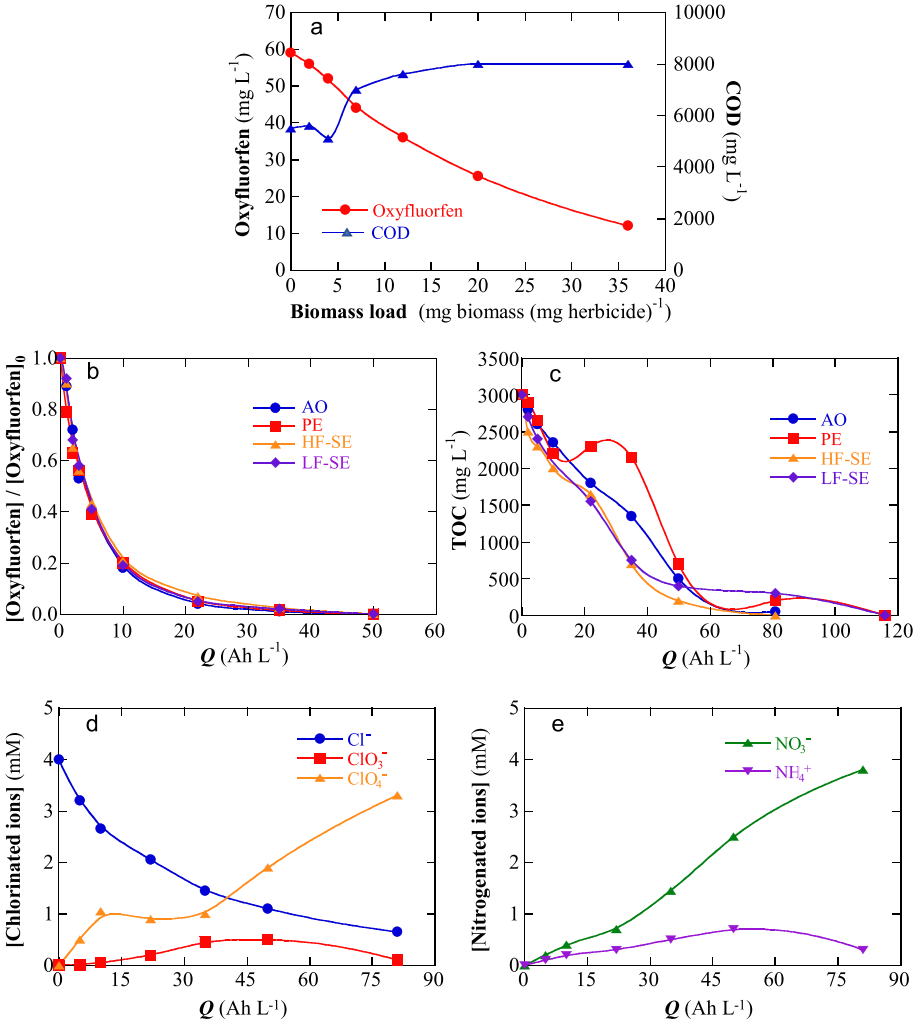


**Fig. 25.** (a) Oxyfluorfen concentration and COD as a function of the biomass/herbicide ratio (BHR) for the biosorption process on activated sludge of the effluent coming from the washing of a soil spiked with the herbicide and a SDS solubilizing agent. Change of (b) oxyfluorfen concentration and (c) TOC with electric charge consumed for different electrochemical treatments of 2 L of the effluent of the biosorption process at BHR = 20 using a flow plant like of Fig. 5d with a filter-press BDD/stainless steel cell at $j = 30$ mA cm$^{-2}$ and liquid flow rate of 200 L h$^{-1}$. PE with a 4 W UVC lamp, high frequency-SE (HF-SE) with US of 100 MHz and low frequency−SE (LF-SE) with US of 24 Hz. Change of the concentration of (d) chlorinated an (e) nitrogenated species detected during the PE treatment. Adapted from Chair et al. (2017b).

with UVC light and SE. These methods are more powerful than individual AO, photolysis and sonolysis. In chloride medium, the PE process with $RuO_2TiO_2$ and $Ti/Ir_{0.3}Ti_{0.7}O_2$ anodes yields greater mineralization of synthetic clopyralid and glyphosate solutions than using BDD, due to the high oxidation ability of photogenerated $Cl^{\bullet}$ and $Cl_2^{\bullet-}$. The remediation of soil-washing effluents obtained from simulated soils of kaolinite and SDS as surfactant is strongly enhanced using PE and SE instead of AO. The PE treatment yields faster degradation and mineralization of the herbicide and SDS than the SE one. The performance of the combined PE/SE process is superior to that of individual treatments. Other hybrid processes involving AO with ozonation and $H_2O_2$ electrogeneration, electrodialysis/AO, adsorption/AO and SPC/SPEC have been explored. Sequential biological-AO, AO-biological, biosorption-electrochemical and electrochemical-electrochemical treatments have been examined as well.

The research over herbicide remediation in wastewaters and soils with single and combined EAOPs has been limited to synthetic solutions treated in small bench-scale electrochemical systems. Great efforts are then required to demonstrate their possible industrial application. To do this, several future challenges are envisaged, including the need of treating real agricultural wastewaters and contaminated soils, the design and construction of optimized electrochemical systems with stable electrodes at industrial scale and the realization of techno-economic studies to show their viability and economic advantages with respect to commercial technologies.

## Declaration of competing interest

The authors declare that they have no known competing financial interests or personal relationships that could have appeared to influence the work reported in this paper.

## References

Abdessalem, A.K., Oturan, M.A., Oturan, N., Bellakhal, N., Dachraoui, M., 2010. Treatment of an aqueous pesticides mixture solution by direct and indirect electrochemical advanced oxidation processes. Int. J. Environ. Anal. Chem. 90, 468–477, 10.1080/03067310902999132.

Alcaide, F., Álvarez, G., Guelfi, D.R.V., Brillas, E., Sirés, I., 2020. A stable CoSP/MWCNTs air-diffusion cathode for the photoelectro-Fenton degradation of organic pollutants at pre-pilot scale. Chem. Eng. J. 379, 122417 https://doi.org/10.1016/j.cej.2019.122417.

Almazán-Sánchez, P.T., Cotillas, S., Sáez, C., Solache-Ríos, M.J., Martínez-Miranda, V., Cañizares, P., Linares-Hernández, I., Rodrigo, M.A., 2017. Removal of pendimethalin from soil washing effluents using electrolytic and electro-irradiated technologies based on diamond anodes. Appl. Catal. B Environ. 213, 190–197. https://doi.org/10.1016/j.apcatb.2017.05.008.

Alves, S.A., Ferreira, T.C.R., Sabatini, N.S., Trientini, A.C.A., Migliorini, F.L., Baldan, M.R., Ferreira, N.G., Lanza, M.R.V., 2012. A comparative study of the electrochemical oxidation of the herbicide tebuthiuron using boron-doped diamond electrodes. Chemosphere 88, 155–160. https://doi.org/10.1016/j.chemosphere.2012.02.042.

Aquino, J.M., Miwa, D.W., Rodrigo, M.A., Motheo, A.J., 2017. Treatment of actual effluents produced in the manufacturing of atrazine by a photo-electrolytic process. Chemosphere 172, 185–192. https://doi.org/10.1016/j.chemosphere.2016.12.154.

Barbari, K., Delimi, R., Benredjem, Z., Saaidia, S., Djemel, A., Chouchane, T., Oturan, N., Oturan, M.A., 2018. Photocatalytically-assisted electrooxidation of herbicide fenuron using a new bifunctional electrode $PbO_2/SnO_2$-$Sb_2O_3$/Ti//Ti/$TiO_2$. Chemosphere 203, 1–10. https://doi.org/10.1016/j.chemosphere.2018.03.126.

Barbosa, M.P.R., Lima, N.S., de Matos, D.B., Alves Felisardo, R.J., Santos, G.N., Salazar-Banda, G.R., Cavalcanti, E.B., 2018. Degradation of pesticide mixture by electro-Fenton in filter-press reactor. J. Water Process Eng 25, 222–235. https://doi.org/10.1016/j.jwpe.2018.08.008.

Barbosa Ferreira, M., Muñoz-Morales, M., Sáez, C., Cañizares, P., Martínez-Huitle, C.A., Rodrigo, M.A., 2020a. Improving biotreatability of hazardous effluents combining ZVI, electrolysis and photolysis. Sci. Total Environ. 713, 136647 https://doi.org/10.1016/j.scitotenv.2020.136647.

Barbosa Ferreira, M., Solano, A.M.S., dos Santos, E.V., Martínez-Huitle, C.A., 2020b. Coupling of anodic oxidation and soil remediation processes: a review. Materials 13, 4309. https://doi.org/10.3390/ma13194309.

Bavasso, I., Montanaro, D., Di Palma, L., Petrucci, E., 2020. Electrochemically assisted decomposition of ozone for degradation and mineralization of diuron. Electrochim. Acta 331, 135423. https://doi.org/10.1016/j.electacta.2019.135423.

Borràs, N., Oliver, R., Arias, C., Brillas, E., 2010. Degradation of atrazine by electrochemical advanced oxidation processes using a boron-doped diamond anode. J. Phys. Chem. 114, 6613–6621. https://doi.org/10.1021/jp1035647.

Borràs, N., Arias, C., Oliver, R., Brillas, E., 2011. Mineralization of desmetryne by electrochemical advanced oxidation processes using a boron-doped diamond anode and an oxygen-diffusion cathode. Chemosphere 85, 1167–1175. https://doi.org/10.1016/j.chemosphere.2011.09.008.

Borràs, N., Arias, C., Oliver, R., Brillas, E., 2013. Anodic oxidation, electro-Fenton and photoelectro-Fenton degradation of cyanazine using a boron-doped diamond anode and an oxygen-diffusion cathode. J. Electroanal. Chem. 689, 158–167. https://doi.org/10.1016/j.jelechem.2012.11.012.

Boye, B., Michaud, P.-A., Marselli, B., Dieng, M.M., Brillas, E., Comninellis, C., 2002. Anodic oxidation of 4-chlorophenoxyacetic acid on synthetic boron-doped diamond electrodes. New Diamond Front. Carbon Tech. 12, 63–72.

Brillas, E., 2020. A review on the photoelectro-Fenton process as efficient electrochemical advanced oxidation for wastewater remediation. Treatment with UV light, sunlight, and coupling with conventional and other photo-assisted advanced technologies. Chemosphere 250, 126198. https://doi.org/10.1016/j.chemosphere.2020.126198.

Brillas, E., Garcia-Segura, S., 2020. Benchmarking recent advances and innovative technology approaches of Fenton, photo-Fenton, electro-Fenton, and related processes: a review on the relevance of phenol as model molecule. Separ. Purif. Technol. 237, 116337 https://doi.org/10.1016/j.seppur.2019.116337.

Brillas, E., Martínez-Huitle, C.A., 2015. Decontamination of wastewaters containing synthetic organic dyes by electrochemical methods. An updated review Appl. Catal. B: Environ. Times 166–167, 603–643. https://doi.org/10.1016/j.apcatb.2014.11.016.

Brillas, E., Sirés, I., Oturan, M.A., 2009. Electro-Fenton process and related electrochemical technologies based on Fenton's reaction chemistry. Chem. Rev. 109, 6570–6631. https://doi.org/10.1021/cr900136g.

Bringas, E., Saiz, J., Ortiz, I., 2011. Kinetics of ultrasound-enhanced electrochemical oxidation of diuron on boron-doped diamond electrodes. Chem. Eng. J. 172, 1016–1022. https://doi.org/10.1016/j.cej.2011.07.016.

Carboneras Contreras, M.B., Fourcade, F., Assadi, A., Amrane, A., Fernandez-Morales, F.J., 2019. Electro Fenton removal of clopyralid in soil washing effluents. Chemosphere 237, 123337. https://doi.org/10.1016/j.chemosphere.2019.124447.

Carboneras, M.B., Cañizares, P., Rodrigo, M.A., Villaseñor, J., Fernandez-Morales, F.J., 2018. Improving biodegradability of soil washing effluents using anodic oxidation. Bio Technol. 252, 1–6. https://doi.org/10.1016/j.biortech.2017.12.060.

Carboneras, M.B., Rodrigo, M.A., Cañizares, P., Villasenor, J., Fernandez-Morales, F.J., 2020. Removal of oxyfluorfen from polluted effluents by combined bio-electro processes. Chemosphere 240, 124912. https://doi.org/10.1016/j.chemosphere.2019.124912.

Cartaxo, M.A.M., Borges, C.M., Pereira, M.I.S., Mendonça, M.H., 2015. Electrochemical oxidation of paraquat in neutral medium. Electrochim. Acta 176, 1010–1018. https://doi.org/10.1016/j.electacta.2015.07.099.

Chair, K., Bedoui, A., Bensalah, N., Fernández-Morales, F.J., Sáez, C., Cañizares, P., Rodrigo, M.A., 2017a. Combining bioadsorption and photoelectrochemical oxidation for the treatment of soil-washing effluents polluted with herbicide 2,4-D. J. Chem. Technol. Biotechnol. 92, 83–89. https://doi.org/10.1002/jctb.5001.

Chair, K., Bedoui, A., Bensalah, N., Sáez, C., Fernández-Morales, F.J., Cotillas, S., Cañizares, P., Rodrigo, M.A., 2017b. Treatment of soil-washing effluents polluted with herbicide oxyfluorfen by combined biosorption-electrolysis. Ind. Eng. Chem. Res. 56, 1903–1910. https://doi.org/10.1021/acs.iecr.6b04977.

Coria, G., Sirés, I., Brillas, E., Nava, J.L., 2016. Influence of the anode material on the degradation of naproxen by Fenton-based electrochemical processes. Chem. Eng. J. 304, 817–825. https://doi.org/10.1016/j.cej.2016.07.012.

da Silva, L.M., de Oliveira Santiago Santos, G., de Salles Pupo, M.M., Eguiluz, K.I.B., Salazar-Banda, G.R., 2018. Influence of heating rate on the physical and electrochemical properties of mixed metal oxides anodes synthesized by thermal decomposition method applying an ionic liquid. J. Electroanal. Chem. 813, 127–133. https://doi.org/10.1016/j.jelechem.2018.02.026.

Dargahi, A., Nematollahi, D., Asgari, G., Shokoohi, R., Ansari, A., Samarghandi, M.R., 2018. Electrodegradation of 2,4-dichlorophenoxyacetic acid herbicide from aqueous solution using three-dimensional electrode reactor with G/β-$PbO_2$ anode: taguchi optimization and degradation mechanism determination. RSC Adv. 8, 39256–39258. https://doi.org/10.1039/c8ra08471h.

Dargahi, A., Ansari, A., Nematollahi, D., Asgari, G., Shokoohi, R., Samarghandi, M.R., 2019. Parameter optimization and degradation mechanism for electrocatalytic degradation of 2,4-diclorophenoxyacetic acid (2,4-D) herbicide by lead dioxide electrodes. RSC Adv. 9, 5064–5075. https://doi.org/10.1039/c8ra10105a.

de Matos, D.B., Barbosa, M.P.R., Leite, O.M., Steter, J.R., Lima, N.S., Torres, N.H., Marques, M.N., de Alsina, O.L.S., Cavalcanti, E.B., 2020. Characterization of a tubular electrochemical reactor for the degradation of the commercial diuron herbicide. Environ. Technol. 41, 1307–1321, 10.1080/09593330.2018.1531941.

de Mello, R., Santos, L.H.E., Pupo, M.M.S., Eguiluz, K.I.B., Salazar-Banda, G.R., Motheo, A.J., 2018. Alachlor removal performance of Ti/$Ru_{0.3}Ti_{0.7}O_2$ anodes prepared from ionic liquid solution. J. Solid State Electrochem. 22, 1571–1580. https://doi.org/10.1007/s10008-017-3700-6.

Diaw, P.A., Oturan, N., Seye, M.D.G., Coly, A., Tine, A., Aaron, J.-J., Oturan, M.A., 2017. Oxidative degradation and mineralization of the phenylurea herbicide fluometuron in aqueous media by the electro-Fenton process. Sep. Purif. Technol. 186, 197–206. https://doi.org/10.1016/j.seppur.2017.06.005.

Diaw, P.A., Oturan, N., Gaye Seye, M.D., Mbaye, O.M.A., Mbaye, M., Coly, A., Aaron, J.-J., Oturan, M.A., 2020. Removal of the herbicide monolinuron from waters by the electro-Fenton treatment. J. Electroanal. Chem. 864, 114087 https://doi.org/10.1016/j.jelechem.2020.114087.

Ding, X., Wang, S., Shen, W., Mu, Y., Wang, L., Chen, H., Zhang, L., 2017. Fe@$Fe_2O_3$ promoted electrochemical mineralization of atrazine via a triazinon ring opening mechanism. Water Res. 112, 9–18. https://doi.org/10.1016/j.watres.2017.01.024.

dos Santos, E.V., Sáez, C., Martínez-Huitle, C.A., Cañizares, P., Rodrigo, M.A., 2015. The role of particle size on the conductive diamond electrochemical oxidation of soil-washing effluent polluted with atrazine, Electrochem. Commun. Now. 55, 26–29. https://doi.org/10.1016/j.elecom.2015.03.003.

dos Santos, E.V., Sáez, C., Martínez-Huitle, C.A., Cañizares, P., Rodrigo, M.A., 2016. Removal of oxyfluorfen from ex-situ soil washing fluids using electrolysis with diamond anodes. J. Environ. Manag. 171, 260–266. https://doi.org/10.1016/j.jenvman.2016.01.027.

dos Santos, E.V., Sáez, C., Cañizares, P., Martínez-Huitle, C.A., Rodrigo, M.A., 2017a. UV assisted electrochemical technologies for the removal of oxyfluorfen from soil washing wastes. Chem. Eng. J. 318, 2–9. https://doi.org/10.1016/j.cej.2016.03.015.

dos Santos, E.V., Sáez, C., Cañizares, P., Martínez-Huitle, C.A., Rodrigo, M.A., 2017b. Treating soil-washing fluids polluted with oxyfluorfen by sono-electrolysis with diamond anodes. Ultrason. Sonochem. 34, 115–122. https://doi.org/10.1016/j.ultsonch.2016.05.029.

dos Santos, E.V., Sáez, C., Cañizares, P., Rodrigo, M.A., Martínez-Huitle, C.A., 2018. Coupling photo and sono technologies with BDD anodic oxidation for treating soil-washing effluent polluted with atrazine. J. Electrochem. Soc. 165, E262–E267. https://doi.org/10.1149/2.1281805jes.

El-Ghenymy, A., Rodríguez, R.M., Brillas, E., Oturan, N., Oturan, M.A., 2014. Electro-Fenton degradation of the antibiotic sulfanilamide with Pt/carbon-felt and BDD/carbon-felt cells. Kinetics, reaction intermediates, and toxicity assessment. Environ. Sci. Pollut. Res. 21, 8368–8378. https://doi.org/10.1007/s11356-014-2773-3.

Feng, Y., Liu, J., Zhu, L., Wei, J., 2013. Combined technology for clomazone herbicide wastewater treatment: three-dimensional packed-bed electrochemical oxidation and biological contact degradation. Water Sci. Technol. 68, 257–260. https://doi.org/10.2166/wst.2013.162.

Fernández-Domene, R.M., Sánchez-Tovar, R., Lucas-Granados, B., Muñoz-Portero, M.J., Ramírez-Grau, R., García-Antón, J., 2018a. Visible-light photoelectrodegradation of diuron on $WO_3$ nanostructures. J. Environ. Manag. 226, 249–255. https://doi.org/10.1016/j.jenvman.2018.08.044.

Fernández-Domene, R.M., Sánchez-Tovar, R., Lucas-Granados, B., Muñoz-Portero, M.J., García-Antón, J., 2018b. Elimination of pesticide atrazine by photoelectrocatalysis using a photoanode based on $WO_3$ nanosheets. Chem. Eng. J. 350, 1114–1124. https://doi.org/10.1016/j.cej.2018.06.015.

Fontmorin, J.-M., Fourcade, F., Geneste, F., Floner, D., Huguet, S., Amrane, A., 2013. Combined process for 2,4-dichlorophenoxyacetic acid treatment-coupling of an electrochemical system with a biological treatment. Biochem. Eng. J. 70, 17–22. https://doi.org/10.1016/j.bej.2012.09.015.

Fontmorin, J.-M., Siguié, J., Fourcade, F., Geneste, F., Floner, D., Soutrel, I., Amrane, A., 2014. Combined electrochemical treatment/biological process for the removal of a commercial herbicide solution, U46D®. Sep. Purif. Technol. 132, 704–711.

https://doi.org/10.1016/j.seppur.2014.06.024.
Forti, J.C., Loretti, G.H., Tadayozzi, Y.S., de Andrade, A.R., 2020. A phytotoxicity assessment of the efficiency 2,4-D degradation by different oxidative processes. J. Environ. Manag. 266, 110588 https://doi.org/10.1016/j.jenvman.2020.110588.
Frangos, P., Shen, W., Wang, H., Li, X., Yu, G., Deng, S., Huang, J., Wang, B., Wang, Y., 2016. Improvement of the degradation of pesticide deethylatrazine by combining UV photolysis with electrochemical generation of hydrogen peroxide. Chem. Eng. J. 291, 215–224. https://doi.org/10.1016/j.cej.2016.01.089.
Ganiyu, S.O., Martínez-Huitle, C.A., 2020. The use of renewable energies driving electrochemical technologies for environmental applications. Curr. Opin. Electrochem 22, 211–220. https://doi.org/10.1016/j.coelec.2020.07.007.
Ganiyu, S.O., Zhou, M., Martínez-Huitle, C.A., 2018. Heterogeneous electro-Fenton and photoelectro-Fenton processes: a critical review of fundamental principles and application for water/wastewater treatment. Appl. Catal. B Environ. 235, 103–129. https://doi.org/10.1016/j.apcatb.2018.04.044.
Ganiyu, S.O., Martínez-Huitle, C.A., Rodrigo, M.A., 2020. Renewable energies driven electrochemical wastewater/soil decontamination technologies: a critical review of fundamental concepts and applications. Appl. Catal. B Environ. 270, 118857 https://doi.org/10.1016/j.apcatb.2020.118857.
García, O., Isarain-Chávez, E., Garcia-Segura, S., Brillas, E., Peralta-Hernández, J.M., 2013. Degradation of 2,4-dichlorophenoxyacetic acid by electro-oxidation and electro-Fenton/BDD processes using a pre-pilot plant. Electrocatalysis 4, 224–234. https://doi.org/10.1007/s12678-013-0135-4.
García, O., Isarain-Chávez, E., El-Ghenymy, A., Brillas, E., Peralta-Hernández, J.M., 2014. Degradation of 2,4-D herbicide in a recirculation flow plant with a Pt/air-diffusion and a BDD/BDD cell by electrochemical oxidation and electro-Fenton process. J. Electroanal. Chem. 728, 1–9. https://doi.org/10.1016/j.jelechem.2014.06.019. EO, EF).
Garcia-Segura, S., Brillas, E., 2017. Applied photoelectrocatalysis on the degradation of organic pollutants in wastewaters. J. Photochem. Photobiol. C Photochem. Rev. 31, 1–35. https://doi.org/10.1016/j.jphotochemrev.2017.01.005.
Garcia-Segura, S., Almeida, L.C., Bocchi, N., Brillas, E., 2011. Solar photoelectro-Fenton degradation of the herbicide 4-chloro-2-methylphenoxyacetic acid optimized by response surface methodology. J. Hazard Mater. 194, 109–118. https://doi.org/10.1016/j.jhazmat.2011.07.089.
Garcia-Segura, S., Cavalcanti, E.B., Brillas, E., 2014. Mineralization of the antibiotic chloramphenicol by solar photoelectro-Fenton: from stirred tank reactor to solar pre-pilot plant. Appl. Catal. B Environ. 144, 588–598. https://doi.org/10.1016/j.apcatb.2013.07.071.
Garcia-Segura, S., dos Santos, E.V., Martínez-Huitle, C.A., 2015. Role of $sp^3/sp^2$ ratio on the electrocatalytic properties of boron-doped diamond electrodes: a mini review. Electrochem. Commun. Now. 59, 52–55. https://doi.org/10.1016/j.elecom.2015.07.002.
Garcia-Segura, S., Brockway Nienhauser, A., Fajardo, A.S., Bansal, R., Coonrod, C.L., Fortner, J.D., Marcos-Hernández, M., Rogers, T., Villagran, D., Wong, M.S., Westerhoff, P., 2020. Disparities between experimental and environmental conditions: research steps toward making electrochemical water treatment a reality. Curr. Opin. Electrochem 22, 9–16. https://doi.org/10.1016/j.coelec.2020.03.001.
Garrido-Ramírez, E.G., Mora, M.L., Marco, J.F., Ureta-Zañartu, M.S., 2013. Characterization of nanostructured allophane clays and their use as support of iron species in a heterogeneous electro-Fenton system. Appl. Clay Sci. 86, 153–161. https://doi.org/10.1016/j.clay.2013.10.001.
Garza-Campos, B.R., Guzmán-Mar, J.L., Reyes, L.H., Brillas, E., Hernández-Ramírez, A., Ruiz-Ruiz, E.J., 2014. Coupling of solar photoelectro-Fenton with a BDD anode and solar heterogeneous photocatalysis for the mineralization of the herbicide atrazine. Chemosphere 97, 26–33. https://doi.org/10.1016/j.chemosphere.2013.10.044.
Gençten, M., Özcan, A., 2015. A detailed investigation on electro-Fenton treatment of propachlor: mineralization kinetic and degradation intermediates. Chemosphere 136, 167–173. https://doi.org/10.1016/j.chemosphere.2015.04.101.
González-Cadena, J., Amador-Hernández, J., Velázquez-Manzanares, M., 2013. Study of electrochemical behavior of the atratone herbicide. Sustain. Environ. Res. 23, 253–257.
Gozzi, F., Sirés, I., Thiam, A., de Oliveira, S.C., Machulek Jr., A.M., Brillas, E., 2017. Treatment of single and mixed pesticide formulations by solar photoelectro-Fenton using a flow plant. Chem. Eng. J. 310, 503–513. https://doi.org/10.1016/j.cej.2016.02.026.
Gozzi, F., Sirés, I., de Oliveira, S.C., Machulek Jr., A., Brillas, E., 2018. Influence of chelation on the Fenton-based electrochemical degradation of herbicide tebuthiuron. Chemosphere 199, 709–717. https://doi.org/10.1016/j.chemosphere.2018.02.060.
Guelfi, D.R.V., Gozzi, F., Machulek Jr., A., Sirés, I., Brillas, E., de Oliveira, S.C., 2018. Degradation of herbicide S-metolachlor by electrochemical AOPs using a boron-doped diamond anode. Catal. Today 313, 182–188. https://doi.org/10.1016/j.cattod.2017.10.026.
Guelfi, D.R.V., Brillas, E., Gozzi, F., Machulek Jr., A., de Oliveira, S.C., Sirés, I., 2019a. Influence of electrolysis conditions on the treatment of herbicide bentazon using artificial UVA radiation and sunlight. Identification of oxidation products. J. Environ. Manag. 231, 213–221. https://doi.org/10.1016/j.jenvman.2018.10.029.
Guelfi, D.R.V., Ye, Z., Gozzi, F., de Oliveira, S.C., Machulek Jr., A., Brillas, E., Sirés, I., 2019b. Ensuring the overall combustion of herbicide metribuzin by electrochemical advanced oxidation processes. Study of operation variables, kinetics and degradation routes. Separ. Purif. Technol. 211, 637–645. https://doi.org/10.1016/j.seppur.2018.10.029.
Guo, X., Liu, H., Miao, J., Ma, Z., 2017. Photocatalytic and photoelectrochemically degradation of chlorsulfuron herbicide. IOP Conf. Ser. Mater. Sci. Eng 274, 12094. https://doi.org/10.1088/1757-899X/274/1/012094.
Gusiatin, Z.M., Kulikowska, D., Klik, B., 2020. New-generation washing agents in remediation of metal-polluted soils and methods for washing effluent treatment: a review. Int. J. Environ. Res. Publ. Health 17, 6220. https://doi.org/10.3390/ijerph17176220.
Hasanzadeh, A., Khataee, A., Zarei, M., Joo, S.W., 2018. Photo-assisted electrochemical abatement of trifluralin using a cathode containing a C60-carbon nanotubes composite. Chemosphere 199, 510–523. https://doi.org/10.1016/j.chemosphere.2018.02.061.
Jović, M., Manojlović, D., Stanković, D., Gašić, U., Jeremić, D., Brćeski, I., Roglić, G., 2015. Electrochemical degradation of triketone herbicides and identification of their main degradation products. Clean 43, 1093–1099. https://doi.org/10.1002/clen.201300951.
Kamaraj, R., Vasudevan, S., 2019. Sulfur-doped carbon-chain network as high-performance electrocatalyst for electro-Fenton system. Chemistry 4, 2428–2435. https://doi.org/10.1002/slct.201803765.
Khataee, A., Sajjadi, S., Hasanzadeh, A., Vahid, B., Joo, S.W., 2017. One-step preparation of nanostructured martite catalyst and graphite electrode by glow discharge plasma for heterogeneous electro-Fenton like process. J. Environ. Manag. 199, 31–45. https://doi.org/10.1016/j.jenvman.2017.04.095.
Khongthon, W., Jovanovic, G., Yokochi, A., Sangvanich, P., Pavarajarn, V., 2016. Degradation of diuron via an electrochemical advanced oxidation process in a microscale-based reactor. Chem. Eng. J. 292, 298–307. https://doi.org/10.1016/j.cej.2016.02.042.
Komtchou, S., Dirany, A., Drogui, P., Delegan, N., El Khakani, M.A., Robert, D., Lafrance, P., 2016. Degradation of atrazine in aqueous solution with electro-photocatalytic process using $TiO_2$-x photoanode. Chemosphere 157, 79–88. https://doi.org/10.1016/j.chemosphere.2016.05.022.
Komtchou, S., Dirany, A., Drogui, P., Robert, D., Lafrance, P., 2017. Removal of atrazine and its by-products from water using electrochemical advanced oxidation processes. Water Res. 125, 91–103. https://doi.org/10.1016/j.watres.2017.08.036.
Lan, H., Jiao, Z., Zhao, X., He, W., Wang, A., Liu, H., Liu, R., Qu, J., 2013. Removal of glyphosate from water by electrochemically assisted $MnO_2$ oxidation process. Separ. Purif. Technol. 117, 30–34. https://doi.org/10.1016/j.seppur.2013.04.012.
Lan, H., He, W., Wang, A., Liu, R., Liu, H., Qu, J., Huang, C.P., 2016. An activated carbon fiber cathode for the degradation of glyphosate in aqueous solutions by the electro-Fenton mode: optimal operational conditions and the deposition of iron on cathode on electrode reusability. Water Res. 105, 575–582. https://doi.org/10.1016/j.watres.2016.09.036.
Li, P., Zhao, G., Li, M., Cao, T., Cui, X., Li, D., 2012. Design and high efficient photoelectric-synergistic catalytic oxidation activity of 2D macroporous SNO2/1D TiO2 nanotubes. Appl. Catal. B Environ. 111–112, 578–585. https://doi.org/10.1016/j.apcatb.2011.11.010.
Lima, A.C.D.A., Melo, A.M.D.S., Pires, E.V., Ferreira, R.C.D.S., Sant'Ana, A.E.G., Goulart, M.O.F., de Abreu, F.C., 2010. Electroanalytical studies of sulfentrazone in protic medium, its degradation by the electro-Fenton process, and toxicity assessment using ss-DNA. Chemosphere 81, 884–889. https://doi.org/10.1016/j.chemosphere.2010.08.003.
Lima, N.S., Souza, A.M., Torres, N.H., Bergamasco, R., Marques, M.N., Garcia-Segura, S., Sanchez de Alsina, O.L., Cavalcanti, E.B., 2019. Relevance of adjuvants and additives of pesticide commercial formulation on the removal performance of glyphosate by electrochemically driven processes. J. Clean. Prod. 212, 837–846. https://doi.org/10.1016/j.jclepro.2018.12.007.
Liu, R., Liu, Y., Liu, C., Luo, S., Teng, Y., Yang, L., Yang, R., Cai, Q., 2011. Enhanced photoelectrocatalytic degradation of 2,4-dichlorophenoxyacetic acid by $CuInS_2$ nanoparticles deposition onto $TiO_2$ nanotube arrays. J. Alloys Compd. 509, 2434–2450. https://doi.org/10.1016/j.jallcom.2010.11.040.
Liu, K., Yu, M., Wang, H., Wang, J., Liu, W., Hoffmann, M.R., 2019a. Multiphase porous electrochemical catalysts derived from iron-based metal-organic framework compounds. Environ. Sci. Technol. 53, 6474–6482. https://doi.org/10.1021/acs.est.9b01143.
Liu, Y., Zhu, K., Sun, Q., Sun, Y., Zhu, H., Huang, L., Hao, X., 2019b. Electrochemical degradation of atrazine on Pt anode with cathodic electro-generation of $H_2O_2$.IOP Conf. Ser. Earth Environ. Sci. 371, 42018, 10.1088/1755-1315/371/4/042018.
Lizama-Bahena, C., Alvarez-Gallegos, A., Hernandez, J.A., Silva-Martinez, S., 2015. Elimination of bio-refractory chlorinated herbicides like atrazine, alachlor, and chlorbromuron from aqueous effluents by Fenton, electro-Fenton, and peroxi-coagulation methods. Desalin. Water Treat 55, 3683–3693, 10.1080/19443994.2014.939858.
Llanos, J., Raschitor, A., Cañizares, P., Rodrigo, M.A., 2018. Exploring the applicability of a combined electrodialysis/electro-oxidation cell for the degradation of 2,4-dichlorophenoxyacetic acid. Electrochim. Acta 269, 415–421. https://doi.org/10.1016/j.electacta.2018.02.153.
Long, L., Bai, C., Zhang, S., Deng, S., Tian, D., Shen, F., Zhang, Y., Wu, J., He, J., Yang, G., 2019. Boosted charge transfer from single crystalline titanium nanotubes for a dual-purpose PEC system. Int. J. Hydrogen Energy 44, 17622–17629. https://doi.org/10.1016/j.ijhydene.2019.05.164.
Lou, Y.-Y., Geneste, F., Soutrel, I., Amrane, A., Fourcade, F., 2020. Alachlor dechlorination prior to an electro-Fenton process: influence on the biodegradability of the treated solution. Separ. Purif. Technol. 232, 115936 https://doi.org/10.1016/j.seppur.2019.115936.
Mahour, R., Khan, M.F., Forbes, S., Perez-Estrada, L.A., 2014. Pesticides and

herbicides. Water Environ. Res. 86, 1545–1578, 10.2175/106143014X14031280668777.
Malakootian, M., Shahesmaeili, A., Faraji, M., Amiri, H., Silva Martinez, S., 2020. Advanced oxidation processes for the removal of organophosphorus pesticides in aqueous matrices: a systematic review and meta-analysis. Process Saf. Environ. Protect. Met. 134, 292–307. https://doi.org/10.1016/j.psep.2019.12.004.
Malpass, G.R.P., Miwa, D.W., Gomes, L., Azevedo, E.B., Vilela, W.F.D., Fukunaga, M.T., Guimaraes, J.R., Bertazzoli, R., Machado, S.A.S., Motheo, A.J., 2010a. Photo-assisted electrochemical degradation of the commercial herbicide atrazine. Water Sci. Technol. 62, 2729–2736. https://doi.org/10.2166/wst.2010.207.
Malpass, G.R.P., Miwa, D.W., Machado, S.A.S., Motheo, A.J., 2010b. $SnO_2$-based materials for pesticide degradation. J. Hazard Mater. 180, 145–151. https://doi.org/10.1016/j.jhazmat.2010.04.006.
Malpass, G.R.P., Miwa, D.W., Santos, R.L., Vieira, E.M., Motheo, A.J., 2012. Unexpected toxicity decrease during photoelectrochemical degradation of atrazine with NaCl. Environ. Chem. Lett. 10, 177–182. https://doi.org/10.1007/s10311-011-0340-4.
Malpass, G.R.P., Salazar-Banda, G.R., Miwa, D.W., Machado, S.A.S., Motheo, A.J., 2013. Comparing atrazine and cyanuric acid electro-oxidation on mixed oxide and boron-doped diamond electrodes. Environ. Technol. 34, 1043–1051, 10.1080/09593330.2012.733420.
Martínez-Huitle, C.A., Brillas, E., 2009. Decontamination of wastewaters containing synthetic organic dyes by electrochemical methods. A general review. Appl. Catal. B Environ. 87, 105–145. https://doi.org/10.1016/j.apcatb.2008.09.017.
Martínez-Huitle, C.A., Panizza, M., 2018. Electrochemical oxidation of organic pollutants for wastewater treatment. Curr. Opin. Electrochem. 11, 62–71. https://doi.org/10.1016/j.coelec.2018.07.010.
Martínez-Huitle, C.A., Rodrigo, M.A., Sirés, I., Scialdone, O., 2015. Single and coupled electrochemical processes and reactors for the abatement of organic water pollutants: a critical review. Chem. Rev. 115, 13362–13407. https://doi.org/10.1021/acs.chemrev.5b00361.
McBeath, S.T., Wilkinson, D.P., Graham, N.J.D., 2019. Application of boron-doped diamond electrodes for the anodic oxidation of pesticide micropollutants in a water treatment process: a critical review. Environ. Sci.: Water Res. Technol 5, 2090–2107. https://doi.org/10.1039/c9ew00589g.
Millán, M., Rodrigo, M.A., Fernández-Marchante, C.M., Canizares, P., Lobato, J., 2019. Powering with solar energy the anodic oxidation of wastewater polluted with pesticides. ACS Sustain. Chem. Eng. 7, 8303–8309. https://doi.org/10.1021/acssuschemeng.8b06704.
Monteil, H., Péchaud, Y., Oturan, N., Oturan, M.A., 2019. A review on efficiency and cost effectiveness of electro- and bio-electro-Fenton processes: application to the treatment of pharmaceutical pollutants in water. Chem. Eng. J. 376, 119577 https://doi.org/10.1016/j.cej.2018.07.179.
Montes, I.J.S., Silva, B.F., Aquino, J.M., 2017. On the performance of a hybrid process to mineralize the herbicide tebuthiuron using a DSA® anode and UVC light: a mechanistic study. Appl. Catal. B Environ. 200, 237–245. https://doi.org/10.1016/j.apcatb.2016.07.003.
Moraleda, I., Oturan, N., Saez, C., Llanos, J., Rodrigo, M.A., Oturan, M.A., 2020. A comparison between flow-through cathode and mixed tank cells for the electro-Fenton process with conductive diamond anode. Chemosphere 238, 124584. https://doi.org/10.1016/j.chemosphere.2019.124854.
Moreira, F.C., Boaventura, R.A.R., Brillas, E., Vilar, V.J.P., 2017. Electrochemical advanced oxidation processes: a review on their application to synthetic and real wastewaters. Appl. Catal. B Environ. 202, 217–261. https://doi.org/10.1016/j.apcatb.2016.08.037.
Murati, M., Oturan, N., Aaron, J.-J., Dirany, A., Tassin, B., Zdravkovski, Z., Oturan, M.A., 2012. Degradation and mineralization of sulcotrione and mesotrione in aqueous medium by the electro-Fenton process: a kinetic study. Environ. Sci. Pollut. Res. 19, 1563–1573. https://doi.org/10.1007/s11356-011-0667-1.
Murati, M., Oturan, N., Zdravkovski, Z., Stanoeva, J.P., Aaron, S.E., Aaron, J.-J., Oturan, M.A., 2014. Application of the electro-Fenton process to mesotrione aqueous solutions: kinetics, degradation pathways, mineralization, and evolution of toxicity. Macedonian J. Chem. Chem. Eng 33, 121–137.
Nidheesh, P.V., Divyapriya, G., Oturan, N., Trellu, C., Oturan, M.A., 2019. Environmental applications of boron-doped diamond electrodes: 1. Applications in water and wastewater treatment. ChemElectroChem 6, 2124–2242. https://doi.org/10.1002/celc.201801876.
Niu, J., Bao, Y., Li, Y., Chai, Z., 2013. Electrochemical mineralization of pentachlorophenol (PCP) by Ti/$SnO_2$-Sb electrodes. Chemosphere 92, 1571–1577. https://doi.org/10.1016/j.chemosphere.2013.04.035.
Oturan, M.A., Aaron, J.J., 2014. Advanced oxidation processes in water/wastewater treatment: principles and applications. a review. Crit. Rev. Environ. Sci. Technol. 44, 2577–2641, 10.1080/10643389.2013.829765.
Oturan, M.A., Edelahi, M.C., Oturan, N., El Kacemi, K., Aaron, J.-J., 2010. Kinetics of oxidative degradation/mineralization pathways of the phenylurea herbicides diuron, monuron and fenuron in water during application of the electro-Fenton process. Appl. Catal. B Environ. 97, 82–89. https://doi.org/10.1016/j.apcatb.2010.03.026.
Oturan, M.A., Oturan, N., Edelahi, M.C., Podvorica, F.I., Kacemi, K.E., 2011. Oxidative degradation of herbicide diuron in aqueous medium by Fenton's reaction based advanced oxidation processes. Chem. Eng. J. 171, 127–135. https://doi.org/10.1016/j.cej.2011.03.072.
Oturan, N., Brillas, E., Oturan, M.A., 2012. Unprecedented total mineralization of atrazine and cyanuric acid by anodic oxidation and electro-Fenton with a boron-doped diamond anode. Environ. Chem. Lett. 10, 165–170. https://doi.org/10.1007/s10311-011-0337-z.
Özcan, L., Mutlu, T., Yurdakal, S., 2018. Photoelectrocatalytic degradation of paraquat by Pt loaded $TiO_2$ nanotubes on Ti anodes. Materials 11, 11091715. https://doi.org/10.3390/ma11091715.
Panizza, M., Cerisola, G., 2009. Direct and mediated anodic oxidation of organic pollutants. Chem. Rev. 109, 6541–6569. https://doi.org/10.1021/cr9001319.
Pedersen, N.L., Nikbakht Fini, M., Molnar, P.K., Muff, J., 2019. Synergy of combined adsorption and electrochemical degradation of aqueous organics by granular activated carbon particulate electrodes. Separ. Purif. Technol. 208, 51–58. https://doi.org/10.1016/j.seppur.2018.05.023.
Pereira, G.F., Rocha-Filho, R.C., Bocchi, N., Biaggio, S.R., 2015. Electrochemical degradation of the herbicide picloram using a filter-press flow reactor with a boron-doped diamond or β-$PbO_2$ anode. Electrochim. Acta 179, 588–598. https://doi.org/10.1016/j.electacta.2015.05.134.
Pereira, G.F., Silva, B.F., Oliveira, R.V., Coledam, D.A.C., Aquino, J.M., Rocha-Filho, R.C., Bocchi, N., Biaggio, S.R., 2017. Comparative electrochemical degradation of the herbicide tebuthiuron using a flow cell with a boron-doped diamond anode and identifying degradation intermediates. Electrochim. Acta 247, 860–870, 1016/j.electacta.2017.07.054.
Pinto, C.F., Antonelli, R., de Araujo, K.S., Fornazari, A.L.D.T., Fernandes, D.M., Granato, A.C., Azevedo, E.B., Malpass, G.R.P., 2019. Experimental-design-guided approach for the removal of atrazine by sono-electrochemical-UV-chlorine techniques. Environ. Technol. 40, 430–440, 10.1080/09593330.2017.1395480.
Pipi, A.R.F., Neto, S.A., De Andrade, A.R., 2013. Electrochemical degradation of diuron in chloride medium using DSA® based anodes. J. Braz. Chem. Soc. 24, 1259–1266, 10.5935/0103-5053.20130159.
Pipi, A.R.F., De Andrade, A.R., Brillas, E., Sirés, I., 2014a. Total removal of alachlor from water by electrochemical processes. Separ. Purif. Technol. 132, 674–683. https://doi.org/10.1016/j.seppur.2014.06.022.
Pipi, A.R.F., Sirés, I., De Andrade, A.R., Brillas, E., 2014b. Application of electrochemical advanced oxidation processes to the mineralization of the herbicide diuron. Chemosphere 109, 49–55. https://doi.org/10.1016/j.chemosphere.2014.03.006.
Rajput, H., Dhir, A., Sangal, V.K., 2018a. GO mediated $TiO_2$ nanotube electrode for the photoelectrocatalytic degradation of pentachlorophenol. J. Electrochem. Soc. 165, H16–H26. https://doi.org/10.1149/2.0871802jes.
Rajput, H., Sangal, V.K., Dhir, A., 2018b. Synthesis of highly stable and efficient Ag loaded GO/$TiO_2$ nanotube electrodes for the photoelectrocatalytic degradation of pentachlorophenol. J. Electroanal. Chem. 814, 118–126. https://doi.org/10.1016/j.jelechem.2018.02.053.
Raschitor, A., Llanos, J., Cañizares, P., Rodrigo, M.A., 2017. Novel integrated electrodialysis/electro-oxidation process for the efficient degradation of 2,4-dichlorophenoxyacetic acid. Chemosphere 182, 85–89. https://doi.org/10.1016/j.chemosphere.2017.04.153.
Raschitor, A., Llanos, J., Rodrigo, M.A., Cañizares, P., 2019. Combined electrochemical processes for the efficient degradation of non-polar organochlorine pesticides. J. Environ. Manag. 248, 109289 https://doi.org/10.1016/j.jenvman.2019.109289.
Ribeiro, A.R., Nunes, O.C., Pereira, M.F.R., Silva, A.M.T., 2015. An overview on the advanced oxidation processes applied for the treatment of water pollutants defined in the recently launched Directive 2013/39/EU. Environ. Int. 75, 33–51. https://doi.org/10.1016/j.envint.2014.10.027.
Rodrigo, M.A., Oturan, M.A., Oturan, N., 2014. Electrochemically assisted remediation of pesticides in soils and water: a review. Chem. Rev. 114, 8720–8745. https://doi.org/10.1021/cr500077e.
Roselló-Márquez, G., Fernández-Domene, R.M., Sánchez-Tovar, R., García-Carrión, S., Lucas-Granados, B., García-Antón, J., 2019. Photoelectrocatalyzed degradation of a pesticides mixture solution (chlorfenvinphos and bromacil) by $WO_3$ nanosheets. Sci. Total Environ. 674, 88–95. https://doi.org/10.1016/j.scitotenv.2019.04.150.
Rubí-Juárez, H., Cotillas, S., Sáez, C., Cañizares, P., Barrera-Díaz, C., Rodrigo, M.A., 2016a. Use of conductive diamond photo-electrochemical oxidation for the removal of pesticide glyphosate. Separ. Purif. Technol. 167, 127–135. https://doi.org/10.1016/j.seppur.2016.04.048.
Rubí-Juárez, H., Cotillas, S., Sáez, C., Cañizares, P., Barrera-Díaz, C., Rodrigo, M.A., 2016b. Removal of herbicide glyphosate by conductive-diamond electrochemical oxidation. Appl. Catal. B Environ. 188, 305–312. https://doi.org/10.1016/j.apcatb.2016.02.006.
Sánchez-Montes, I., Pérez, J.F., Sáez, C., Rodrigo, M.A., Cañizares, P., Aquino, J.M., 2020. Assessing the performance of electrochemical oxidation using DSA® and BDD anodes in the presence of UVC light. Chemosphere 238, 124575. https://doi.org/10.1016/j.chemosphere.2019.124575.
Samarghandi, M.R., Nemattollahi, D., Asgari, G., Shokoohi, R., Ansari, A., Dargahi, A., 2019. Electrochemical process for 2,4-D herbicide removal from aqueous solutions using stainless steel 316 and graphite anodes: optimization using response surface methodology. Separ. Sci. Technol. 54, 478–493, 10.1080/01496395.2018.1512618.
Samet, Y., Agengui, L., Abdelhédi, R., 2010a. Anodic oxidation of chlorpyrifos in aqueous solution at lead dioxide electrodes. J. Electroanal. Chem. 650, 152–158. https://doi.org/10.1016/j.jelechem.2010.08.008.
Samet, Y., Agengui, L., Abdelhédi, R., 2010b. Electrochemical degradation of chlorpyrifos pesticide in aqueous solutions by anodic oxidation at boron-doped diamond electrodes. Chem. Eng. J. 161, 167–172. https://doi.org/10.1016/j.cej.2010.04.060.
Santos, T.A.S., Silva, R.S., Eguiluz, K.I.B., Salazar-Banda, G.R., 2015. Development of Ti/$(RuO_2)_{0.8}(MO_2)_{0.2}$ (M=Ce, Sn or Ir) anodes for atrazine electro-oxidation.

Influence of the synthesis method. Mater. Lett. 146, 4–8. https://doi.org/10.1016/j.matlet.2015.01.145.
Santos, T.E.S., Silva, R.S., Meneses, C.T., Martínez-Huitle, C.A., Eguiluz, K.I.B., Salazar-Banda, G.R., 2016. Unexpected enhancement of electrocatalytic nature of Ti/($RuO_2$)x-($Sb_2O_5$)y anodes prepared by the ionic liquid-thermal decomposition method. Ind. Eng. Chem. Res. 55, 3182–3187. https://doi.org/10.1021/acs.iecr.5b04690.
Santos, G.O.S., Eguiluz, K.I.B., Salazar-Banda, G.R., Saez, C., Rodrigo, M.A., 2020a. Photoelectrolysis of clopyralid wastes with a novel laser-prepared MMO-$RuO_2TiO_2$ anode. Chemosphere 244, 125455. https://doi.org/10.1016/j.chemosphere.2019.125455.
Santos, G.O.S., Gonzaga, I.M.D., Eguiluz, K.I.B., Salazar-Banda, G.R., Saez, C., 2020b. Improving biodegradability of clopyralid wastes by photoelectrolysis: the role of the anode material. J. Electroanal. Chem. 864, 114084. https://doi.org/10.1016/j.jelechem.2020.114084.
Saylor, G.L., Zhao, C., Kupferle, M.J., 2018. Synergistic enhancement of oxidative degradation of atrazine using combined electrolysis and ozonation. J. Water Process Eng 21, 154–162. https://doi.org/10.1016/j.jwpe.2017.12.010.
Sirés, I., Brillas, E., Oturan, M.A., Rodrigo, M.A., Panizza, M., 2014. Electrochemical advanced oxidation processes: today and tomorrow. A review. Environ. Sci. Pollut. Res. 21, 8336–8367. https://doi.org/10.1007/s11356-014-2783-1.
Souza, F.L., Teodoro, T.Q., Vasconcelos, V.M., Migliorini, F.L., Lima Gomes, P.C.F., Ferreira, N.G., Baldan, M.R., Haiduke, R.L.A., Lanza, M.R.V., 2014. Electrochemical oxidation of imazapyr with BDD electrode in titanium substrate. Chemosphere 117, 596–603. https://doi.org/10.1016/j.chemosphere.2014.09.051.
Souza, F.L., Lanza, M.R.V., Llanos, J., Sáez, C., Rodrigo, M.A., Cañizares, P., 2015a. A wind-powered BDD electrochemical oxidation process for the removal of herbicides. J. Environ. Manag. 158, 36–39. https://doi.org/10.1016/j.jenvman.2015.04.040.
Souza, F.L., Sáez, C., Lanza, M.R.V., Cañizares, P., Rodrigo, M.A., 2015b. Removal of herbicide 2,4-D using conductive-diamond sono-electrochemical oxidation. Separ. Purif. Technol. 149, 24–30. https://doi.org/10.1016/j.seppur.2015.05.018.
Souza, F.L., Sáez, C., Llanos, J., Lanza, M.R.V., Cañizares, P., Rodrigo, M.A., 2015c. Solar-powered CDEO for the treatment of wastewater polluted with the herbicide 2,4-D. Chem. Eng. J. 277, 64–69. https://doi.org/10.1016/j.cej.2015.04.118.
Souza, F., Sáez, C., Lanza, M., Cañizares, P., Rodrigo, M.A., 2016a. Towards the scale-up of electrolysis with diamond anodes: effect of stacking on the electrochemical oxidation of 2,4 D. J. Chem. Technol. Biotechnol. 91, 742–747. https://doi.org/10.1002/jctb.4639.
Souza, F.L., Saéz, C., Lanza, M.R.V., Cañizares, P., Rodrigo, M.A., 2016b. Removal of pesticide 2,4-D by conductive-diamond photoelectrochemical oxidation. Appl. Catal. B Environ. 180, 733–739. https://doi.org/10.1016/j.apcatb.2015.07.038.
Souza, F.L., Sáez, C., Lanza, M.R.V., Cañizares, P., Rodrigo, M.A., 2016c. The effect of the $sp^3/sp^2$ carbon ratio on the electrochemical oxidation of 2,4-D with p-Si BDD anodes. Electrochim. Acta 187, 119–124. https://doi.org/10.1016/j.electacta.2015.11.031.
Souza, F., Quijorna, S., Lanza, M.R.V., Sáez, C., Cañizares, P., Rodrigo, M.A., 2017. Applicability of electrochemical oxidation using diamond anodes to the treatment of a sulfonylurea herbicide. Catal. Today 280, 192–198. https://doi.org/10.1016/j.cattod.2016.04.030.
Souza, F.L., Rocha, R.S., Ferreira, N.G., Rodrigo, M.A., Lanza, M.R.V., 2019. Effects of coupling hybrid processes on the treatment of wastewater containing a commercial mixture of diuron and hexazinone herbicides. Electrochim. Acta 328, 135013. https://doi.org/10.1016/j.electacta.2019.135013.
Souza, F.L., Sáez, C., Cañizares, P., Rodrigo, M.A., 2020. Improving photolytic treatments with electrochemical technology. Sep. Purif. Technol. 235, 116229 https://doi.org/10.1016/j.seppur.2019.116229.
Stirling, R., Walker, W.S., Westerhoff, P., Garcia-Segura, S., 2020. Techno-economic analysis to identify key innovations required for electrochemical oxidation as point-of-use treatment systems. Electrochim. Acta 338, 135874. https://doi.org/10.1016/j.electacta.2020.135874.
Thiam, A., Salazar, R., 2019. Fenton-based electrochemical degradation of metolachlor in aqueous solution by means of BDD and Pt electrodes: influencing factors and reaction pathways. Environ. Sci. Pollut. Res. 26, 2580–2591. https://doi.org/10.1007/s11356-018-3768-2.
Thiam, A., Sirés, I., Salazar, R., Brillas, E., 2018. On the performance of electrocatalytic anodes for photoelectro-Fenton treatment of synthetic solutions and real water spiked with the herbicide chloramben. J. Environ. Manag. 224, 340–349. https://doi.org/10.1016/j.jenvman.2018.07.065.
Tran, N., Drogui, P., Doan, T.L., Le, T.S., Nguyen, H.C., 2017. Electrochemical degradation and mineralization of glyphosate herbicide. Environ. Technol. 38, 2939–2948, 10.1080/09593330.2017.1284268.
Tran, M.H., Nguyen, H.C., Le, T.S., Dang, V.A.D., Cao, T.H., Le, C.K., Dang, T.-D., 2019. Degradation of glyphosate herbicide by an electro-Fenton process using carbon felt cathode. Environ. Technol. 2019, 1660411, 10.1080/09593330.2019.1660411.
Trellu, C., Chakraborty, S., Nidheesh, P.V., Oturan, M.A., 2019. Environmental applications of boron-doped diamond electrodes: 2. Soil remediation and sensing applications. ChemElectroChem 6, 2143–2156. https://doi.org/10.1002/celc.201801877.
Vagi, M.C., Petsas, A.S., 2019. Recent advances on the removal of priority organochlorine and organophosphorus biorecalcitrant pesticides defined by Directive 2013/39/EU from environmental matrices by using advanced oxidation processes: an overview (2007-2018). J. Environ. Chem. Eng, 102940. https://doi.org/10.1016/j.jece.2019.102940.
Valenzuela, A.L., Vasquez-Medrano, R., Ibanez, J.G., Frontana-Uribe, B.A., Prato-Garcia, D., 2017. Remediation of diquat-contaminated water by electrochemical advanced oxidation processes using boron-doped diamond (BDD) anodes. Water Air Soil Pollut. 228, 67. https://doi.org/10.1007/s11270-017-3244-5.
Wang, X., Zhu, K., Ma, X., Sun, Z., Hu, X., 2018. Degradation of diuron by heterogeneous electro-Fenton using modified magnetic activated carbon as the catalyst. RSC Adv. 8, 19971–19978. https://doi.org/10.1039/c8ra02776e.
Wang, H.-X., Zhu, L.-N., Guo, F.-Q., 2019. Photoelectrocatalytic degradation of atrazine by boron-fluorine co-doped TiO2 nanotube arrays. Environ. Sci. Pollut. Res. 26, 33847–33855. https://doi.org/10.1007/s11356-018-2569-y.
Wei, J., Feng, Y., Sun, X., Liu, J., Zhu, L., 2011. Effectiveness and pathways of electrochemical degradation of pretilachlor herbicides. J. Hazard Mater. 189, 84–91. https://doi.org/10.1016/j.jhazmat.2011.02.002.
Wu, T.-N., 2010. Electrochemical removal of pentachlorophenol in a lab-scale platinum electrolyzer. Water Sci. Technol. 62, 2313–2320. https://doi.org/10.2166/wst.2010.096.
Xin, Y., Liu, H., Han, L., Zhou, Y., 2011. Comparative study of photocatalytic and photoelectrocatalytic properties of alachlor using different morphology $TiO_2$/Ti photoelectrodes. J. Hazard Mater. 192, 1612–1618. https://doi.org/10.1016/j.jhazmat.2011.07.005.
Xu, F., Chang, L., Duan, X., Bai, W., Sui, X., Zhao, X., 2019. A novel layer-by-layer CNT/$PbO_2$ anode for high-efficiency removal of PCP-Na through combining adsorption/electrosorption and electrocatalysis. Electrochim. Acta 300, 53–66. https://doi.org/10.1016/j.electacta.2019.01.090.
Yang, Y., Cui, L., Li, M., Yao, Y., 2019a. Electrochemical removal of metribuzin in aqueous solution by a novel $PbO_2$/$WO_3$ composite anode: characterization, influencing parameters and degradation pathways. J. Taiwan Inst. Chem. Eng 102, 170–181. https://doi.org/10.1016/j.jtice.2019.05.023.
Yang, Y., Cui, L., Li, M., Zhang, L., Yao, Y., 2019b. Electrocatalytic degradation of the herbicide metamitron using lead dioxide anode: influencing parameters, intermediates, and reaction pathways. Environ. Sci. Pollut. Res. 26, 27032–27042. https://doi.org/10.1007/s11356-019-05868-7.
Zaouak, A., Matoussi, F., Dachraoui, M., 2013. Electrochemical oxidation of herbicide bifenox acid in aqueous medium using diamond thin film electrode. J. Environ. Sci. Health B 48, 878–884, 10.1080/03601234.2013.796827.
Zaviska, F., Drogui, P., Blais, J.-F., Mercier, G., Lafrance, P., 2011. Experimental design methodology applied to electrochemical oxidation of the herbicide atrazine using Ti/$IrO_2$ and Ti/$SnO_2$ circular anode electrodes. J. Hazard Mater. 185, 1499–1507. https://doi.org/10.1016/j.jhazmat.2010.10.075.
Zazou, H., Oturan, N., Zhang, H., Hamdani, M., Oturan, M.A., 2017. Comparative study of electrochemical oxidation of herbicide 2,4,5-T: kinetics, parametric optimization and mineralization pathway. Sustain. Environ. Res. 27, 15–23. https://doi.org/10.1016/j.serj.2016.11.008.
Zhang, Y.-N., Dai, W., Wen, Y., Zhao, G., 2017. Efficient enantioselective degradation of the inactive (S)-herbicide dichlorprop on chiral molecular-imprinted $TiO_2$. Appl. Catal. B Environ. 212, 185–192. https://doi.org/10.1016/j.apcatb.2017.04.062.
Zhao, K., Quan, X., Chen, S., Yu, H., Zhang, Y., Zhao, H., 2018. Enhanced electro-Fenton performance by fluorine-doped porous carbon for removal of organic pollutants in wastewater. Chem. Eng. J. 354, 606–619. https://doi.org/10.1016/j.cej.2018.08.051.
Zhao, R., Zhang, X., Chen, F., Man, X., Jiang, W., 2019. Study on electrochemical degradation of nicosulfuron by $IrO_2$ -based DSA electrodes: performance, kinetics, and degradation mechanism. Int. J. Environ. Res. Publ. Health 16, 16030343. https://doi.org/10.3390/ijerph16030343.
Zhu, K., Qi, H., Sun, X., Sun, Z., 2019a. Anodic oxidation of diuron using $Co_3O_4$/graphite composite electrode at low applied current. Electrochim. Acta 299, 853–862. https://doi.org/10.1016/j.electacta.2019.01.072.
Zhu, K., Wang, X., Ma, X., Sun, Z., Hu, X., 2019b. Comparative degradation of atrazine by anodic oxidation at graphite and platinum electrodes and insights into electrochemical behavior of graphite anode. Electrocatalysis 10, 35–44. https://doi.org/10.1007/s12678-018-0493-z.